

UNIVERSITY OF BELGRADE
FACULTY OF TECHNOLOGY AND METALLURGY

Rouaida Mohamed Abozaid

**PHYSIC MECHANICAL PROPERTIES OF
POLYMER COMPOSITES WITH
NANOMODIFIED SINGLE CRYSTALS**

Doctoral Dissertation

Belgrade, 2019.

UNIVERZITET U BEOGRADU
TEHNOLOŠKO-METALURŠKI FAKULTET

Rouaida Mohamed Abozaid

**FIZIČKO MEHANIČKA SVOJSTVA
POLIMERNIH KOMPOZITA SA
NANOMODIFIKOVANIM
MONOKRISTALIMA**

Doktorska Disertacija

Beograd, 2019.

Supervisors

Dr Vesna Radojević, full professor, University of Belgrade
Faculty of Technology and Metallurgy

Dr Zorica Lazarević, Associate Research Professor, University of Belgrade,
Institute of Physics

Member of Committes

Dr Petar Uskoković, full professor, University of Belgrade
Faculty of Technology and Metallurgy

Dr Radmila Jančić Heinemann, full professor, University of Belgrade
Faculty of Technology and Metallurgy

Dr Dušica Stojanović, Associate Research Professor, University of Belgrade
Faculty of Technology and Metallurgy

Dr Ivana Radović, Research Professor, University of Belgrade
Vinča Nuclear Institute

Date: _____

To my husband

ACKNOWLEDGEMENTS

I would like to express my enormous gratitude to all of those who stood by me regarding this work; particularly my supervisor Prof Dr Vesna Radojević for her generous support and assistance. Without her, I would not have been capable to bring this to an end.

I would like to express the deepest appreciation to my other advisor, Dr Zorica Lazarević from Institute of Physics, who has attitude and the substance of a genius: she continually and convincingly conveyed a spirit of adventure in regard to research. Without her guidance and persistent help this dissertation would not have been possible. It has been an honor to be their PhD student.

I would like to thank my rest of committee members Prof Dr Petar Uskoković and Dr Dušica Stojanović my thesis examiners for their interest in my work and for their insightful suggestions and comments on my thesis.

I would also like to thank Prof Dr Radmila Jančić and all of the teaching staff members of Material Science and Engineering Faculty of Belgrade University whose insightful wide knowledge of the field helped me to go ahead and finish my study.

I would like to thank the various members of with whom I had the opportunity to work and have not already mentioned who provided a friendly and cooperative atmosphere at work and also useful feedback and insightful comments on my work, and for always making me feel so welcome. I was fortunate to have the chance to work with Dr Ivana Radović who patiently taught me number of laboratory techniques, and worked closely with me. Special thanks to Dr Martina Gilić (the Institute of Physics Belgrade) for technical help for recording Raman spectra and for the valuable discussion. Also, I want to express my gratitude to our dear colleagues who have helped in the photoluminescence measurement, Dr Dragutin Šević and Dr Maja Rabasović (the Institute of Physics Belgrade). Last but not least, thanks to my colleague Dr Nataša Tomić, to help with FTIR hardness measurements and discussions.

My final gratitude always goes to my beloved husband Dr. Abdalla Tawengi and my five lovely kids for being so patient to keep me cheerful during my whole study periods.

FIZIČKO MEHANIČKA SVOJSTVA POLIMERNIH KOMPOZITA SA NANOMODIFIKOVANIM MONOKRISTALIMA

Rezime

U okviru ove doktorske disertacije ispitana je mogućnosti modifikacije površine monokristala tokom sinteze optoelektronskih kompozitnih materijala s polimernom matricom kontrolisanih optičkih svojstava. Na ovaj način se poboljšava povezanost strukture kao i veza matrica-monokristal što utiče na fizičko-mehanička svojstva kompozita. Izbor materijala pao je na poli(metil-metakrilat)-PMMA kao polimernu matricu i monokristale kalcijum volframata dopiranog neodijumom ($\text{CaWO}_4:\text{Nd}^{3+}$) i kvantne tačke kadmijum selenid/cink sulfid (CdSe/ZnS). Poli(metil-metakrilat) je polimer izuzetnih optičkih svojstava i transparentan je u celoj oblasti vidljivog elektromagnetnog zračenja. Zbog toga ne bi trebalo da utiče na optička svojstva ugrađenih monokristala. Kao modifikator površine korišćen je silan i to 3-merkaptopropil-trimetoksi-silan (MPTMS) zbog obezbeđivanja dobre transparentnosti u kompozitu.

Istraživanja su izvedena u dva pravca: a) sinteza monokristalnog $\text{CaWO}_4:\text{Nd}^{3+}$ kao funkcionalnog nosioca u kompozitu, modifikacija površine i procesiranje laminatnog kompozita sa poli(metilmetakrilatom); b) sinteza i karakterizacija kompozita ugradnjom modifikovanih kvantnih tačaka CdSe/ZnS . Na ovako organizovan način istraživanja može se pratiti uticaj modifikacije površine monokristala na optička, termička i mehanička svojstva dobijenog kompozita. Dobijen je i karakterisan visoko kvalitetni monokristal ($\text{CaWO}_4:\text{Nd}^{3+}$) metodom po Čohralskom. Nakon sečenja kristala u planparalelne pločice, procesirani su laminatni kompoziti sa poli(metil-metakrilat)-om.

Ugradnjom optoelektronskih čestica ili pločica u polimernu matricu menja se granična površina prelamanja elektromagnetnog zraka, sa vazduh-kristal na polimer-kristal. Modifikacijom površine čestice pojavljuje se još jedna granična površina kristal/silan-polimer. Pored toga, optička svojstva procesiranih kompozita zavise od veličine, oblika, sadržaja i raspodele monokristalnih čestica tako da takođe treba uspostaviti korelaciju između ovih parametara. Zbog toga je tokom istraživanja ispitan uticaj modifikatora površine monokristala i na makro i na nano nivou, tj. kod laminatnog kompozita i kod nanokompozita s kvantnim tačkama. Pokazalo se da modifikacija kod

laminatnog kompozita ne remeti optička svojstva, dok kod nanokompozita čak i popravlja one pomeraje u spektru koji su se dogodili tokom ugradnje čestica u polimer. U svakom slučaju, termička i mehanička svojstva kompozita su bitno poboljšana, što uz održana, pa čak i poboljšana optička svojstva, dovodi do dobijanja visokokvalitetnih optičkih polimernih kompozita.

Ključne reči: Polimerni kompoziti, monokristali, kvantne tačke, modifikacija površine, silani,

UDK:

Naučna oblast: Tehnološko inženjerstvo

Uža naučna oblast: Inženjerstvo materijala

PHYSIC MECHANICAL PROPERTIES OF POLYMER COMPOSITES WITH NANOMODIFIED SINGLE CRYSTALS

Abstract

Within this doctoral dissertation the possibility of modification of the surface of single crystals during the synthesis of optoelectronic composite materials with a polymer matrix of controlled optical properties was examined. In this way, the connection between the structure and the matrix-single crystals bond is improved, which affects the physic-mechanical properties of the composite. Poly(methyl-methacrylate) - PMMA was used as a polymeric matrix and single crystals of neodymium doped calcium tungstate ($\text{CaWO}_4:\text{Nd}^{3+}$) and quantum dots cadmium-selenide/zinc-sulfide (CdSe/ZnS). Poly(methyl-methacrylate) is a polymer of exceptional optical properties and it is transparent throughout whole wavelength range of visible electromagnetic radiation. Therefore, it should not have to affect the optical properties of the embedded single crystals. 3-mercaptopropyl-trimethoxy-silane (MPTMS) was used as a surface modifier with aim to provide good transparency in the composite.

The investigations were conducted in two directions: a) synthesis of single crystal $\text{CaWO}_4:\text{Nd}^{3+}$ as a functional carrier in the composite, surface modification and processing of laminate composite with poly (methyl methacrylate); b) synthesis and characterization of composites by incorporating modified quantum points CdSe/ZnS . In this way, the influence of modification of the surface of the single crystals on the optical, thermal and mechanical properties of the composite obtained can be monitored. A high quality single crystal of neodymium doped calcium tungstate $\text{CaWO}_4:\text{Nd}^{3+}$ was obtained by Czochralski method. After plating the crystals, laminate composites with poly (methyl methacrylate) were processed.

By installing optoelectronic particles or sheets in the polymer matrix, the boundary surface of the electromagnetic reflection is changed, with the air-crystal on the polymer-crystal. By modifying the surface of the particle, another boundary surface of the crystal/silane polymer appears. In addition, the optical properties of processed composites depend on the size, shape, content, and distribution of single crystalline particles, so also the correlation between these parameters should also be established. Therefore, during the

research, the influence of the surface modifier on the surface of the single crystals was studied both at macro and nano levels, in the laminate composite and in the nanocomposite with quantum dots. It has been shown that the modification in the laminate composite does not disturb the optical properties, while in the nanocomposite it even corrects those scattering in the spectrum agreed upon during the incorporation of the particles into the polymer. In any case, the thermal and mechanical properties of the composites have been significantly improved. So, optical polymer composites of high quality with undisturbed, moreover improved optical properties were processed.

Keywords: Polymer composites, single crystals, quantum dots, surface modification, silanes

UDK:

Field of Academic Expertise: Technology Engineering

Specialized Field of Academic Expertise: Materials Engineering

Contents

THEORETICAL PART	12
1. Introduction.....	13
2. COMPOSITE MATERIALS.....	15
2.1. Classification of composites	16
2.2. Properties of composite materials	20
2.3. Polymers and polymer matrix composites.....	22
2.3.1. Polymers and polymerization	22
2.3.2. Polymer matrix.....	25
2.3.3. Thermoplastic polymer matrix.....	25
2.3.4. Thermosetting polymer as matrix	27
2.3.5. Poly (methyl methacrylate).....	28
3. Modification of matrix-active medium interface	29
3.1. Silanes	30
3.1.1. Reaction of silane bonding	31
4. Optical active single crystals.....	34
4.1. Optical absorption in a semiconductor	35
5. Neodymium doped calcium tungstate single crystal, $\text{CaWO}_4:\text{Nd}^{3+}$ as optical materials: properties and crystal growth.....	37
6. Methods of single crystal growth.....	39
7. Nano single crystals and quantum dots.....	46
8. Optical active composite materials with polymer matrix.....	47
8.1. Influence of interface modification on the optical properties of composites	49
9. Methods of characterization of optical active materials and composites	50
EXPERIMENTAL PART	58
10. Experimental procedures.....	59
10.1. Crystal growth	59
10.2. Preparation of PMMA- $\text{CaWO}_4:\text{Nd}^{3+}$ layered composite.....	60
10.2.1. Materials	60
10.2.2. Film deposition.....	60
10.3. Methods of characterization of single crystal	61
10.4. Preparation of PMMACdSe/ZnS quantum dots composites	66
10.4.1. Materials.....	66
10.4.2. Modification of CdSe/ZnS QD`s surface	67

10.4.3. Preparation of PMMA-CdSe/ZnS films	67
10.4.4. Preparation of PMMA-CdSe/ZnS nanofibers	67
10.3.4. Characterization of samples	68
11. RESULTS AND DISCUSSION	71
11.1. Single crystal	71
11.2. Layered composite PMMA- CaWO ₄ :Nd ³⁺	80
11.3. Composite films PMMA- CdSe/ZnS quantum dots.....	84
11.4. Composite PMMA-CdSe/ZnS nanofibers	91
CONCLUSION	100
LIST OF REFERENCES	105
PRILOG 1.	115
Izjava o autorstvu.....	115
PRILOG 2.	116
Izjava o istovetnosti štampane i elektronske verzije doktorskog rada	116
PRILOG 3.	117
Izjava o korišćenju	117
Biography	119
Biografija	119

THEORETICAL PART

1. Introduction

Functional composites with a polymer matrix represent high performance materials in which specific properties can be designed depending on the application and the requirements in the exploitation. They are subject of great interest because of the possibility of adjusting properties by controlling the composition and morphology by different process techniques or by modifying the polymer matrix.

The structure of the composite represents a synergy of continuous phase called the matrix and one or more of the discontinuous phases, called the reinforcement or functional filler. The discontinuous phase has a reinforcement function, and it can also modify some other properties of the composite, such as optical, thermal, electrical or magnetic. The resulting properties of the composite materials depend on the properties and content of the constituents, their interactions, and the distribution of constituents, the geometry, and the orientation of the discontinuous phase.

The structure and properties of the interface between constituents in the composite material play a very important role in determining the physical and mechanical properties of composite materials. In the field of processing functional composite materials, the role of the interface is important because it is very important to preserve the original functional properties of components that are incorporated into composite (optical, electrical, thermal, magnetic ...) [1].

Composites with a polymeric matrix based on single crystals have great potential in the field of optical communication systems where the active micros to nano crystals are dispersed in an optically transparent matrix. When the electromagnetic wave passes through matter, one part of the atoms and the molecule of the environment are excited. For some materials, a small amount of energy deposited is released by photon emission at a higher energy level (up conversion) or lower energy (down conversion). Inorganic single crystals form a group of high density luminescent materials. Thanks to their high density and a large number of atoms, they can be used when high stopping power are required or high conversion efficiency of electrons or photons. For integrated nano-photon systems, it would be particularly useful if a laser source on a nano scale was available, characterized by high monochromaticity and coherence, and which is necessary for the processing of

optical information. So, as it was mentioned before the main feature in optical active composites is interface between transparent polymer matrix and single crystal and phenomenology of light transparency through it.

Research in the framework of this dissertation will be developed in order to examine the effects of processing on the properties of composites with a polymer matrix with embedded single crystals of different dimensions and levels of organization. For the good physical and mechanical properties of the composite material it is extremely important to achieve a connection between the matrix and the particles of the filler. Usually the silanes are used as coupling agents. These organic-inorganic compounds have dual-function molecules. On the one hand, they react with the particles of the filler, creating a stable Si-O-Si type bond, and on the other hand, they bond to an organic matrix creating covalent bonds.

Special attention will be paid to modifying the surface of the single crystal for better compatibility with the matrix. In addition to other physical-mechanical properties, the optical properties of single crystals will be especially monitored, which are now being modified in the process of incorporation in the matrix. For the propagation of optical rays the inter surface changes from single crystal-air through single crystal-polymer to single crystal-silane- polymer.

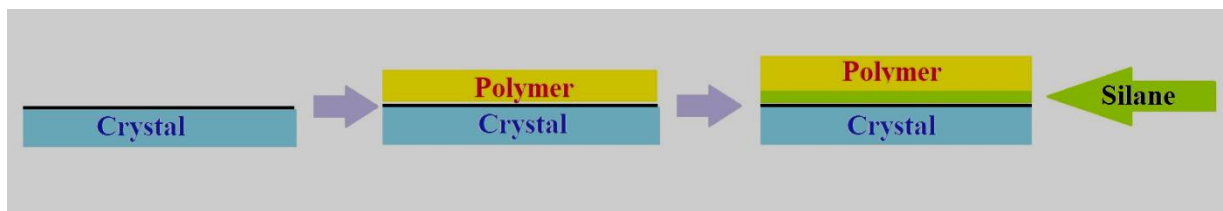


Figure 1. Interfaces in polymer matrix composites.

Single crystals represent perfect crystals whose crystal lattices are continuous throughout the bulk, without the presence of the grain boundary, i.e. the whole bulk is one crystal, without changing the layout and packing of atoms in all directions. A whole series of optoelectronic semiconductor single crystals represent materials for energy conversion due to their electronic configuration. Namely, the energy flow between the valentine and the conductive zone allows the absorption of electromagnetic radiation and the emission of photons at a higher (up conversion) or lower energy level (down conversion). Inorganic

single crystals form a group of high density luminescent materials. Thanks to their high density and a large number of atoms, they can be used when high power stops are required or high conversion efficiency of electrons or photons.

Lately, one of the single crystals that attract attention is calcium tungstate as a carrier material in which active ions of rare countries can be incorporated. In addition to laser application, single crystals of neodymium-doped calcium tungstate ($\text{CaWO}_4:\text{Nd}^{3+}$) are also interesting for acoustic-optical filters, LEDs and sensors. Therefore, it is very important to optimize the process of crystal growth in order to obtain high quality single crystals.

Quantum dots-QD are semiconductors single crystal nanostructures, whose charge-occupancy carriers are spatially limited in all three dimensions. The material from which the QD are made defines their characteristic energy values; however, the exact values of the energy gap are determined by the point size. The consequence of this is the fact that quantum dots made of the same material but of different sizes emit radiation of different wavelengths. The QD`s are sensitive to oxidation so t protection is performed by coating other single crystal materials. Thus, the core-shell structures of the type II-VI, IV-VI, and III-V semiconductors (CdS/ZnS , CdSe/ZnS , CdSe/CdS and InAs/CdSe) are formed. Polymers doped with optoelectronic active supplements allow the energy of nuclear radiation or UV rays to be converted into the radiation energy in the second part of the electromagnetic spectrum (up and down conversion).

2. Composite materials

Composite materials are multicomponent, multiphase materials composed of two or more phases separated by an intermediate boundary, whose physical and mechanical properties in the composite differ significantly from the initial properties of the components they make. Designing composite materials is done in order to improve the structural, thermal, chemical and other characteristics of the starting materials [1, 2]. The construction of composite materials is done to improve the structural, thermal, chemical and other characteristics of the starting materials. The development of modern composites is focused on the possibility of designing their structure and properties by various methods of synthesis and processing. By combining the constituent of the composite at the

macroscopic, microscopic and nano levels, a resulting set of properties of the composite material could be obtained.

Each composite has certain characteristics that distinguish it from other materials: high strength and stiffness, low density and mass, corrosion resistance and high temperature, chemical inertia, processing ability and shaping in different shapes, durability, as well as improved characteristics of the obtained composite materials provide a wide range of applications. In search of new composite materials, there were always combinations between the basic classes of materials: metals, ceramics and polymers.

2.1. Classification of composites

The great need for composite materials in different areas of human activity creates difficulties in their classification, but the most common way of classifying composite materials is according to the type of matrix shape and according to of the geometry of reinforcement (Figure 2, Table 1).

The materials most commonly used as matrix are polymers, metals, ceramics and carbon. The matrix in composite materials participates with 30-40 volumes by performing numerous functions:

1. Accepts external stress and transmits it to amplification;
2. Protects reinforcement against environmental impact and wear;
3. Determines the thermo-mechanical stability of the composite, durability, toughness, shear, compression and tensile strength of the composite;
4. Connecting constituents into a common entity.

Composites with polymer matrix are most used in room temperature conditions, because at elevated temperatures the polymer decomposition occurs. Such composites are elastic, robust and economical for production and therefore have a wide scope of application. The fibers that enter them are usually continuous or short. Depending on the character of the changes that occur during processing and the application area, thermoplastic and thermosetting polymer matrices are distinguished.

Composites with a metal matrix feature excellent mechanical properties, but the combination of fiber and metal matrix is limited by the chemical reactions that can be

drawn between them. Strengthening the metal nut with particles and fibers improves specific strength and creep resistance, and the temperature interval of their use is expanded up to several hundred degrees, for this type of matrix the most commonly used are continuous and short fibers, viscera and particles. This type of composite is obtained by first consolidating the reinforcing matrix, followed by the formation by forging, rolling and extruding.

Composites with a ceramic matrix contain a ceramic matrix that can be oxidized (Al_2O_3 , SiO_2 , barium, lithium, calcium-alumo silicates), which is reinforced with particles or short single crystals particles or fibers-whiskers. The advantage of ceramics is creep resistance and stability at extremely high temperatures and corrosion resistance, high hardness, while the greatest lack of tendency to crack fracture, then low resistance to bending and stretching, low toughness and low strength to impact.

Composites can be classified according to geometry of reinforcements (Table 1). Three main categories:

- Reinforced by particles;
- Fibres reinforced;
- Layered structures.

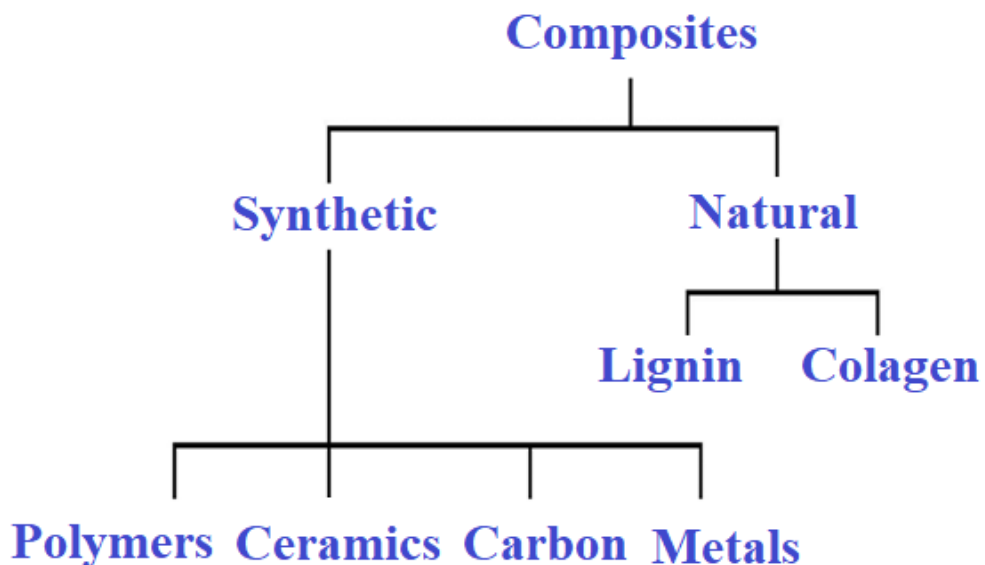



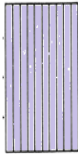




Figure 2. Classification of composites according matrix material.

Table 1. Classification of composites by geometry of reinforcements

Composites					
Particles		Fibers		Layered	
Large	Small	Short Fibers	Continuous Fibers	Laminate	Sandwich
					

In composites reinforced by particles, particles can be of different size, with a fine or coarse particles of 10 nm to 1 μm , as well as distinctive shapes: spherical, cubic, tetragonal, plate-shaped or irregular. A particle can be organic and inorganic, can classify as natural or synthetic, and the dependencies of the functions they can be inert, semi-active or active. Low cost particle size and relatively easy to obtain composite with particles enabled widely use in composites with metal and ceramic matrix [3]. This group includes micro- and macro-composite materials reinforced with large particles and nanocompatible materials so-called. dispersion reinforced composites. The difference between these two types of composites is in the amplification mechanism. The term of the large particle says that the interaction between the continuous phase-matrix and particles as reinforcements can not be observed at atomic or molecular levels. In most of the composite materials in this group, particulate matter is a mechanically firmer and harder phase, and the matrix material is a ductile and tough phase. In this way, the particles slow down the plastic and viscous deformation of the matrix. In the mechanical load of composite materials, the matrix as a continuous phase transmits stress to particles. The degree of amplification depends to a large extent on the strength of the bond between the matrix and the particles. In dispersion reinforced composite materials the particles are much smaller and their

diameter ranges from up to. Mechanisms of interaction between the particle and the matrix are at atomic and molecular levels and they determine the degree of amplification. In these composite materials, the matrix suffers a whole load while the role of particles in preventing movement of dislocations.

A particularly interesting area is the research of new types of nanocomposites. Addition of nano dimensions inorganic filler (<100 nm) in polymers cause completely new effects in the structure. Developmental researches in this field result in new types of hybrid organic/inorganic composites. These materials have superior mechanical, optical, electrical and electrochemical properties between organic polymers and inorganic ceramic/glass materials. Some examples include: the addition of special types of clay (bentonite) scattered in layers in a polymer matrix give the composite material impermeable to water and oxygen; or the addition of SiO₂ nanoparticles into the automotive tire, instead of the char, a smaller friction factor and better recycling of the tire is achieved.

The fiber is a thin, a flexible material whose one dimension is many time is bigger from the other two. The fibers are the most beneficial reinforcement of the discontinuous solid phase following the fact that the combining of this material with some other kind of matrices leads to the achievement of superior physical and mechanical characteristics, and the strength of composite between the fibers and the matrix has a verified by rule of mixing. The woven fibers of the composite depend on a higher factor: the materials, the fibers length, the fiber diameter, cross section shape and others. The fibers can be continuous or short, as well as individual, in the form of monofilament, or in the form of a sheet - a multifilament. Structure of fibers can be distinguished: non-crystal (glass), single crystal (polystyrene), polycrystalline (metal, ceramics), high-phase, and on the basis of geometrical parameters is done on the whisker, fiber and wire.

Short fibers are fibers in which the ratio of length and fiber diameter, with an average length of 6 to 50 mm. Depending on the thickness of the fiber and the method of obtaining polymeric composites in the microstructure, it is possible to achieve different fiber orientation from random two-dimensional and random three-dimensional to complete unidirectional orientation of short fibers.

In relation to polymers that are reinforced with continuous fibers, they have much less strength than modules, but these two types are used much more in various areas: automotive industry, electrical components, shipbuilding, building construction, etc. The reasons for this wide use are as follows: a) relatively easy to install and process and can be

massively produced, b) relatively cheap, c) the mechanical properties of short-fiber reinforced polymers are better than clean plates and for many uses are good enough to be competitive metals and g) if there is no fiber orientation, particle-reinforced polymers and short fiber reinforced polymers can be isotropic.

The layered structure could be in form laminate and sandwich structure. Laminate have a many layers of different structure, bout matrices or reinforcements, while sandwich structure have one layer in the middle covered by harder material [4-6]. The laminate can consist of layers with different orientation of unidirectional fibers. The properties of the composite in the form of laminate are anisotropic. The laminate possesses a transversal isotropic symmetry, a form of orthotropic symmetry, with three mutually administrative levels of symmetry, characterized by isotropy in all directions governing the fiber direction. The lamina is oriented in the main material coordinate system 1-2-3, in which the axis 1 coincides with the fiber direction, the axis 2 is governed by the axis 1 in the level of lamination 1-2, and the axis 3 is straight at 1-2. Layered structures are also very suitable for optical composite with single crystal wafer and polymer layers.

2.2. Properties of composite materials

Composite materials are made by artificial joints having two or more materials of different properties with the aim of obtaining materials whose characteristic properties do not have any of the starting constituents individually. On such way, unusual combination of properties can be achieved, such as stiffness, strength, mass, high temperature behavior, chemical resistance, hardness or electric and thermal conductivity. Some of the general advantages of composite materials in comparisons with classical materials are: a) high strength with exceptionally low mass, b) possibility making very complex shapes, c) reducing the cost of subsequent processing of parts, d) the possibility connecting parts during the production process itself, e) stability of dimensions in extreme cases working conditions, f) corrosion resistance. The composite response to the applied loading depends on: a) the properties of the matrix and the reinforcement, b) the size distribution and dispersion of constituents, c) the volume fraction of the constituents, d) the form of the constituents, and e) the nature and the strength of the relationship between the constituents.

Due to the phenomenon of synergy, that is, obtaining of better properties of composite material than a simple sum of the corresponding properties of the constituents, the composite material are classified in the class of synergistic materials, which indicates that the properties of the composite are essentially determined by the mechanisms of interaction between its constituents.

The physic-mechanical properties of the composite are determined by the properties of their constituents, the distribution of constituents and their interaction. The properties of the composite can be described by the sum of the products of the properties of constituents and their volume fraction, so-called a mixing rule that can be written in the general form in the form of an equation:

$$\text{Composite properties, } P_c = \sum_i^N (\text{constituents properties, } P_i) \times (\text{volume fraction of constituent, } v_i)$$

If the constituents react in a synergistic way then the properties of composites cannot be expressed by the mixing rule, i.e. there is an inequality:

$$\text{Composite properties, } P_c \neq \sum_i^N (\text{constituents properties, } P_i) \times (\text{volume fraction of constituent, } v_i)$$

Cases when inequality is valid are much more frequent than cases when the rule applies mixing to calculate the properties of a composite. The orientation of the discontinuous phase affects the isotropy of the properties of the material. Reinforcement in the shape of approximately equiaxial particles determines the complete isotropy of the properties of composites. If the particle dimensions are not identical, the composite is isotropic only when the particles are randomly oriented, as is the case with the composite reinforced by randomly oriented, short fibers. If all the particles are oriented in the same direction during the course of production, anisotropy is blamed. Composites reinforced with long fibers exhibit pronounced anisotropy properties, as well as a laminar composite material that is always anisotropic. Properties of orthotropic materials differ in three different directions.

Some properties of the material, such as density, specific heat, the absorption and are not directly related to isotropy and using scalar quantities which have certain intensity for both isotropic and for non-isotropic material. On the other hand, properties such as

stiffness, Poisson's ratio, thermal expansion, expansion due to moisture, thermal and electrical conduction are related to direction and they are function of orientations in anisotropic material. Fiber reinforced composites can exhibit varying degrees of anisotropy and variability properties. The greatest difference is observed between the properties in the longitudinal (in the direction of the fiber direction) and transversal (orthogonal to fiber direction) direction.

2.3. Polymers and polymer matrix composites

2.3.1. Polymers and polymerization

Polymers are molecules consisting of many constituent units - monomers. Today, according to IUPAC, the polymer is defined as a substance consisting of molecules that are characterized by multiple repetitions of constituent units in the molecular chain and are so large that their properties do not change significantly if a molecular chain is incorporated or washed away by several constituent units. Polymers are macromolecular substances.

Macromolecules are large molecules consisting of several hundred or thousands of molecules. Chemical reactions to which monomer molecules connect in macromolecules are called polymerization reactions. Polymers are represented by the chemical formula of the remainder of the monomer or the basic motif, denoted by the bracket and the number, n , the basic motifs - "measure" in the macromolecule chain, which is called the polymerization degree and is denoted by X . The polymers can be classified according to different criteria which are: origin, chemical composition of monomers, and way of connecting to macromolecules, mechanism of formation reaction, properties and method of processing, then according to areas of application, etc.

According to their origin, polymers are divided into two large groups: natural and synthetic. Natural polymers are starch, cellulose, wool, silk, as well as biopolymers from which living organisms, DNA and proteins are built. Synthetic polymers, which are still called synthetic resins, are divided into degrees (condensation) and chain (addition) by the way of polymerization reaction. In the form of polymer chains, they are divided into linear, branched and cross-linked, which are formed by connecting at least two chains.

The structure of the polymer is mostly amorphous, which means that within these substances there is no proper arrangement of the particles that build the polymer. But some

polymers can have partially ordered structures/crystallites. By modifying the polymer, achieved in different ways, a wide variety of materials bearing the general name of the plastic mass is obtained. Polymers that consist of the same repeating units are called homopolymers, while those containing two or more different types of repeating units are called copolymers. By way of binding the monomer units, the copolymers can be statistically random, in which the repeating units are randomly distributed, alternating, in which the units are alternately arranged alternately, block copolymers, in which units are repetition is in the form of blocks and grafted copolymers, which consists of a basic chain to which the side chain is composed of other monomer units.

For the synthesis of macromolecules from monomers, two methods are used: polymerization and polycondensation.

Polymerization is a reaction by which chemical compounds of a small molecular weight (monomers), or mixtures of several such compounds, react each other until the free functional groups are exhausted, resulting in the formation of molecules with a much higher molecular weight than the reactants. This is a special case of the addition reaction and refers to the merging of a large number of monomer molecules, which have a multiple connection, without allocating side products. Therefore, the polymer and the monomer have the same elemental chemical composition. Polycondensation is a process of substitution in which the polymer is formed by extracting by-products, usually small molecules. In polycondensation monomers must have at least two functional groups. The polycondensation product has a different elemental composition from the starting monomers.

Under the supramolecular structure, the macromolecular packing is assumed to be spatial separated continents of different degrees of order, shape and layout in the space. Molar mass and molecule interaction determine the physical state of a substance. Unlike low molecular weight substances, polymers can have two aggregate states - solid and liquid. The boiling temperature of the polymer is higher than the degradation temperature, which is why they cannot exist in a gaseous state. In addition to the stated aggregate (liquid and solid) and phase states (amorphous and crystalline), physical states were introduced to characterize the polymer (Table 2). Thermoplastic - amorphous polymers can occur in three physical states - glass, highly elastic and plastic [7, 8].

Table 2. The physical states of polymers

Temperature →	Physical states	
	Liquid (Easy movement of macromolecular chains)	
	Amorphous Movement of chains under stress	Crystalline Heavy chain movements
	Glassy state Only locally moving chain segments at stress	

Due to the analogy in the behavior of silicate glass, a typical representative of amorphous bodies, which do not change the structure when moving from liquid to solid state (degree the polymers in a solid-amorphous state are called glasses. That's why the transition from a highly elastic to a solid state is called transition to glassy state. It's not followed by a suddenly change temperature, like which is the case in the crystallization of low molecular substances, because the structure of the polymer practically does not change. Transition to glassy state is played in an interval of about 10 °C, and the mean temperature of that interval is marked with T_g , glass transition temperature. When macromolecules settled from solution or by curing melt, they can be in an amorphous or partially crystalline state depending on the chemical composition of the monomer, the flexibility of the macromolecular chains and interactions within a single macromolecule and between different macromolecules. If macromolecular chains have large side groups, such as polystyrene or poly(methyl methacrylate), they will remain the form of a tangled club in transition to a solid state and will have an amorphous structure. The macromolecules of the polymer in the amorphous state are completely unordered so that there is practically no change in degree of determination of macromolecules during the transition from melt to solid state. They most often retain the shape of a tangled club, but with slightly smaller dimensions than in a good solvent. Amorphous polymers are thermoplastic, transparent and anisotropic, ie they have the same properties in all directions.

2.3.2. Polymer matrix

Polymer composites representing multiphase materials are composed of two or more components, where the polymer forms a continuous phase, a matrix, and fillers or reinforcing additives represent structural parts. The structure and properties of the matrix determine the chemical and thermal resistance of composite materials, and also affect some mechanical and physical properties. Depending on the character of the changes that occur during processing, thermoplastic and thermosetting polymer matrices are distinguished. The polymeric composite material represents a polymer continuous phase in which one or more discontinuous phases are incorporated. If the discontinuous phase is circular, harder and stronger than the continuous polymer phase, it is called an amplifying phase or short amplification while the continuum phase is called a matrix. The shape of the discontinuous phase may be different and can be approximated by the sphere (particles), the cylinder (fibers, sticks), the plating layer (laminated), irregular plates (flakes) or irregular particles (filler).

2.3.3. Thermoplastic polymer matrix

Polymers whose structure are in the form of linear or branched macromolecules are usually thermoplastic polymers. Thermoplastic polymers are used in short fiber composites. Thermoplastic polymers can be completely non-crystalline or partially crystalline (Figure 3). Polymers relatively simply form non-crystalline structures, because their chains are very long and flexible, and as such they are difficult to order in the correct crystalline structures. The most common polymer structure consists of interwoven macromolecules. Thermoplastic polymers first soften after heating, and then transferred to viscous liquids without chemical changes. The cooled material again solidifies and goes into its original state. This softening and curing process can be repeated unlimited times.

Thermoplastic polymers include: polyacrylates, polyethylene, polypropylene, polyvinyl chloride, polystyrene, polyamides, polycarbonates, and others (Figure 4).

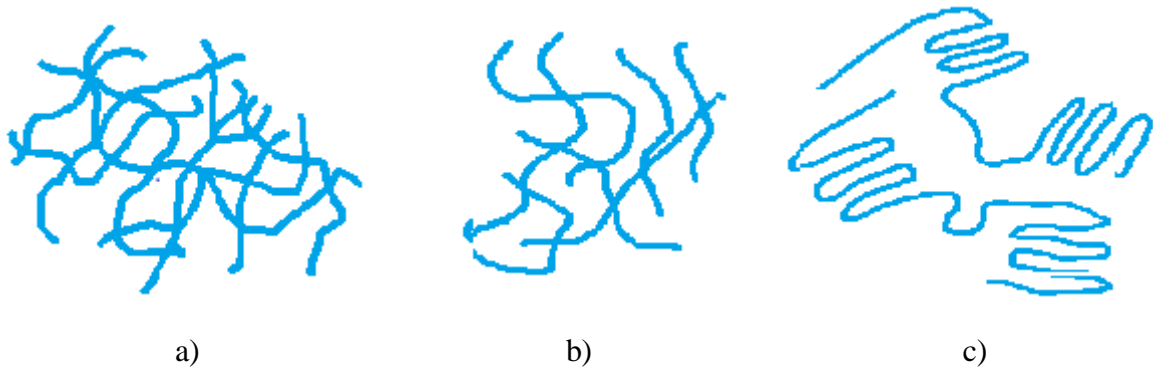


Figure 3. Schematic representation of structures: a) fully cross-linked thermosetting polymer, b) non-crystalline thermoplastic polymer, c) partially crystalline thermoplastic polymer.

The introduction of new thermoplastic resins: polyetheretherketone (PEEK), polyetherketone (PEK), polyethylene sulfide (PES), etc., as a matrix influenced the improvement of the toughness of the matrix and the characteristic of resistance to the impact of the composite, the method of forming the composite was shortened.

$\left[\text{CH}_2 - \underset{\begin{array}{c} \text{C}=\text{O} \\ \\ \text{O} \\ \\ \text{CH}_3 \end{array}}{\overset{\text{CH}_3}{\text{C}}} \right]_n$	$\left[\text{CH}_2 - \text{CH}_2 \right]_n$	$\left[\text{CH}_2 - \underset{\text{Cl}}{\text{CH}} \right]_n$
Poly (methylmethacrylate)	Polyethylene	Poly (vinyl chloride)

Figure 4. Formulas of some thermoplastic polymers.

2.3.4. Thermosetting polymer as matrix

Thermoreactive (thermosetting) polymers most commonly build a solid three-dimensional network. When processing by heating or with the addition of some chemical compounds, they switch to hard and insoluble products, which cannot be converted to plastic state again. The reason for this is that when processing, under these conditions, chemical reactions occur, resulting in the formation of a networked spatial non-crystalline structure. For the production of composites, most commonly used are phenol formaldehyde, polyester, epoxy resins.

Polymer matrix composites with fibers are thermosetting resins or duromers and thermoplastic resins or plastomers. Thermosetting resins in composites are used with continuous fibers, polyester with glass, and phenol formaldehyde and epoxy resins with carbon, glass and/or aramid fibers (Figures 5 and 6).

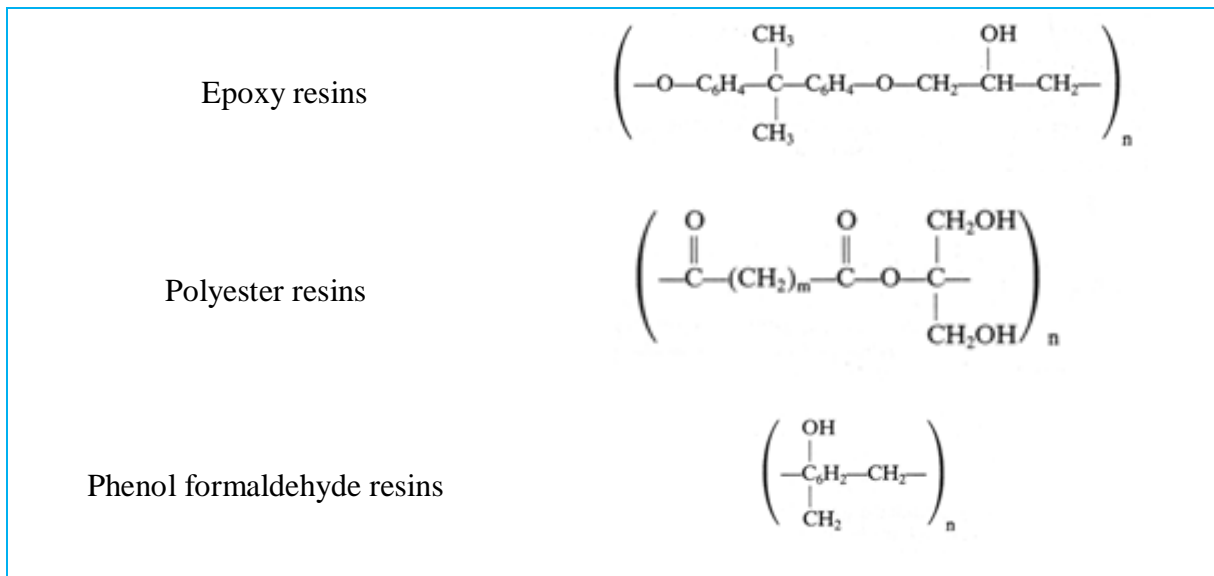


Figure 5. The most frequently used a thermosetting resin as the matrix in polymer composites [8].

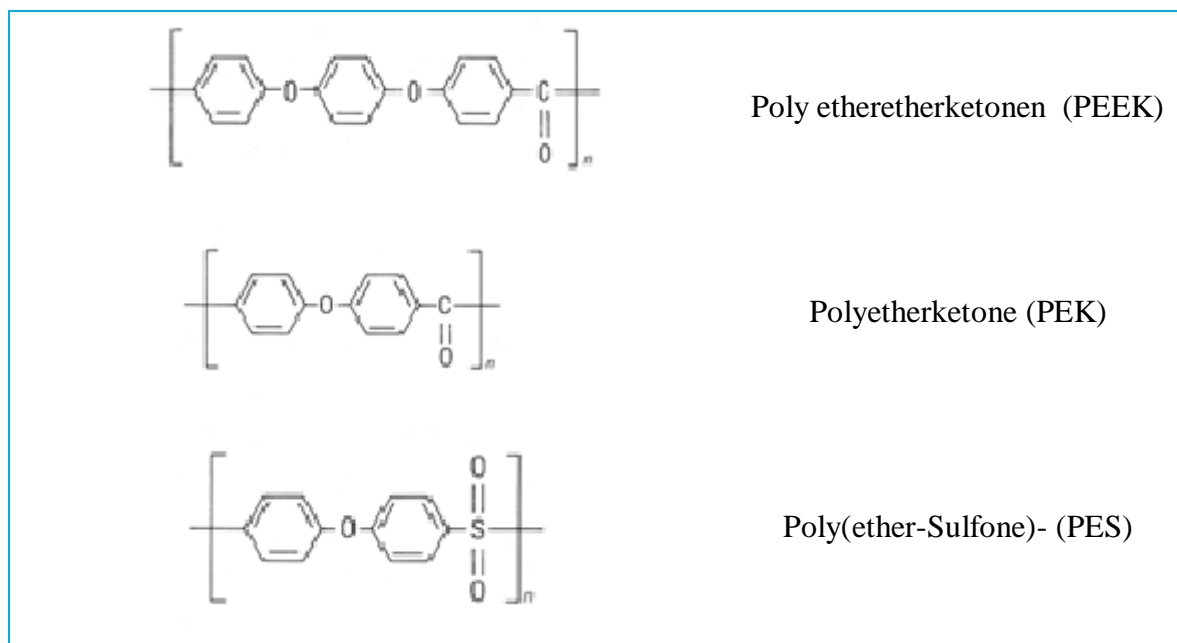


Figure 6. Formulas of some thermosetting resins and polymers.

2.3.5. Poly (methyl methacrylate)

Poly(methyl methacrylate) is a synthetic polymer that appeared on the market in the 1930. under the name Plexiglas. PMMA is the most widely used vinyl polymer of the group of acrylates. Polyacrylates are marketed in the form of powder or in the form of plates, rods, tubes and blocks. Due to its good properties, but also a relatively low price, PMMA has found great application in the automotive industry, home appliance production, construction, etc. Because of its transparency and resistance to atmospheric conditions in combination with high strength and surface hardness, it is often used as a replacement for glass. Its optical properties are remarkable, better than glass. It spills up to 92% of the light in an interval of 380 to 780 nm. As for chemical stability, it is extremely stable, it is not subject to oxidation, nor to the action of acids, bases and UV rays. It is amorphous and can be processed to a great extent.

The quality and durability of the product depends on the amount of residual monomer in the polymerization reaction, or the way the reaction is performed. Poor PMMA properties are brittle and flammable.

The PMMA polymerization reaction is carried out with radical initiators in suspension or in weight. The rate of reaction and the amount of newly formed polymer grow together with the degree of conversion. The initiator of the reaction is usually benzoyl peroxide. PMMA belongs to thermoplastic polymers. PMMA has a high glass temperature, $T_g \approx 120$ °C. The hardness of the surface is small and easy to scratch, but it has a high impact resistance. It is not resistant to chemicals and is dissolved in organic solvents, such as aromatic hydrocarbons, esters and dioxane. It is resistant to atmospheric conditions. It is absorbed in organic glass and is most often used for this purpose from all other organic glasses. It can replace inorganic glass, because it is colorless and transparent. Transparent is visible in the wavelength range of electromagnetic radiation [9].

3. Modification of matrix-active medium interface

The structure and properties of the interface between constituents in the composite material play a very important role in determining the physical and mechanical properties of composite materials. In particular, large differences between the thermal and elastic properties of the constituents are confronted over the interface, that is, the stresses acting on the matrix are transferred to the reinforcement through the interface. The boundary surface is defined as the connection between the matrix and the reinforcement. Indeed, especially in polymeric composites, the fiber-matrix region has the structure and mechanical properties different from both the matrix and the reinforcement. It is possible to gradually change the mechanical properties from one boundary surface to another border area across the border region. This region is known as the intermediate region and its size depends on the composite to the composite depending on the chemical nature of the matrix material and reinforcement. Nature of connections on boundary surfaces in composite materials can be established with different nature of bonding:

- a) adsorption and wettability,
- b) electrostatic attraction,
- c) chemical bonding,
- d) interdiffusion,
- e) mechanical adhesion.

When two electro neutral surfaces are brought in close contact, they come to physical attraction at the contact points. Such a mechanism for making reinforcement-matrix connections is called adsorption and wettability.

The forces of attracting established between two surfaces with different polarity, a purely positively, and the other a purely negative charge, as in the case of the acid-base interaction or in the formation of an ionic bond. This mechanism is called electro-static attraction.

Inter-diffusion is a form of connecting two polymer surfaces through a diffusion of polymer molecules from one surface to a molecular net of the second surface in contact. The chemical binding mechanism is important in the connection of the reinforcement and polymer matrix (the chemical bond is realized through chemical groups on the surface of reinforcement with compatible chemical groups in the matrix)/ Mostly, that is, when bonding of inorganic reinforcement with polymer matrices over the silane as a coupling agent.

Some fiber-matrix connections are realized by the mechanism of mechanical adhesion by pure mechanical connection of two surfaces. A resin that completely flies the surface of the fibers is accompanied by every detail of the surface of the fibers. The strength of this intermediate level is not large enough to tensile, but the shear strength along the intermediate surface can be very significant and depends on the degree of roughness of the surfaces.

3.1. Silanes

The most commonly used coupling agents are silane based products, compounds having bifunctional molecules. Silanes, as coupling agents, have the ability to form a lasting chemical bond between organic and inorganic substances, which, in the absence of silanes, create weak links. Good bonding allows a flexible organic matrix to withstand the stress by which the material is exposed during exploitation to solid inorganic particles of the filler [10-13].

The general formula shown in Figure 7 shows that there are two reaction points. The hydrolysable group is X (mainly it is alkoxy, acyloxy, halogen or amino), which during the hydrolysis forms a silanol group, which, furthermore, can form a siloxane group

by condensation. They are forming very stable bonds by reacting with oxides of aluminum, zirconium, titanium, nickel, until condensation occurs, while weaker bond are formed with oxides of boron, iron, and carbon. The non-hydrolyzed group is R, which is responsible for reactivity. Bonding of loxysilane from the particle solution can produce several structures: a) covalent, b) self-organizing and c) polycondensed. The final structure depends largely on the temperature at which the silanisation is carried out and on the amount of water present in the solvent or on the surface of the particles.

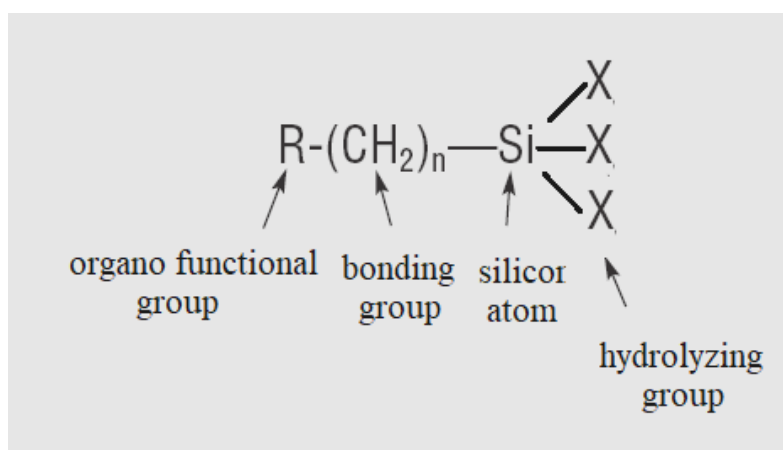


Figure 7. Formula of trialkoxysilane.

3.1.1. Reaction of silane bonding

Most commonly used silanes with one reaction group and three hydrolyzing substituent's. The reaction is carried out in four steps: firstly, the hydrolysis of alkoxy into the silanol group results in condensation (water is separated), and a form is obtained which bonds to the substrate with hydrogen bonds. The resulting compound is dried or heated to separate the water molecules and the resulting covalent bond, Figures 8, 9 and 10. When it comes to the initiation caused by hydrolysis, the reaction proceeds spontaneously and very quickly. Most commonly, one bond between the substrate and the silane is formed, while the other connections are either condensed or free. The R group remains free to form other covalent bonds or physical bonding.

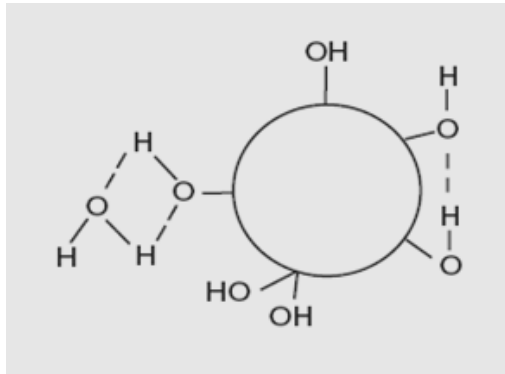


Figure 8. The surface of particle and the bonds that are formed.

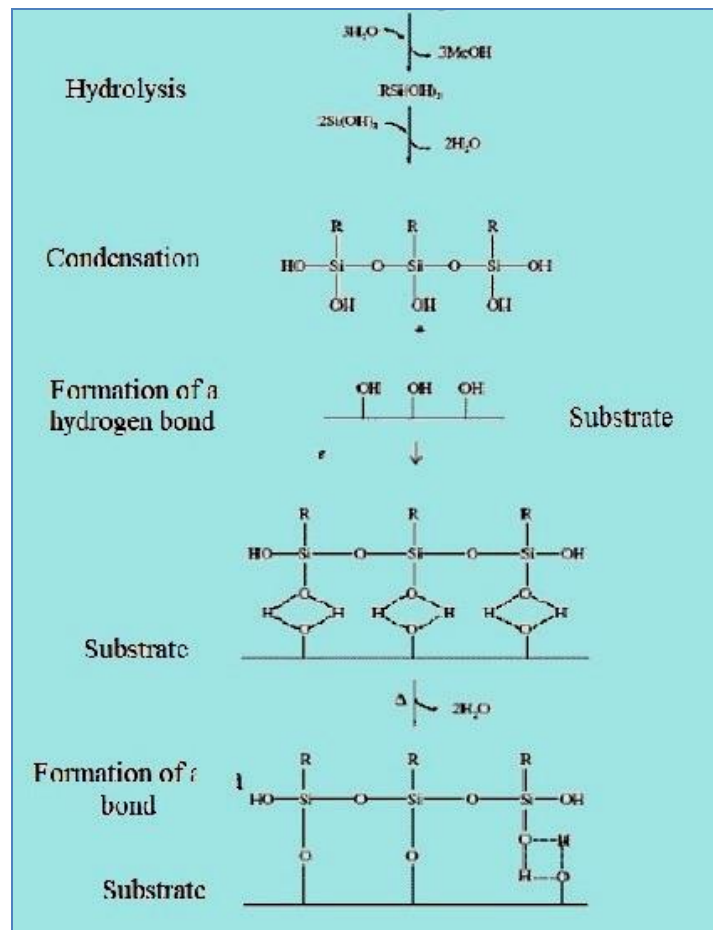


Figure 9. Reaction of silanes and formation a bonds.

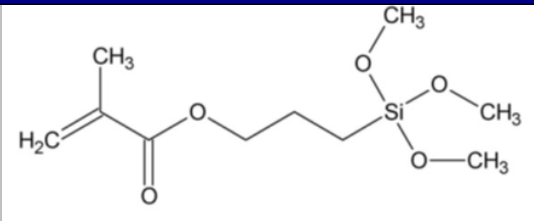
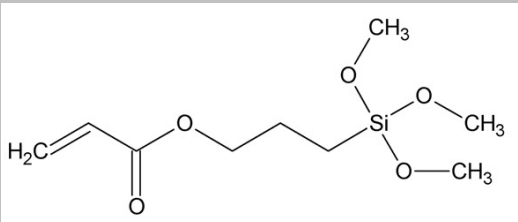
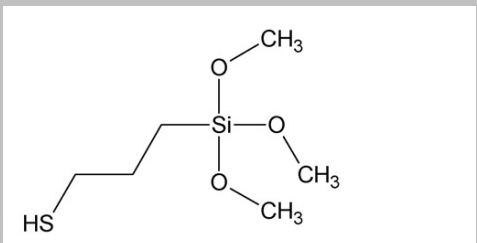
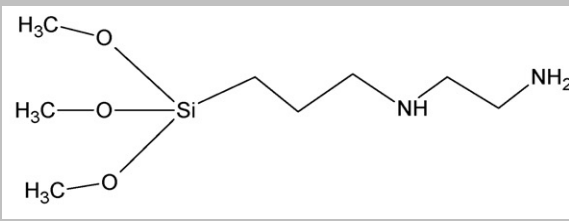
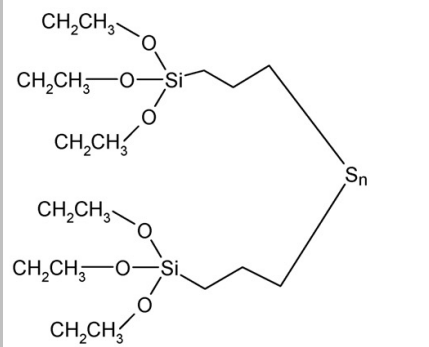
<i>Silane</i>	<i>Formula</i>
a) 3-methacryloyloxypropyltrimethoxysilane	
b) 3-acryloyloxypropyltrimethoxysilane	
c) 3-mercaptopropyltrimethoxysilane	
d) N-[3-(trimethoxysilyl)propylethylenediamine]	
e) bis-[3-(triethoxysilyl)propyl]polysulfide (n = 2-4, poly).	

Figure 10. Formulas of some silanes: a) 3-methacryloyloxypropyltrimethoxysilane, b) 3-acryloyloxypropyltrimethoxysilane, c) N-[3-(trimethoxysilyl)propylethylenediamine], d) 3-mercaptopropyltrimethoxysilane and e) bis-[3-(triethoxysilyl)propyl]polysulfide (n = 2-4, poly) [14].

4. Optical active single crystals

The fields of application of semiconductor materials are expanding day by day. One of the important areas was the production of optoelectronic appliances. Light has many features that make it very suitable for transmitting information, such as:

- Resistance to electromagnetic fields. As the light particles are not electrified, electromagnetic phenomena such as lightning have no effect on them.

- Crossing two optical beams without interference. Two unbound light beams can be crossed without any effect on one another. This feature can be used in the production of very complex devices. In case of crossing two electronic signals there is a loss of information.

- High speed information transfer.

- Optical air management. Optical air can be easily controlled using a lens. This feature can be used to quickly change the configuration of the car.

- Special functions devices. This is the most interesting feature of optical devices and has potential application in fast transmission and processing of information. An important example is the lens, which when applied in an appropriate relationship object - an image can produce a Fourier transform image object.

- The wave nature of light. As light is scattered at large distances in comparison with electrons, its wavy nature can be applied to making special devices.

- Nonlinear interaction. Many materials have a non-linear response to the effect of optical air.

- Easy connection to electronics. Optical and electronic interaction can be easily connected in semiconductor devices. This feature has led to the production of the most important opto-electronic devices such as laser, detector and modulator [15-18].

In the case of semiconductor materials, the interaction between light, i.e. photons and the semiconductor material itself, takes place through an electron. In light of the corresponding energy into semiconductor material can cause the creation of pairs of electrons and cavities. These electrons and cavities can be used to convert the energy of photons into electricity. This interaction is based on the operation of solar cells and optical detectors. In the same way it is possible to obtain light by recombination of electrons and vacancies.

4.1. Optical absorption in a semiconductor

When the semiconductor material is placed on the path to the light beam, the transition from the valence to the conductive band can occur. This phenomenon is called photon absorption. Photon absorption is the strongest when photon directly induces the transition of electrons from the valence band to the conductive. Since the photon moment is much smaller than the moment of the electron, the law of energy maintenance requires that the passage of the electron cavity be vertical in the k-space as shown in Figure 11a).

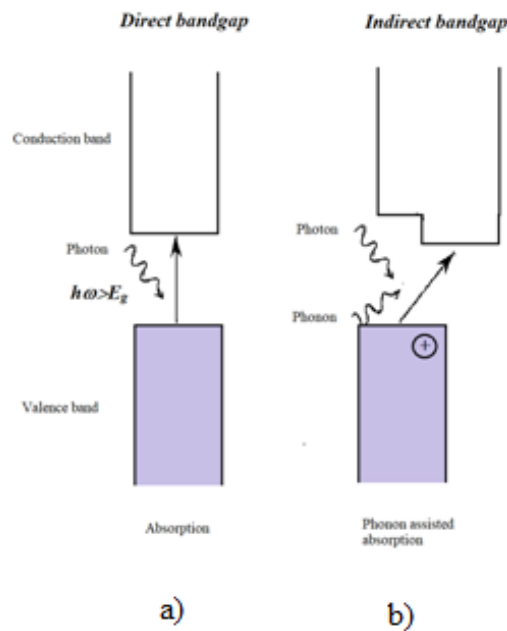


Figure 11. Interaction of optoelectronic material with light wave.

Such transitions are only possible with materials having a direct energy flow. When the semiconductor does not have a direct energy circuit impossible, the vertical k is transmitted and the electron can absorb the photon only if the phonon (or vibration of the crystal lattice) participates in the process as shown in Figure 11b). Such processes are not as strong as those in which phonon does not participate. The transition coefficient for materials with an indirect projection is less than the coefficient of transition of materials with a straight-line gap of about 100 times. Materials such as GaAs, InP, InGaAs have strong optical absorption because it is played without the participation of phonons. On the

other hand, Si and Ge have indirect energy circuits so absorption is poor. Literature data presents that in the particular case of CaWO_4 [19] E_g ranges from 4.4 to 6.8 eV.

When the absorption coefficient is known, it is necessary to find out the conditions in which the pairs of the electron - vacancy will arise. If with $P_{\text{op}}(0)$ we denote the intensity of light that strikes the semiconductor material per unit area, then the intensity in point x is then equal:

$$P_{\text{op}}(x) = P_{\text{op}}(0) \exp(-\alpha x) \quad (1)$$

The energy absorbed in seconds per unit area in the region of thickness dx between the points x and $x+dx$ is:

$$P_{\text{op}}(x) - P_{\text{op}}(x+dx) = P_{\text{op}}(0)[\exp(-\alpha x) - \exp(-\alpha(x+dx))] = P_{\text{op}}(x) \alpha dx \quad (2)$$

If this absorbed energy produces a pair of electron-vacancy with energy $h\omega$, the speed of producing energy carrier is:

$$G_L = \alpha P_{\text{op}}(x) / h\omega \quad (3)$$

When the light ray falls to the semiconductor material and creates a pair of electron-vacancy, the performance of the detector depends on the collection of these carriers and the change in the conductivity of the material. In the absence of an electric field, a pair of electron-vacancy will be recombined and will not generate a detectable signal. An important feature of the detector is the intensity of an I_L current that occurs under the influence of the optical air of certain strength

$$R_{\text{ph}} = I_L / P_{\text{op}} * A \quad (4)$$

Where R_{ph} is the responsibility, I_L photo current produced in the device with surface A .

The response of the detector depends largely on the wavelength of light [20-22]. If the wavelength is greater than the break wavelength (λ_c), the photons will not be absorbed and photo streams will not be created. Otherwise, if the wavelength is less than λ_c , the photon energy will be higher than the energy of the circuit and the difference will be released in the form of heat.

For collecting pairs of electron-cavity, an electric field is required. This can be generated using a preload on an undoped semiconductor or using a p-n diodes. In this way, a photo conductor detector is obtained for which the pairs of electron cavities change the conductivity of the semiconductor material.

5. Neodymium doped calcium tungstate single crystal, $\text{CaWO}_4:\text{Nd}^{3+}$ as optical materials: properties and crystal growth

A crystalline oxide materials play an important role in the development of lasers. Drawn crystals were initially applied in the production of semiconductors. In recent years, however, a very rapid progress in this area lies in the growth of refractory oxide and salt crystals are dielectrics. Of a large number of scientists has been largely stimulated by the need for a base material for lasers, and the need for auxiliary materials for laser and modulator harmonic generation.

The first material of this type which has been widely studied as a base material for the laser was a calcium tungstate (scheelite) CaWO_4 . Nassau and Van Uiteret the first 1960 show growth scheelite structure type obtained by drawing. Nassau and co-authors in a series of reports show growing conditions CaWO_4 adding rare earth. The first objective of this study was the preparation of such a solid laser crystal, which is the active ion Nd^{3+} . Describes a growth of the crystal by the addition of CaWO_4 with Nd^{3+} as an active ion. The described defects are formed during crystal growth, as well as the results obtained by a variety of methods for characterization.

"In recent years, molybdates and tungstates belonging to the scheelite-type tetragonal structure [23-28] have been extensively investigated by the scientific community for technological applications in acousto-optic filters [28], solid state lasers [29, 30], light-emitting diodes [31], photocatalysts [32, 33], phosphors [34-36], scintillators [37-39], microwave dielectrics [40, 41], and cryogenic scintillation detectors [42, 43]. Among these materials, the pure or rare earth-doped calcium tungstate (CaWO_4) has been studied because of its photoluminescence (PL) emissions in the visible wavelength regions of the electromagnetic spectrum [44-48]." [48]

Tungsten and its alloys because of their unique characteristic have wide application in many sectors of the industrial production [23, 49]. "Tungstates are natural minerals. Furthermore, they can be made synthetically. The mineral name associated with these materials is CaWO_4 . The name used to describe the common crystal structure of these materials is scheelite [50]. The scheelite- ABO_4 ($A=\text{Ca}$ and $B=\text{W}$) crystal structure (Figure 12) [23] is characterized by the tetragonal space group $I4_1/a$ (n° 88). The B atoms are surrounded by four O atoms in an approximately tetrahedral symmetry configuration, and the A atoms are surrounded by eight O atoms in an approximately octahedral symmetry. Many material properties can be associated to the existence of these $[\text{BO}_4]$ (Figure 12b) and $[\text{AO}_8]$ (Figure 12a) approximate polyhedrons into crystalline structure. The B cation tetrahedra (with W) behave as rigid structural elements with no observed cation oxygen compression [51]. On the other hand, compression of the eight-coordinated $A=\text{Ca}$ polyhedron, is more favorable parallel to c than perpendicular to c ." [50]

"Various techniques such as the Czochralski technique, flux method, and solid-state reactions have been used to synthesize single crystals, whiskers, and powder of $\text{CaWO}_4:\text{Nd}^{3+}$ [23, 52, 53]. Some attempts were made on the preparation of single crystal films, but these experiments had limited success because of the high vaporization pressure of WO_3 and obtained films did not have a uniform structure." [52] The growth of single crystals from melt by the Czochralski method has a number of advantages, such as the absence of contact between the crystal and the crucible walls, that essentially reduces stresses in the crystals; the possibility to control the crystal growth visually and the processes which occur at crystal-melt interface, relative simplicity of its technical realization. Moreover, the method allows to grow large-size and sufficiently perfect high-melting oxide crystals, to control the character of the melt convection and as consequence to choose the most optimal conditions for the growth of optically homogeneous crystals. Possibilities of the method are able to provide the obtaining of crystals of different shape.

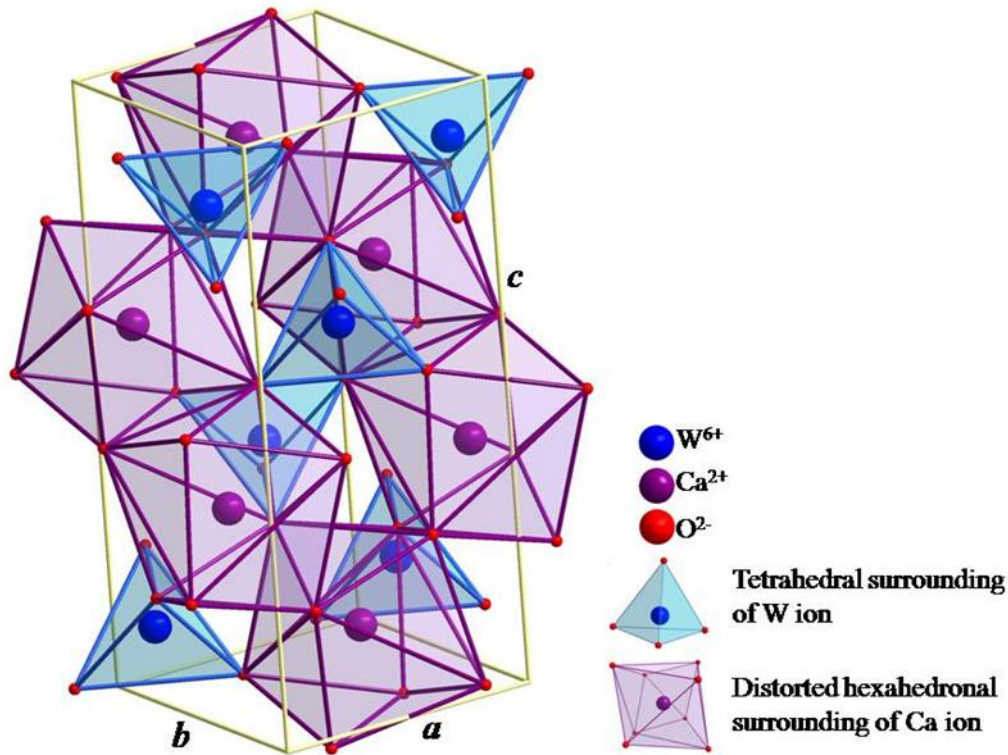


Figure 12. These figure shows unit cell of $\text{CaWO}_4:\text{Nd}^{3+}$ single crystal [23].

6. Methods of single crystal growth

Methods of crystal growth

Methods that are commonly used for the preparation of the crystals are as follows: growth of the crystal from the melt, the growth of a vapor-phase growth from the saturated solution [54-61]. The method which is the most used today is the growth of crystals from the melt.

Bridgman method

This method is developed based on work Tammann, Obreimov and Schubnikov [60-63]. The Bridgman method of crystal growth is perhaps the simplest melt-based technique (Figure 13). The primary advantage of the Bridgman method is its simplicity and ease of implementation. For this method of crystal growth apparatus is used which consists of a vertical furnace, which is the means of a plate divided into two chambers: an upper

and a lower. The upper chamber furnace is heated to a temperature which is 50-80 °C to above the melting point of the material to be crystallized, and the lower furnace chamber is situated at a temperature that is 50-80 °C to lower than the melting point of the material. Also, use the crucible with conical bottom to facilitate crystallization.

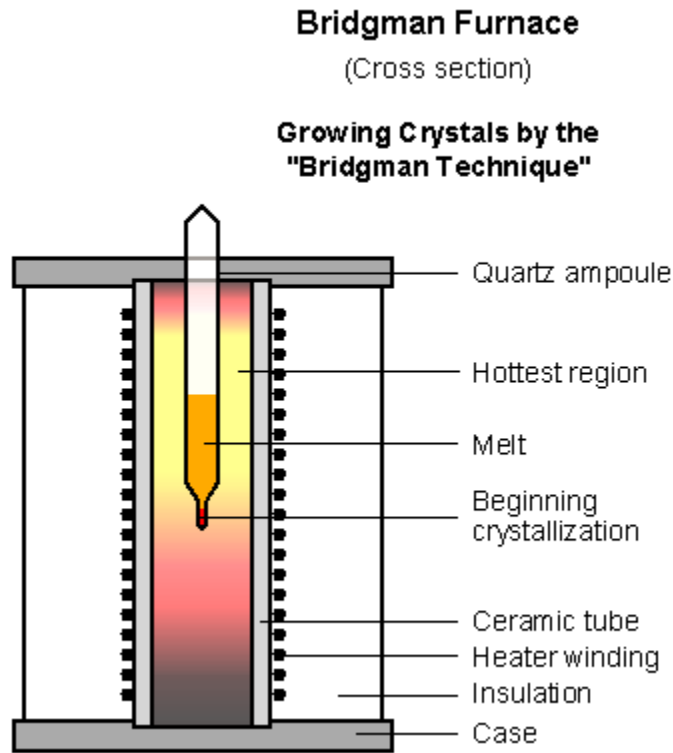


Figure 13. Scheme devices for crystal growth by the Bridgman method.

The device has the following parts: 1. thermal insulations; 2. pipe; 3. thermocouple; 4. furnace threaded; 5. panel - a protector against radiation; 6 ceramic or metal holder. The method consists in the fact that the crucible with a batch has been placed on the holder in the upper furnace chamber and is performed to gradually warm up to the melting of the batch.

For the realization of the process of growth, the crucible with molten by means of the holder descends, in the above, warm, to the lower, cold, furnace chamber. In the tip of the cone, which first comes in a cold area, the call is created, which begins the crystallization. Crystallized, island, the cone gradually increases. When the entire melt crystallized, cooling is carried out, crucible descends gradually, and reduces the power supply.

The optimal conditions for crystal growth were: apparatus, which is to be thermally and mechanically stable, as crystal growth rate, which should be in the interval of 1-10 mm

h^{-1} . At low speeds the growth of high-quality single crystal was obtained, while at high speeds the growth of high-quality polycrystal is obtained.

Verneuil method

Method Verneuil [64-66] represents the melting process in flames (Figure 14). The funnel-shaped container is a tank whose bottom is perforated. The tank is filled with powder (e.g. Al_2O_3), and above the funnel is a hammer (hammer mechanism), and below the funnel of the burner. Oxygen is introduced through the pipe to the hopper, and the hydrogen is fed directly into the torch. On the bottom side, into the chamber is introduced a carrier of refractory material, which can be moved in the vertical direction. Hammer is put in motion after the ignition flame. Also, the hammer strikes on the tank at regular intervals, so that the powder passes through the perforated bottom, and a stream of oxygen affected, passing through the hopper and the burner, and finally dropped on a carrier. By means of a flame, which is directed towards the carrier, the powder is melted and forms a small ball of growing. The rest of the powder falling on the carrier, is also melting. During the process, the carrier is cooled, and it allows the growth of crystals. Device for crystal growth according to the method Verneja include: 1. hammer; 2. a reservoir; 3. the burner; 4. the chamber of refractory material; 5. growing a crystal; 6. a carrier of refractory materials; 7. momentum to set the size of the growing crystal.

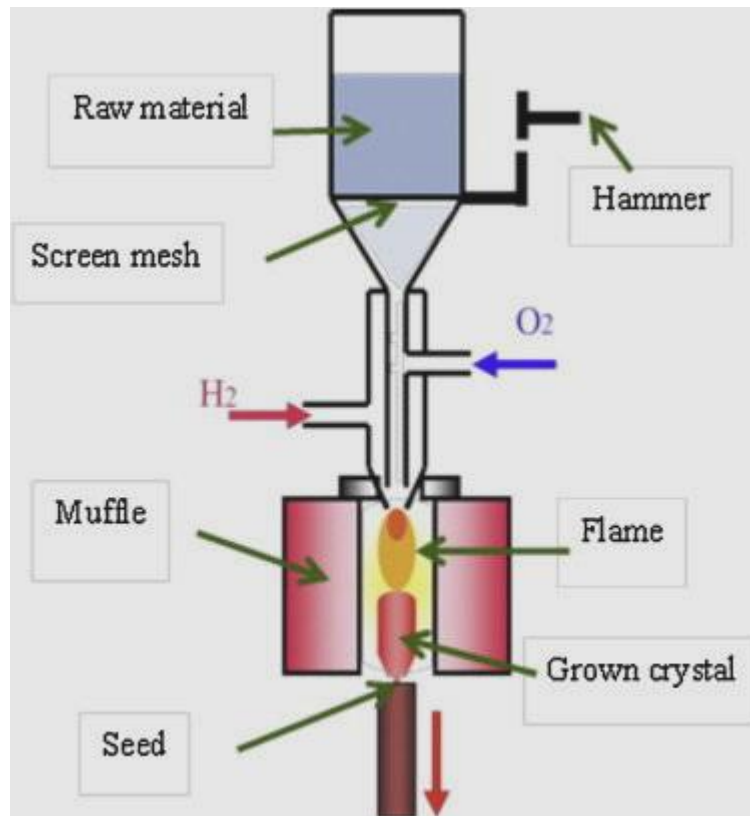


Figure 14. Scheme devices for crystal growth according to the method Verneuil.

The zone melting method

Today this technique [67, 68] is used mainly for treatment of a large number of materials. It is also used to obtain single crystals. Figure 15 shows the simplest layout apparatus. Device for crystal growth by the method of the zone melting is composed of: 1 heater, 2 primers, 3 melt, 4. polycrystalline rod.

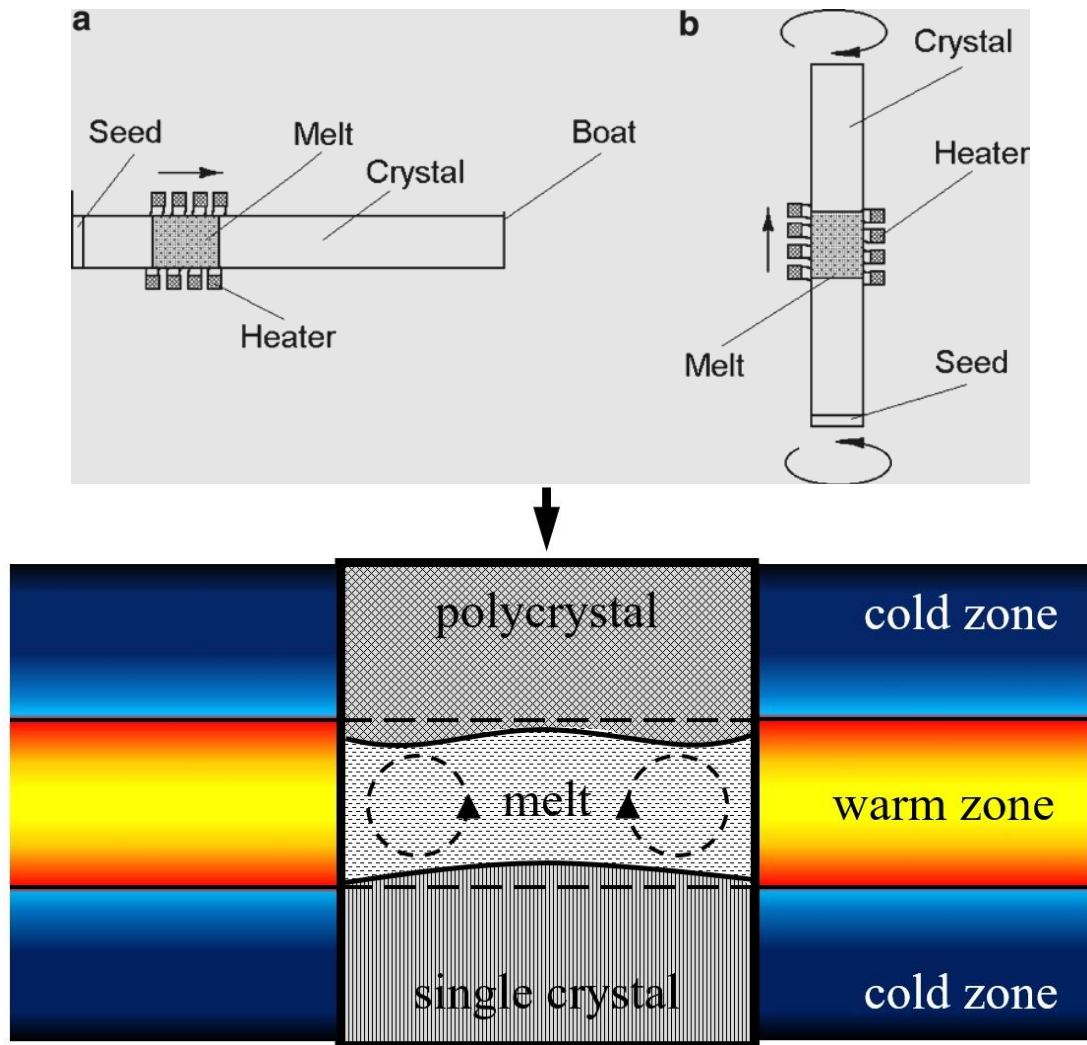


Figure 15. Schematic representation of the device for crystal growth method zonal melting.

The method consists in the fact that the call is placed on one end of the tray, in which the polycrystalline. A small area of material melts, then moving slowly toward the calls until it is completely moisten, then the direction of the opposite zone. This polycrystalline melt, and the melted material crystallizes the calls, and it grows to form a single crystal. Optimal growing conditions are minimal mechanical and thermal changes and the slow rate of growth.

Floating zone method

This method is used to obtain crystals [69, 70], which is necessary to avoid the use of crucible (Figure 16). The procedure for obtaining single crystals consists in the fact that

the seeds, and polycrystal fastened vertically to the bottom and top of this unit. Seed and polycrystalline approaching, until their tops do not touch, and then in the area of contact, performs melt. The tops of seed and polycrystals melt at a time, and give the melted zone.

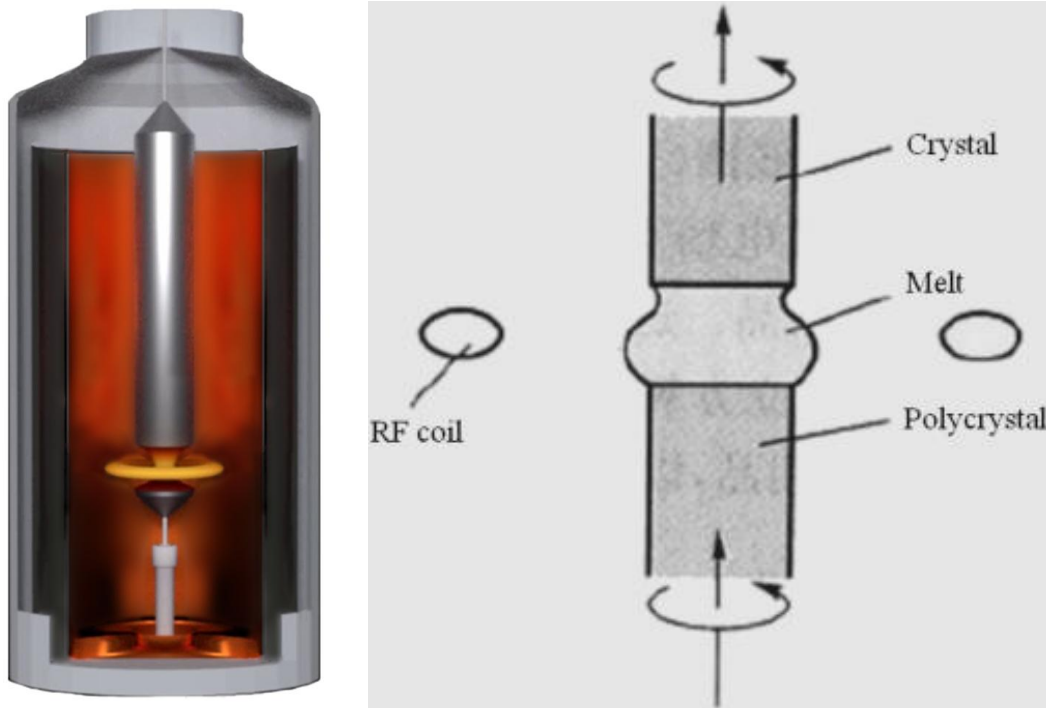


Figure 16. Scheme devices for crystal growth by floating zone technique.

The direction of movement is obtained by zone vertically upwards. Thus, the polycrystal melt, and the melted material was crystallized in the seed, such seed grow and become a single crystal. Seed and polycrystal may stand motionless, opposite one another, are fastened by means of the jaw, or to rotate in opposite directions, in order to achieve good mixing and reduction of the temperature gradient.

Growth of the crystal from the melt according to the Czochralski method

Crystal growth, or by the Czochralski method (1918) is a popular method for the growth of the crystal, because larger crystals are obtained in a relatively short period of time (Figure 17) [71]. The material, which is growing, it melts in the crucible. Seed is then immersed into the melt, and slowly pulls up. At the same time, seed rotates to achieve thermal symmetry, but also at the same time perform the mixing of the melt. Important requirements for proper growth of the crystal by this method is constancy feed speed and the speed of rotation, as well as the proper regulation of the temperature of the melt.

Diameter of crystals depends on the melt temperature and the speed of the draw. The maximum size of the crystals, which can in this way be obtained, depending on the volume of melt, crucible size, strength of crystals in a place where it is the smallest diameter. The boundary between the two phases, seed-melt should be handled. If this condition is met, the crystal reduces the mechanical stress, which occurs during cooling. Deformation is removed, while the crystal in a plastic state. It is also important that the crucible is heated constantly. If not, the crystal will grow laterally, to the coldest part, giving a cross section that is not circular. Also, the surface of the melt must be kept clean, because dirt act as nucleation centers.

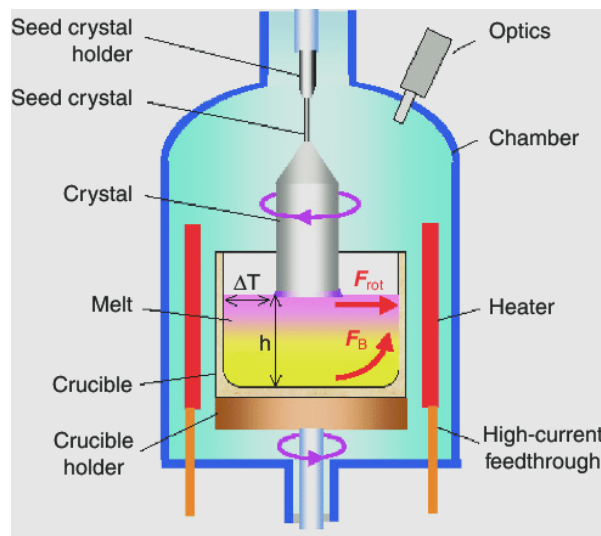


Figure 17. Scheme devices for crystal growth by Czocharalski method.

Conditions for obtaining high-quality single crystals

In inappropriate conditions of crystal growth (the speed of rotation of the seed, the speed for feeding, a temperature gradient) can occur strain in the crystals, a non-homogeneous refractive index, to the formation of cracks, inclusions of gas bubbles, the concentration of impurities caused by inhomogeneity of the material [71]. Such crystals exhibit anisotropy in the optical density, and as such are practically useless for most optical devices. One of the basic requirements to overcome the result of inappropriate growth conditions is to provide a flat-crystal interface (boundary surface of the solid-melt) during the crystal growth process. There are many factors affecting it. But the most significant are the speed of crystal growth, the crystal diameter, the diameter of the vessel, the rotation speed, close to the bottom of the vessel, axial and radial temperature gradient. But it is very

difficult, that all these growth parameters are included in mathematical equations, from beginning to end the process of crystal growth.

7. Nano single crystals and quantum dots

Reduction of system sizes up to a line of 100 nm and less causes quantum phenomena that change the electronic zonal structure, that is, electrical and optical properties of (charge is limited within a very thin layer, in one or more spatial dimension system is treated quantitatively mechanically).

In semiconductors of the discrete value, energies are attained when the thickness of the observed the layer corresponds to de Broglie wavelength [72]:

$$\lambda = h / (3kT_m^*)^{1/2} \quad (5)$$

From expression (5) it can be concluded that the wavelength depends on the effective mass of the electron in semiconductor, T_m^* and temperature, where k is Boltzman's constant.

In bulk single crystals, there is no quantum-confinement, the charge is moving freely, therefore to form, charge carrier gas. As dimensio goes to less values charge gas occurs in two dimensions, so they are called the 2D structures (grapheme, mxene), 1D structure (Quantum wires) and quantum dots of 0D-structure. Because, one of charge carriers are vacancies in quantum dots the energy levels are expressed by discrete states analogous to the energy states in the atom, so these structures are called artificial atoms.

QD`s are semiconductor crystal structure who have possibility to absorb white light, and then reemit in particular wave length [73]. This wave length could be modified by size and material of QD`s, and can vary from blue to near infra red. So, the QD with diameter of 2 nm emitted green light, while the QD with diameter of 5 nm emitted red light. By changing the size and shape of QDs, their optoelectronic properties can be successfully tailored [74-77]. Due to his ability and their photostability, they are being used for light emitting devices (LED), biosensing, fluorescent labeling, laser technology and solar cells [78-86]. Photostability of QDs can be increased with passivation of the surface, which is usually achieved by coating, i.e. by creating core-shell structure [77]. This method is well-known and proven to be successful on the example of CdSe QDs

coated with ZnS [78]. Luminescence and photostability are increased because the energy band gap of CdSe falls inside ZnS band gap, thus confining the photo-generated electrons and holes in CdSe [79].

8. Optical active composite materials with polymer matrix

The development of modern composite materials spread to a considerable extent based on the possibilities designing their structure and properties, different methods of synthesis and fabrication. Different set of properties of composite material is achieved not only by the combination of one-material in macroscopic, but also in microscopic and nano level. In search for new composite materials, new combinations between the basic ones (metals, ceramics and polymers) are constantly emerging. Synthesis of materials from simpler to more complex materials are carried out by appropriate specific methods of manufacturing, changing the structure from nano to macro dimension to achieve optimum desired properties. This approach enables the development of structurally very complex multifunctional materials, in which the design of the structure extends from nano (nanocomposite), to the macro level (macro-composite materials).

The basic concept of optically active composites with polymer matrix is that some optical medium (mostly inorganic) is embedded in transparent polymer. The shape of the functional medium could be the sphere (particles), the cylinder (fibers), the correct plate or rods (mica, clay, particles of glass). The size, shape, size distribution and volume content define the microstructure, and determine the type and extent of the interaction between filler and the matrix. The filler content is represented by a volume or mass fraction, and it is certainly the most important parameter, which, in addition to the properties of the constituents, determines the properties of the composite. It represents easily controlled variable, through which the properties of the composite change. The distribution of the reinforcement content is a measure of the homogeneity and uniformity of the system. Particularly in the case of nano and micro particles due to poor surface treatment conditions of the particles, there may be aggregation of especially nano and meso particles, which brings in sufficient unevenness, forming an aggregate skeleton in the framework of weaker links. The non uniformity of the composite should be avoided because it reduces the values of the properties of the system that is determined by the weakest bond in the

material. During processing of these composites should be pay attention that some processing parameters can affect optical activity of functional filler. The scattering problem and the dielectric properties are two important factors that should be discussed about optical active composites. There are a wide spectrum of research of influence of incorporation of 3D [87], 2D [88-92], 1D [93, 94] and 0D [95], structures in polymer matrix.

Since the wavelength of light that QDs emit depends on nanocrystal's size due to quantum confinement effect, one can control the desired emitted color by tuning the size of CdSe/ZnS. This phenomenon and various effects related to it are already being thoroughly investigated [96-99]. Furthermore, optical degradation of CdSe/ZnS QDs upon gamma-ray irradiation, along with blue shift (blueing), photo-oxidation and photo-bleaching are known research topics covered so far [100-102].

These unique optical and electronic properties of core-shell QDs have opened the door for their use in polymer nanocomposites meant for sensing, membranes, photovoltaic cells, bio-labeling and optical amplification [103, 104]. Poly(methyl methacrylate) (PMMA) (Figure 18) is widely used as a material for optical purposes, due to its excellent optical, thermal, mechanical and chemical properties [105-110]. Therefore, PMMA has already been employed as a matrix material for nanocomposites with CdSe/ZnS QDs. The effects of different solvents and PMMA on QDs quantum efficiency have already been presented, and it has been established that the choice of a solvent greatly influences quantum efficiency of QDs [111]. According to previous researches, it is assumed that QDs can be uniformly dispersed within the polymer in the form of nanofibers. Agglomeration of QDs could be prevented, with the perpetuation of their optical properties, by using electrospinning technique for the processing of nanocomposites [112]. It is a well-established, simple method for the production of fine, continuous nanofibers [113-115].

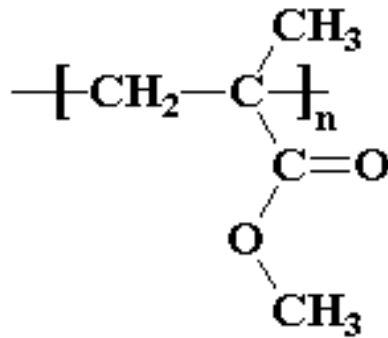


Figure 18. Structural formula of polymethylmethacrylate (PMMA).

8.1. Influence of interface modification on the optical properties of composites

In processing of composite materials the modification of matrix-particle interface and established bonding is responsible for behavior of composite, like thermal, optical or mechanical. So, in the many researches the modification of particle surface is performed with the aim of improving those properties. The modification could be chemical or physical treatment. The use of silane is common way of chemical treatment [116]. Coupling agent molecule could be adsorbed on the surface of nanoparticles, and promote the better deagglomeration in polymer nanocomposite because of steric hindrance [117]. In this work the modification of QD`s was performed by 3-mercaptopropyltrimethoxy silane (MPTMS) (Figure 19). This choice should be useful for optical properties of nanocomposite, because of weak dipole-dipole bonding established between modified QD`s and PMMA matix." [118].

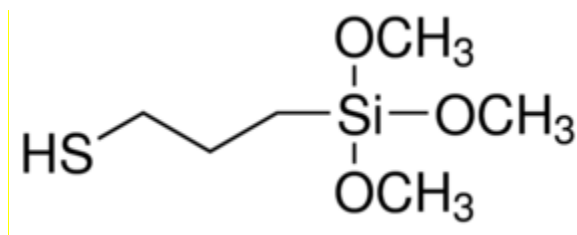


Figure 19. Structural formula of 3-mercaptopropyltrimethoxysilane (MPTMS).

9. Methods of characterization of optical active materials and composites

Various experimental techniques have been utilized to characterize single crystal, polymer nanocomposites and the samples of pure PMMA, and composites with unmodified and silane modified QD`s CdSe/ZnS. Different types of characterization techniques are available to study the physical and chemical properties of the crystal. Some of them are:

X-ray diffraction (XRD)

X-ray powder diffraction (XRD) [119] is a rapid analytical technique primarily used for phase identification of a crystalline material and can provide information on unit cell dimensions (Figure 20). Collection of XRD data by single crystal X-ray diffraction analysis and powder X- ray diffraction analysis to confirm the structure of the grown crystals. Bragg first suggested the use of X-rays as a tool for investigating the structure of crystals. Bragg considered X-ray diffraction from a crystal as a problem of reflection from atomic planes.

The peaks in a X-ray diffraction pattern are directly related to the atomic distances given by Bragg's law: $2d \sin\theta = n \lambda$ [120]. Where d is the inter-plane distance, θ is the scattering angle, n is an integer representing the order of the diffraction peak and λ the wavelength of the X-ray.

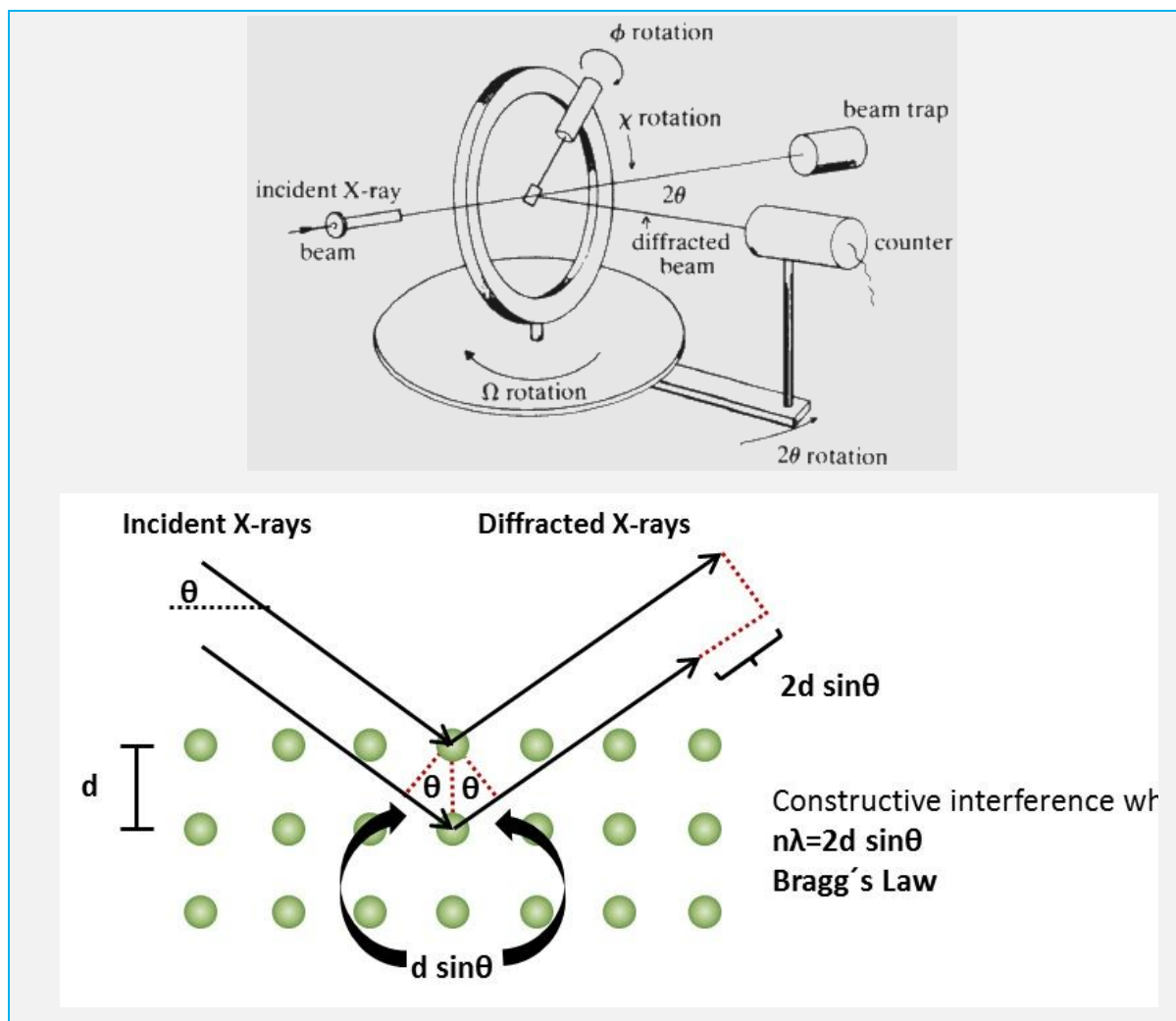


Figure 20. Schematic diagram of XRD according Bragg's law.

Fourier transform infrared spectroscopy

Fourier transform infrared spectroscopy (FTIR) (Figure 21) is a powerful tool for identifying types of chemical bonds in a molecule by producing an Infrared absorption spectrum that like a molecular “finger print” Fourier transform infrared spectroscopy (FTIR) is an analytical technique used to identify organic (and in some cases inorganic) materials [121]. This technique measures the absorption of various infrared light wave lengths by the material of interest. These infrared absorption bands identify specific molecular component and structures.

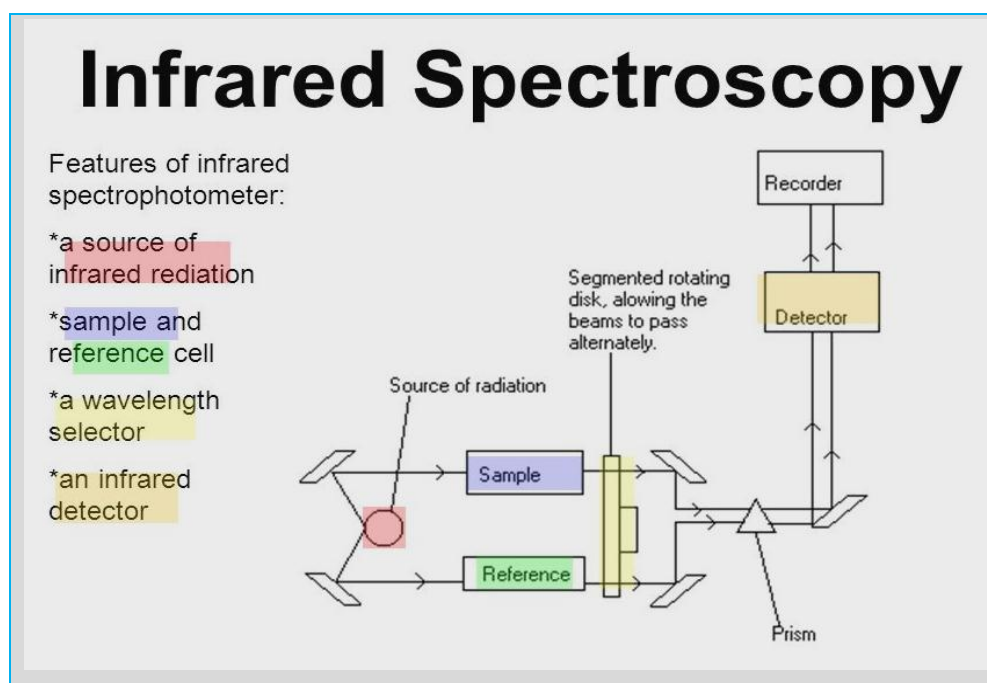
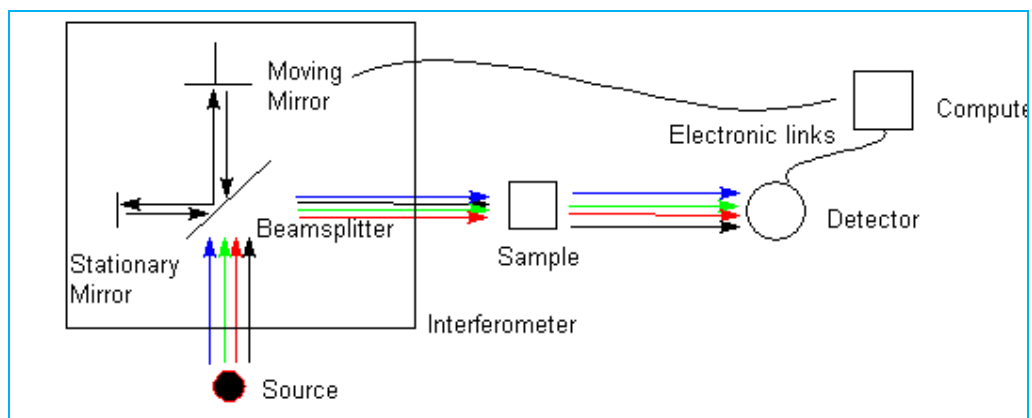


Figure 21. Schematic of FT-IR imaging set-up.

Raman spectroscopy

When light is scattered from a molecule or crystal, most photons are elastically scattered [122]. The scattered photons have the same energy (frequency) and, therefore, wavelength, as the incident photons. Raman scattering can occur with a change in vibration, rotational or electronic energy of a molecule. If the scattering is elastic, the process is called Rayleigh scattering. If it's not elastic, the process is called Raman

scattering [122]. In quantum mechanics the scattering is described as an excitation to a virtual state lower in energy than a real electronic transition with nearly coincident de-excitation and a change in vibration energy. Figure 22 shows Raman experiments.

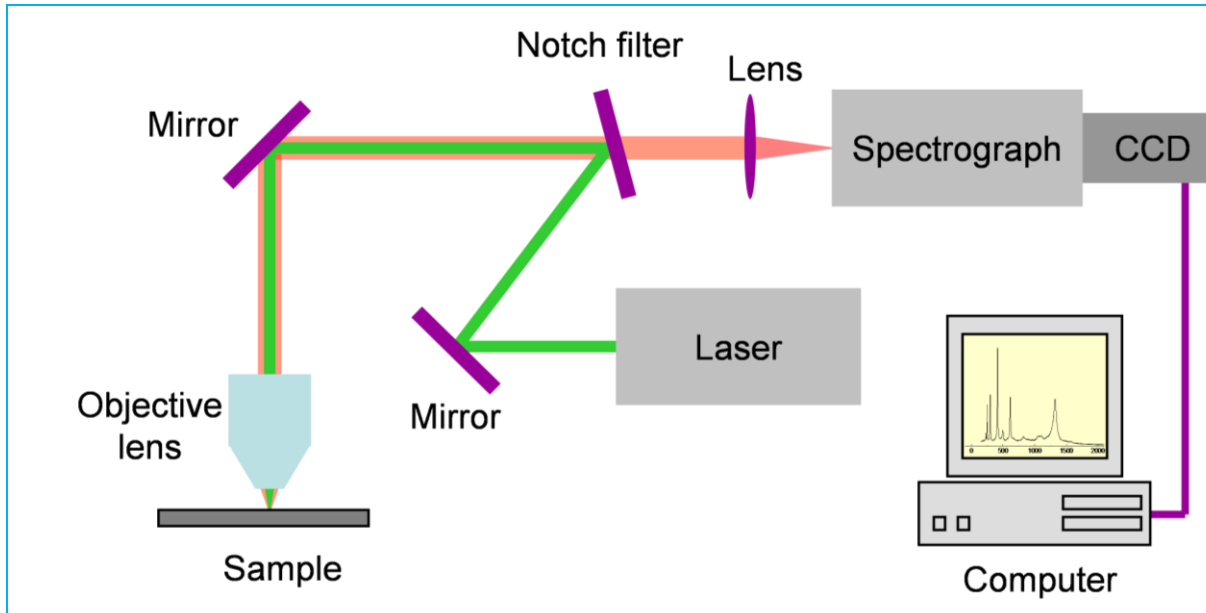


Figure 22. Schematic of Raman experiments.

Scanning electron microscopy (SEM)

Scanning electron microscope (SEM) is one of the common methods for imaging the microstructure and morphology of the materials. In SEM, an electron beam with low energy is radiated to the material and scans the surface of the sample. Several different interactions occur as the beam reaches and enters the material, which lead to the emission of photons and electrons from or near the sample surface. Optical microscopy has the limit of resolution of $\sim 2,000 \text{ \AA}$ by enlarging the visual angle through optical lens. Light microscopy has been, and continues to be, of great importance to scientific research. Since the discovery that electrons can be deflected by the magnetic field in numerous experiments in the 1890s [123], electron microscopy has been developed by replacing the light source with highenergy electron beam (Figure 23). In this section, we will, for a split second, go over the theoretical basics of scanning electron microscopy including the resolution limitation, electron beam interactions with specimens, and signal generation.

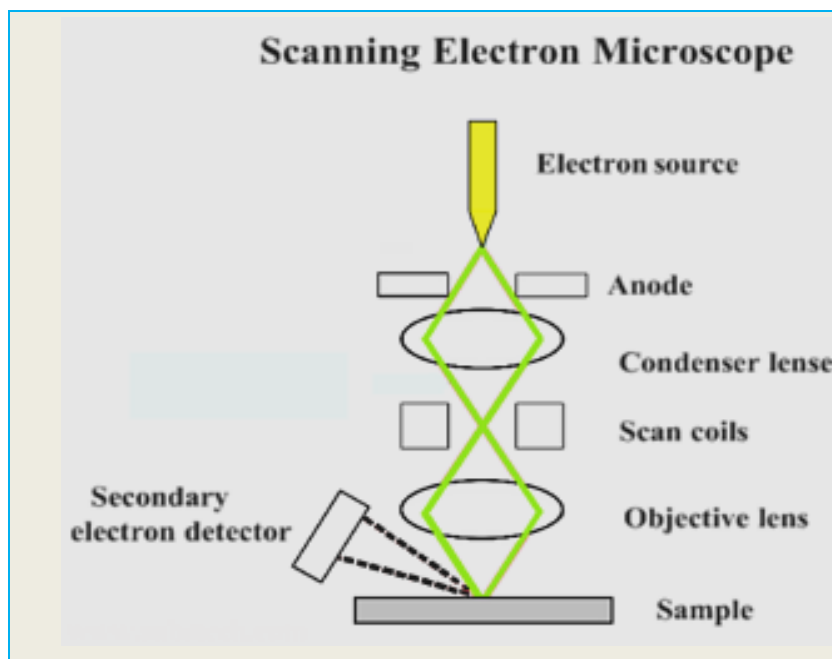


Figure 23. Schematic representation of the basic SEM components [122].

Time resolved laser induced fluorescence measurements

"Time resolved laser induced fluorescence measurements (TRLIF) is a very sensitive and selective method for ultra trace analysis in the different fields of nuclear, environmental, and medical science. This technique is based on laser excitation followed by temporal resolution of the fluorescence signal. The other great advantage of TRLIF is its triple resolution: (1) excitation resolution by the proper choice of the laser wavelength (N₂, tripled or quadrupled Nd:YAG, dye, (2) emission fluorescence, which gives characteristic spectra of the fluorescent cation (free or complexed); and (3) fluorescence lifetime, which is characteristic of its environment (complexation, quenching). These two latter types of data provide useful information on the chemical species present in solution as well as for complexation studies. For example, this technique used as a fluorescent titration method' has allowed the determination of complex formation at a low level between trivalent elements [124]. Excitation part of the system is based on nanosecond Nd:YAG laser and Optical Parametric Oscillator (OPO). The fluorescence detection part of our system is based on picoseconds streak camera. The laser is more than powerful enough (365 mJ at 1064 nm, variable OPO output >5 mJ) for LIBS, but somehow slow (the length of fundamental laser harmonic output pulse is about 5 ns) for fluorescence measurements in our present area of interest, namely plants and food products. Fortunately, the pulse

length of tunable OPO output (320-475 nm) is less than 1 ns, so by means of a correct deconvolution procedure it is possible to measure the fluorescence lifetimes in the range as small as a few nanoseconds [125].

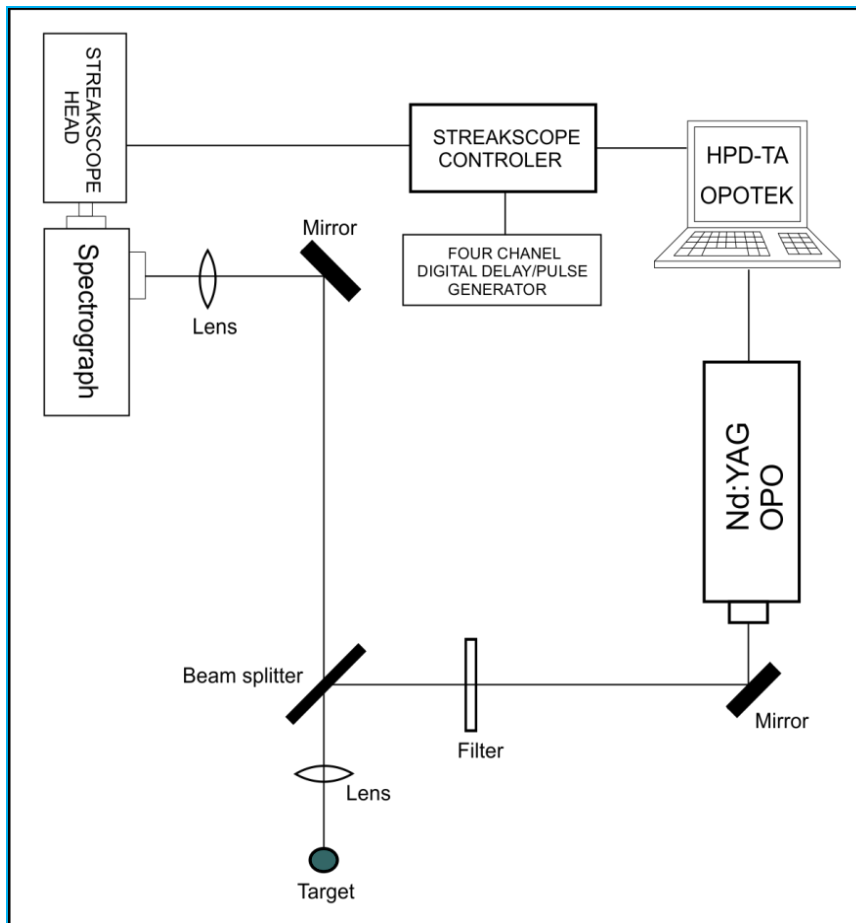


Figure 24. Schematic illustration of experimental setup for TR-LIF spectroscopy [124].

The experimental set-up consists of excitation and detection part (Figure 24). Pulsed excitation was provided by a tunable Nd-YAG laser system (Vibrant model 266 made by Opotek, Inc.). This system incorporates the Optical Parametric Oscillator (OPO) that is pumped by the fourth harmonics of the laser at 266 nm. The laser induced fluorescence in the samples is recorded using streak scope (Hamamatsu model C4334-01) with integrated video streak camera." [125].

The Vickers hardness test method

"The hardness test is a mechanical test for material properties which are used in engineering design, analysis of structures, and materials development. The Vickers hardness test method consists of indenting the test material with a diamond indenter, in the form of a right pyramid with a square base and an angle of 136 degrees between opposite faces subjected to a load of 1 to 100 kgf (Figure 25). The full load is normally applied for 10 to 15 seconds. The two diagonals of the indentation left in the surface of the material after removal of the load are measured using a microscope and their average calculated. The area of the sloping surface of the indentation is calculated. The Vickers hardness is the quotient obtained by dividing the kgf load by the square mm area of indentation." [126]

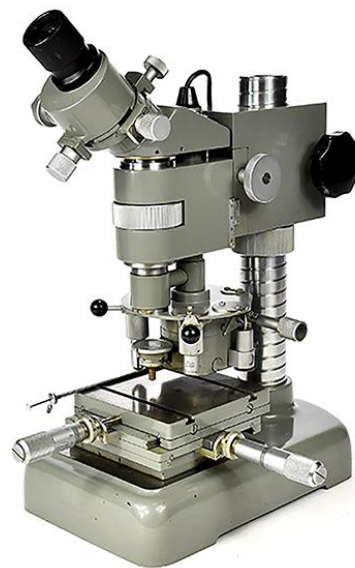
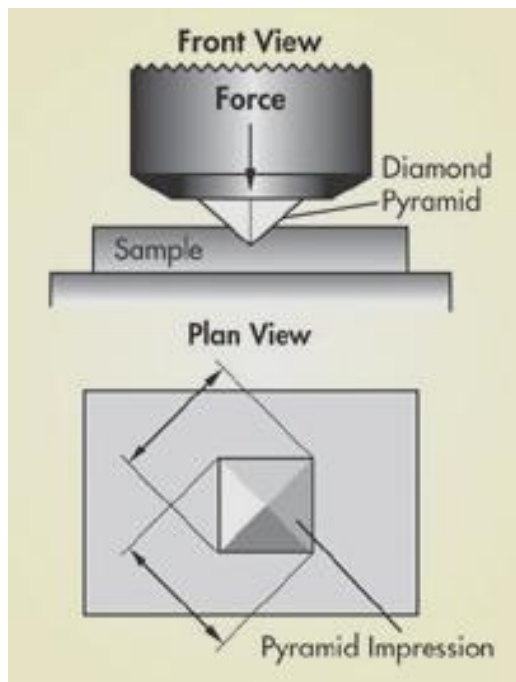


Figure 25. Hardness test equipment.

Differential scanning calorimetry – DSC

A thermal analysis technique is differential scanning calorimetry – DSC. All measurements by DSC provide quantitative and qualitative information about physical and chemical changes that involve endothermic or exothermic processes, or changes in heat

capacity and shows function of time and temperature. The result of a DSC experiment is a heating or cooling curve. Depending on the phase transformations, DSC scans exhibit endothermic and/or exothermic peaks related to absorption or evolution of heat, respectively. A schematic of a DSC curve is shown in the Figure 26 [127]. This curve can be used to calculate enthalpies of transitions. DSC is the most widely used thermal analysis technique with applicability to polymers and organic chemicals, as well as various inorganic materials.

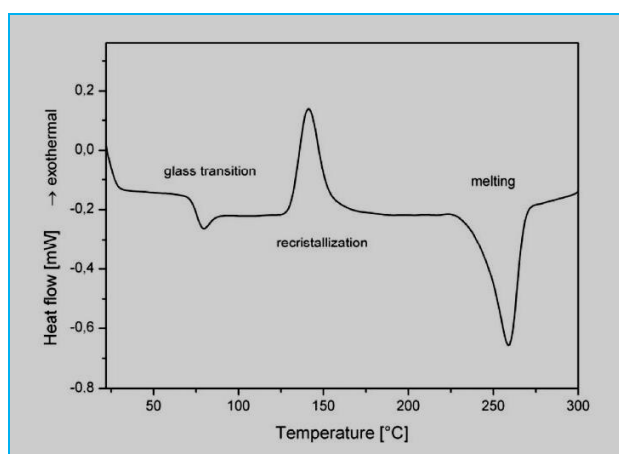


Figure 26. A schematic DSC curve [127].

EXPERIMENTAL PART

10. Experimental procedures

10.1. Crystal growth

Single crystals of $\text{CaWO}_4:\text{Nd}^{3+}$ were grown in an air atmosphere by Czochralski method using a MSR 2 crystal puller as describes in Ref. [23] (Figure 27). The crystals were grown from the starting CaWO_4 and Nd_2O_3 powders in the stoichiometric ratio. The rhodium crucible (4 cm diameter, 4 cm high and 0.2 cm thick) was placed into an alumina vessel surrounded by the ZrO_2 wool isolation.

"The double walls were used for a protection against the high radiation [23, 52]. To decrease the radial temperature gradient in the melt, alumina surrounded the system. The pull rate was in the range $0.54\text{-}12\text{ mm h}^{-1}$, and the best results were obtained for both materials at the pulling rate of 6.7 mm h^{-1} . The crystal rotation rate was evaluated using the hydrodynamics equations, and the critical value was 30 rpm in both cases. The critical diameter of $\text{CaWO}_4:\text{Nd}^{3+}$ crystals were found to be 1 cm. The crucible was not rotated during the growth. After the growth run, the crystal boule was cooled down to room temperature at the rate of about 50 K h^{-1} . In order to reveal strains in the structure, all obtained crystal plates were checked with the polarized light." [52]

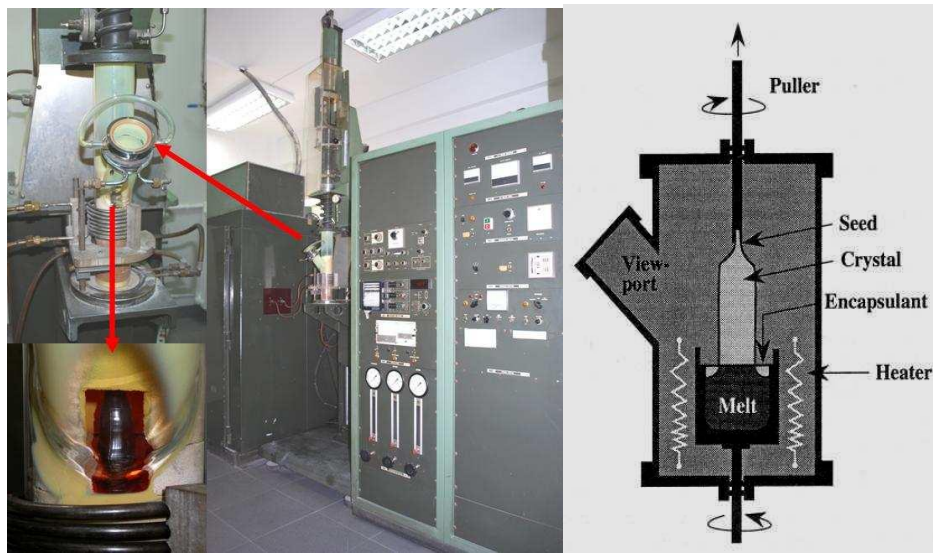


Figure 27. Czochralski crystal growth system.

The observations relating to the dislocation were recorded by observing an etched surface of $\text{CaWO}_4:\text{Nd}^{3+}$ crystal, using a Metaval of Carl Zeiss Java metallographic microscope with magnification of 270x [23, 128]. A selected $\text{CaWO}_4:\text{Nd}^{3+}$ single crystal

was cut into several tiles with the diamond saw. The plates were polished with a diamond paste, which were later used for the characterization of Raman, IR and luminescence spectroscopy. The crystal plane of cleavage of $\text{CaWO}_4:\text{Nd}^{3+}$ crystal is $\langle 001 \rangle$. Thin panels for testing dislocations we obtained by splitting of individual pieces of crystal. A solution for etching the crystals consisted of one part of 40% HF and the two parts of a saturated solution of CrO_3 . The sample was etched for 15 min.

10.2. Preparation of PMMA- $\text{CaWO}_4:\text{Nd}^{3+}$ layered composite

10.2.1. Materials

(3-mercaptopropyl)trimethoxysilane (MPTMS) used as an adhesive promoter and poly(methyl methacrylate) (PMMA, $M_w \sim 350,000$ by GPC) were supplied from Sigma Aldrich. Acetone for dissolving PMMA was purchased from Centrohem ltd.

10.2.2. Film deposition

PMMA was dissolved in acetone in order to obtain 20 wt% solution for layer deposition on $\text{CaWO}_4:\text{Nd}^{3+}$ substrate. A drop coating method was used for PMMA deposition on the $\text{CaWO}_4:\text{Nd}^{3+}$ substrate [129]. In specific, a thin layer on the brass substrate was formed by depositing a single drop of the PMMA solution on its surface. The substrate was then cured in dryer for 12 hours at 60°C . The ultimate thickness of the deposited PMMA was controlled by the weight of a glass cover, which was placed over the drop, so that the obtained film had a thickness value of $30 \pm 3 \mu\text{m}$.

Adhesion promoter – MPTMS was applied by the same method. The substrate was dried for 12 hours at 60°C before PMMA layer deposition. Three samples were tested in this work: i) neat $\text{CaWO}_4:\text{Nd}^{3+}$, ii) $\text{CaWO}_4:\text{Nd}^{3+}/\text{MPTMS}$, iii) $\text{CaWO}_4:\text{Nd}^{3+}/\text{PMMA}$ and iv) $\text{CaWO}_4:\text{Nd}^{3+}/\text{MPTMS}/\text{PMMA}$. This is shown schematically in Figure 28.

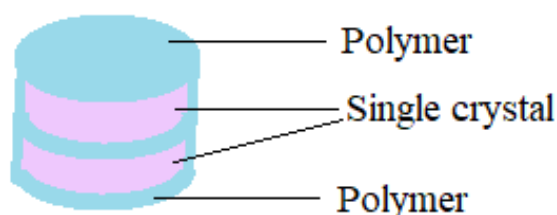


Figure 28. Schematic presentation of layered structures.

10.3. Methods of characterization of single crystal

The Vickers Hardness Number (VHN) was obtained using the following equation:

$$VHN = 2 \cos \frac{22^\circ P}{d^2} = \frac{1.8544P}{d^2},$$

where P (kgf) is the applied load and d (mm) is the length of the indentation diagonal. The micro hardness of the samples was characterized using micro Vickers hardness tester Leitz, Kleinhartepreifer DURIMETI with a load of 4.9 N according to ASTM E384-16 [130].

The structural characteristics were obtained by the XRD powder technique using Philips PW 1050 diffractometer (Figure 29) equipped with a PW 1050 generator, 40kV x 20mA, using Ni filtered Co $K\alpha$ radiation of $\lambda = 1.54178 \text{ \AA}$ at room temperature. Measurements were carried out in the range of $10-90^\circ$ with a scanning step of 0.05° and scanning time 4 s per step. Unit cell parameters were determined by Le Bail's full profile refinement using *FullProf* computing program. The crystallite size and microstrain were determined by using X-Fit software packages which is based on Fundamental Parameter convolution approach [131].



Figure 29. Philips PW1050 diffractometer PW1050.

TriVista 557 (Figure 30) [132] is a triple spectrograph that offers the highest spectral resolution and extreme stray light rejection required for Raman, photoluminescence, and other applications in UV, VIS, and NIR spectral ranges. Its unique optical design (patent pending) allows easy switching between additive and subtractive modes and it can be easily reconfigured to work as a double or a single spectrometer. At the heart of TriVista is industry leading Acton Research Corporation spectrometers. They are known for superb resolution, stray light rejection, excellent imaging and ruggedness. The TriVista can operate from 185 nm to 2.2 μm . Spectral resolution can reach 4 picometers in the VIS spectral range (500 nm). And - extreme stray light rejection allows Raman spectra to be captured as close as 5 wave numbers from the Rayleigh line.



Figure 30. TriVista 557 system [132].

The infrared reflectivity measurements were performed at room temperature with a BOMEM DA-8 Fourier-transform infrared spectrometer (Figure 31) [132]. A hyper beamsplitter and deuterated triglycine sulfate (DTGS) pyroelectric detector were used to cover the wavenumber region from 80 to 650 cm^{-1} . Spectra were collected with 2 cm^{-1} resolution and with 500 interferometer scans added for each spectrum.



Figure 31. A photo of the BOMEM IR spectrometer [23, 132].

Fourier-transform infrared spectroscopy (FTIR) was used for the characterization of the chemical composition of four different modifications of alumina based particles and obtained composite films. Tests were performed using a Nicolet iS10 spectrometer (Thermo Scientific) in the attenuated total reflectance (ATR) mode with a single bounce 45 °F Golden Gate ATR accessory with a diamond crystal, and DTGS detector (Figure 32). FTIR spectra were obtained at 4 cm^{-1} resolution with ATR correction. The FTIR spectrometer was equipped with OMNIC software and recorded the spectra in the wavelength range from $2.5\text{ }\mu\text{m}$ to $20\text{ }\mu\text{m}$ (i.e., $4000\text{-}500\text{ cm}^{-1}$).



Figure 32. Nicolet IS10 FTIR spectrometer.

"The photoluminescence (PL) response is not simple [133]. Photoluminescence emission spectra can be used for investigation of the possible outcomes of photoinduced electrons and holes in a materials, since photoluminescence emission results from the recombination of free charge carriers [134]. The time resolved optical characteristics of samples were analyzed using streak camera and Nd:YAG laser as excitation source (Figure 33). The setup is described in more detail in earlier publication [125]. Shorty, the basic setup of time resolved laser induced fluorescence measurement system consists of Vibrant OPO laser system and Hamamatsu streak camera. The output of the OPO can be continuously tuned over a spectral range from 320 nm to 475 nm. The samples can be also excited by the second harmonic (532 nm) of the Nd-YAG OPO pump laser. After analysis of preliminary results, we decided to use excitation at 532 nm for time resolved analysis of $\text{CaWO}_4:\text{Nd}^{3+}$ near infrared luminescence. This pulsed laser excitation has duration of about 5 ns and repetition rate 10 of Hz. The emission spectra were recorded using a streak scope (Hamamatsu model C4334-01) with integrated video streak camera." [125].

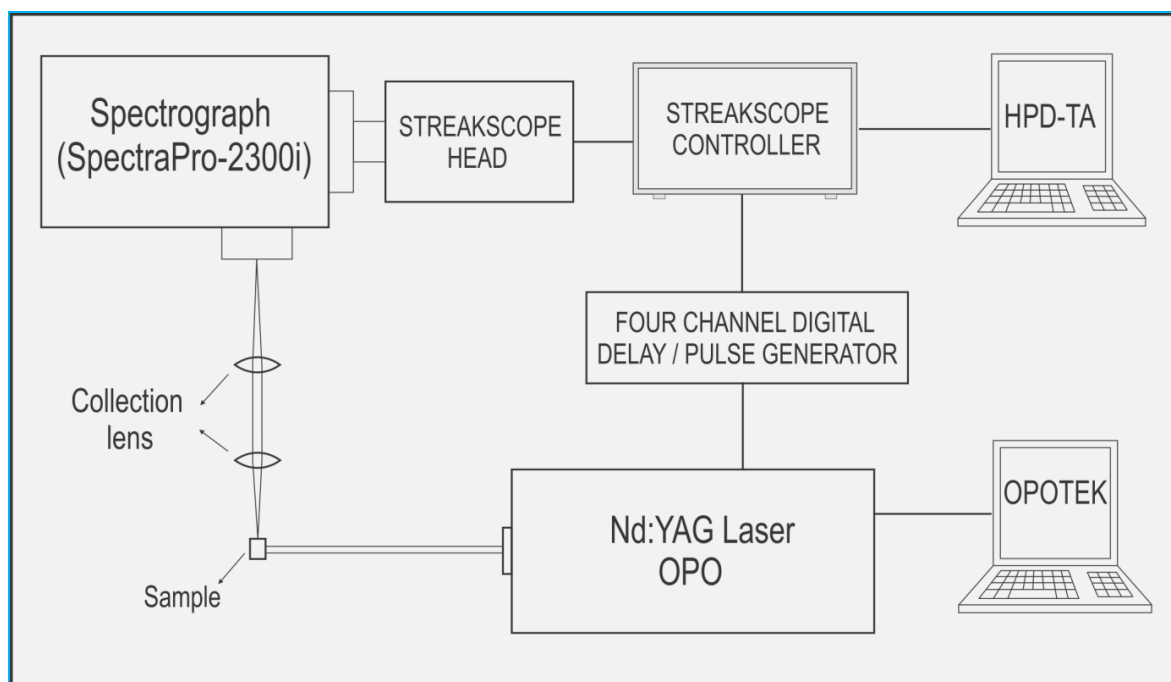


Figure 33. Schematic illustration of experimental setup for time-resolved laser fluorescence (TR-LIF) [23, 125].

10.4. Preparation of PMMACdSe/ZnS quantum dots composites

10.4.1. Materials

Commercially available PMMA (poly(methyl methacrylate)) Acryrex® CM205 (Chi Mei Corp., Korea, $M_w \approx 90400 \text{ g mol}^{-1}$) [135] pellets were used as a matrix material. DMF (dimethylformamide, anhydrous, 99.8 %) supplied by Sigma-Aldrich (United States) was used as organic solvent. The core-shell CdSe/ZnS quantum dots with a mass concentration of 5 mg ml^{-1} in toluene, with emission wavelength 610 nm, were supplied from QD's particles (The Netherlands) and used as received. As a coupling agent 3-mercaptopropyltrimethoxy silane (MPTMS, 95%; Sigma-Aldrich) was used.

A 22 wt% solution of PMMA in DMF was prepared by stirring at room temperature overnight, until homogenization. The CdSe/ZnS QDs/toluene mixture with a predetermined volume (5mg/mL) was placed in an ultrasonic bath and sonicated for 5 minutes to ensure uniform dispersion of the QDs in the mixture and added to the polymer

solution. The concentration of CdSe/ZnS nanoparticles in fibers was 0.06 wt%. The QDs/PMMA solution was then placed and stirred for 60 minutes to ensure dispersion of the QDs in the mixture.

10.4.2. Modification of CdSe/ZnS QD`s surface

"The thiol group grafted samples were prepared as follows [105, 136]: 0.6 ml of MPTMS was mixed with QD`s CdSe/ZnS in 50 ml of dried toluene. This mixture was stirred under reflux condition for 36 h. Then the solid in the mixture was collected by filtration, rinsed with anhydrous ethanol to remove the non reacted MPTMS and dried at 80 °C for 24 h." [118].

10.4.3. Preparation of PMMA-CdSe/ZnS films

"Solution of PMMA in DMF (22 %wt) was prepared by mixing at room temperature overnight, until homogenization. The QD`s CdSe/ZnS was added in polymer solution in concentration of CdSe/ZnS nanoparticles in polymer of 0.06 % w. The QD`s CdSe/ZnS /PMMA solution was then placed and stirred for 60 minutes to ensure dispersion of the QD`s in the mixture. The solution was cast into Petri dish and allowed to dry for 24 h at room temperature and then 24 h more at 60 °C in an oven, to eliminate residual solvent. Two series with unmodified and modified QD`s were processed." [118].

10.4.4. Preparation of PMMA-CdSe/ZnS nanofibers

PMMA-QDs solution was prepared as was described in previous chapter, and one part was used to obtain fibers, which were fabricated by the electrospinning process.

The electrospinning was performed on Electrospinner CH-01, Linari Engineering, Italy, with the flow rate of 1 ml/h, 14 cm distance from collector and voltage power of 28 kV. The resulting fibers were allowed to dry for 48 hours at room temperature and then 6 hours at 50 °C in an oven. Both fibers and film were further dried for 1 hour at 50 °C in a vacuum dryer.

10.3.4. Characterization of samples

"Fourier transform infrared (FTIR) transmission-KBr disk spectroscopy (Hartmann&Braun, MB-series) was performed with aim to approve the chemical bonding of MPTMS silane on the surface of QD`s." [118].

Thermal analysis of composites was performed on a device for differential scanning calorimetry (DSC) in the temperature range from 24 °C to 160 °C (SDT Q600, TA instruments).

An insight of dispersion and deagglomeration of nanoparticles was performed using FESEM (TESCAN MIRA 3) with fracture surfaces sputtered with gold (Figure 34).



Figure 34. FESEM (TESCAN MIRA 3).

"The Raman scattering measurements of CdSe/ZnS QD`s and PMMA-QD`s film were performed using micro-Raman spectrometer TriVista 557 equipped with 100x objectives and a cooled CCD camera. The spectra have been excited by a 532 nm line of Ar⁺ - ion laser with an output power of 40 mW. Spectral resolution of the spectrometer was about 0.34 cm⁻¹." [118].

The time-resolved laser induced fluorescence measurement system uses Nd-YAG Vibrant OPO (Optical Parametric Oscillator) laser as an excitation source. The OPO output is continuously tunable in the range between 320 nm and 475 nm. The emission

spectra and luminescence lifetimes of samples were analyzed by using the Hamamatsu streak camera system. The camera is equipped with the spectrograph.

Thermal analysis of composites was performed on a device for differential scanning calorimetry (DSC) in the temperature range from 24 °C to 160 °C (SDT Q600, TA instruments). The nanoindentation experiments on the powder of pure PMMA and prepared PMMA-CdSe/ZnS films were performed using a Triboscope T950 Nanomechanical Testing System (Hysitron, Minneapolis, MN) equipped with a Berkovich indenter type with in situ imaging mode. A peak load of 2 mN was applied for all samples with the load-hold-unload of 25s for each segment. Nine indentation measurements were performed for each sample and the mean values and standard deviations are reported. The reduced elastic modulus E_r and hardness H results were obtained by the Oliver and Pharr method [137].

RESULTS AND DISCUSSION

11. Results and discussion

11.1. Single crystal

$\text{CaWO}_4:\text{Nd}^{3+}$ single crystals were grown by the Czochralski technique in air. The best results were obtained with a crystal growth rate of 6.7 mm h^{-1} . The critical rotation rate was 30 rpm. The obtained single crystal was about 70 mm in length and 10 mm in diameter (Figure 35) [23].



Figure 35. Photographs of $\text{CaWO}_4:\text{Nd}^{3+}$ single crystal [23].

From the Figure 36a), the dislocations of can be observed [23]. Number of dislocations in $\text{CaWO}_4:\text{Nd}^{3+}$ crystal was 638 per cm^2 . Before individual dislocations can be observed little corner of the border. One of them is shown in Figure 36b).

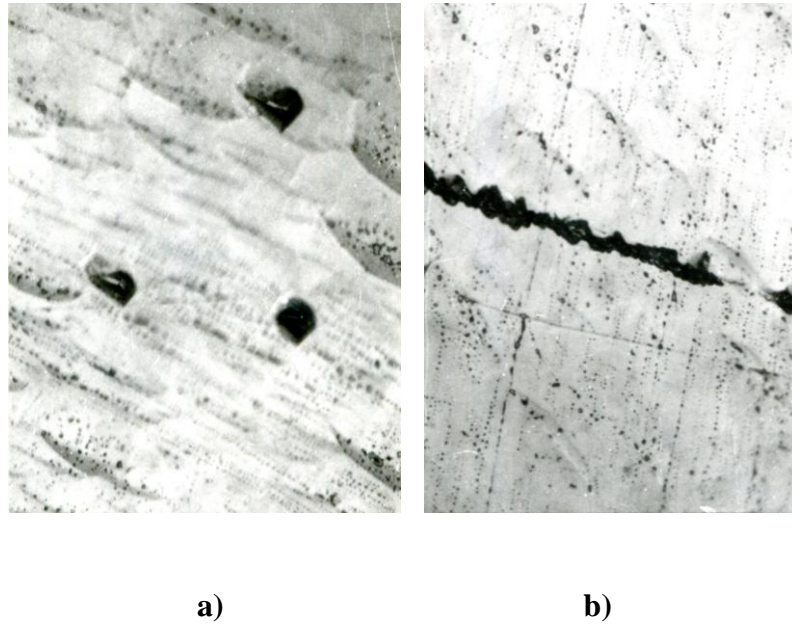


Figure 36. The microscopic image of the surface $\text{CaWO}_4:\text{Nd}^{3+}$ crystal plate in the direction $\langle 001 \rangle$ after etching 15 min: a) appearance of individual dislocations and b) look of low-angle boundaries on the surface. Magnification of 270x [23].

Hardness of the samples was $\text{HV} = 1.156 \text{ GPa}$.

Structure of synthesized $\text{CaWO}_4:\text{Nd}^{3+}$ powdered sample was identified by XRD pattern as shown in Figure 37. The diffractogram confirms that sample is monophased, and that it crystallized in scheelite type of structure in 88. space group, $I4_1/a$. All of the observed diffraction peaks are indexed according to this space group. In this structural type, Ca ions occupy $4b$ Wyckoff positions $[[0, 1/4, 5/8]]$ with local symmetry $\bar{4}$, while W ions occupy $4a$ Wyckoff positions $[[0, 1/4, 1/8]]$ with the same local symmetry. W ions are in tetrahedral surrounding of O ions (coordination number 4), while Ca ions are in distorted hexahedral surrounding of O ions (coordination number 8) as shown in Figure 36. W tetrahedrons share common vertices with Ca polyhedrons, while Ca polyhedrons between each other share common edges (Figure 38). Unit CaWO_4 cell is tetragonal with cell parameters $a = b = 5.24318 \text{ \AA}$ and $c = 11.37104 \text{ \AA}$ according to Inorganic Crystal Structure Database (ICSD) card N° 15586. X-Fit [130] was used to extract the unit cell parameters through peak fitting analysis, which determines the unit cell parameter from least squares analysis of the positions of the peaks. The value crystallite size was 177 nm. In principle, this is expected, because the test sample obtained by milling of the single

crystals. The crystallites were significantly larger and out of range of accurate measurement using XRD methods. On the other hand, the size of microstrain (0.276%) is high, which is also characteristic of the samples obtained by milling of the single crystal.

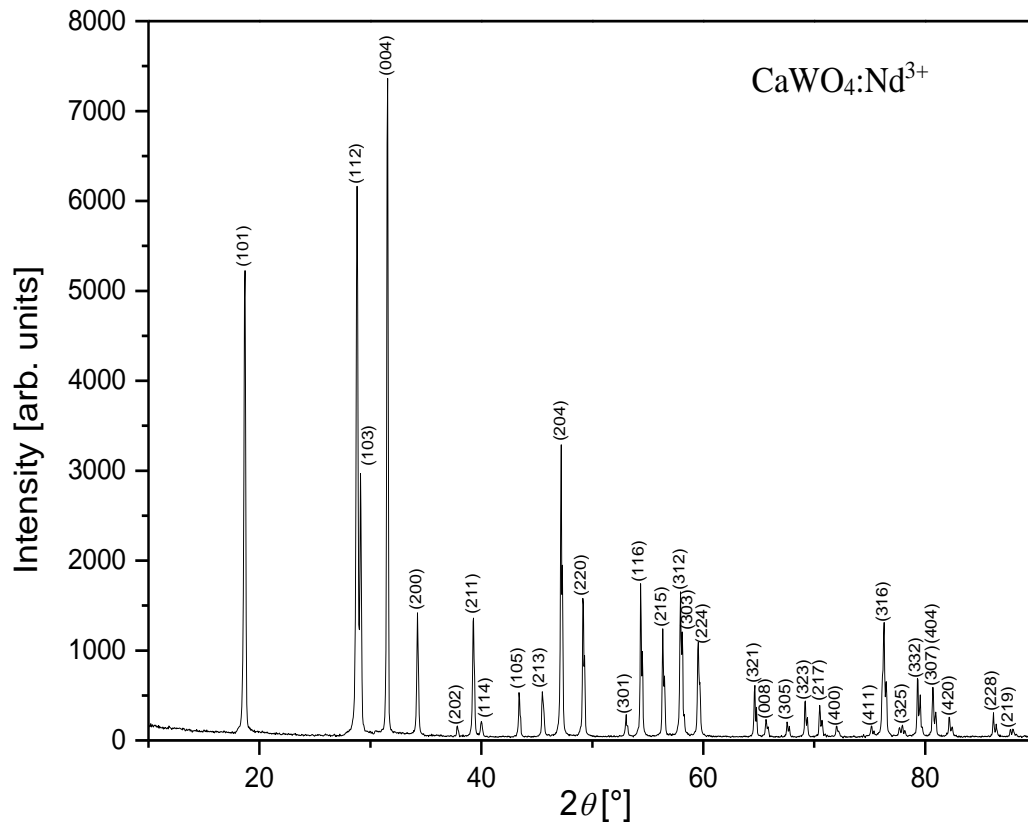


Figure 37. XRD pattern of $\text{CaWO}_4:\text{Nd}^{3+}$. All peaks are indexed according to 88. space group, $I4_1/a$ [23].

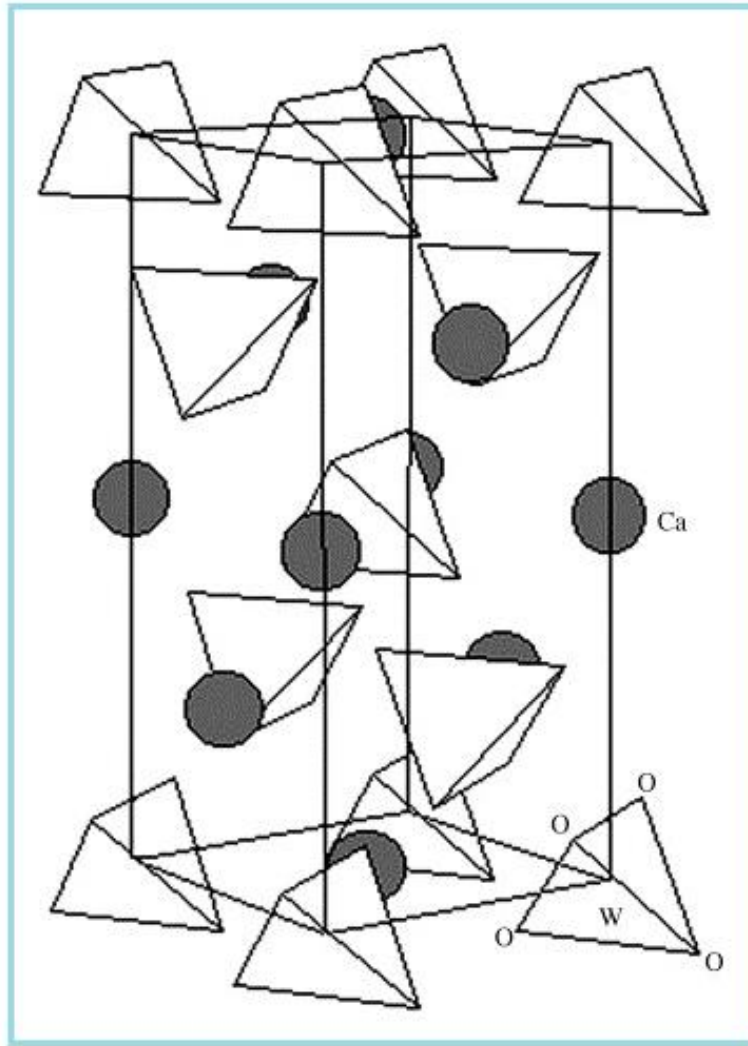


Figure 38. Schematic illustrating the crystal structure of the CaWO_4 crystal unit cell [52].

Factor group analysis in the C space group gives the following set of irreducible representations that characterize all the vibration modes (Raman and infrared) for a tetragonal scheelite primitive cell ($k=0$) [23, 138, 139]:

$$\Gamma_{(\text{Raman} + \text{Infrared})} = 3A_g + 5B_g + 5E_g + 5A_u + 3B_u + 5E_u \quad (6)$$

where the A_g , B_g and E_g are Raman-active modes. The A and B modes are nondegenerate, while the E modes are doubly degenerate. The subscripts "g" and "u" indicate the parity under inversion in centrosymmetric CaWO_4 crystals. The A_u and E_u modes correspond to

the zero frequency of acoustic modes, while the others are optic modes. In addition, the A_g , B_g and E_g modes arise from the same motion in a CaWO_4 phase. Thus, 13 zone-center Raman-active modes for the CaWO_4 crystals are expected, as described in Eqn. (7) [140, 141]:

$$\Gamma_{(\text{Raman})} = 3A_g + 5B_g + 5E_g \quad (7)$$

According to the literature [142, 143], the vibrational modes detected in the Raman spectra of tungstates can be classified into two groups, external and internal modes [144]. In vibrational infrared spectra, $1A_u$ and $1E_u$ acoustic are infrared-inactive mode and $3B_u$ forbidden infrared modes. Therefore, only 8 infrared-active vibration modes remain, as presented by [145]: Eqn. (8)" [48]:

$$\Gamma_{(\text{Infrared})} = 4A_u + 4E_u \quad (8)$$

Figure 39 shows a Raman spectrum of the $\text{CaWO}_4:\text{Nd}^{3+}$ excited 532 nm line of an Ar-ion laser kept at a power of 0.25 mW on sample. The internal vibrations are related to the $[\text{WO}_4]^{2-}$ molecular group with a stationary mass center. The external vibrations or lattice phonons are associated to the motion of the Ca^{2+} cation and rigid molecular units. In the free space, $[\text{WO}_4]^{2-}$ tetrahedrons show T_d -symmetry. In this case, the vibrations of the $[\text{WO}_4]^{2-}$ ions are constituted by four internal modes ($\nu_1(A_1)$, $\nu_2(E)$, $\nu_3(F_2)$ and $\nu_4(F_2)$), one free rotation mode ($\nu_{\text{fr}}(F_1)$) and one transition mode (F_2), When $[\text{WO}_4]^{2-}$ ions are present in a scheelite-type structure, its point symmetry reduces to S_4 . The $3B_u$ vibration is a silent mode. The Raman modes in Figure 39 were detected as $\nu_1(A_g)$, $\nu_3(B_g)$, $\nu_3(E_g)$, $\nu_4(B_g)$, $\nu_2(B_g)$, rotation (E_g) and rotation (A_g) vibrations at 912, 835, 798, 395, 329, 281 and 216 cm^{-1} , respectively, which provide evidence of a Scheelite structure. The well-resolved sharp peaks for the CaWO_4 indicate that the synthesized particles are highly crystallized.

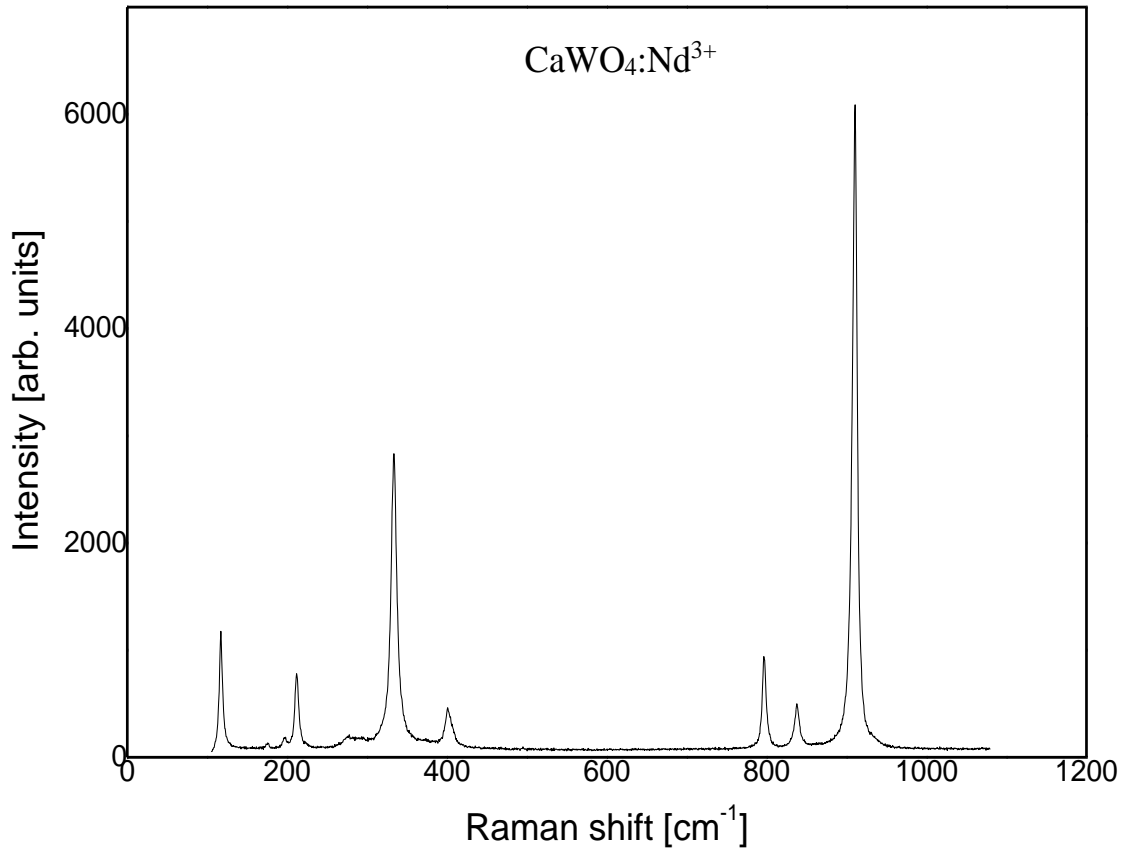


Figure 39. Raman spectrum of $\text{CaWO}_4:\text{Nd}^{3+}$ single crystal, recorded at room temperature [23].

Figure 40 illustrate the IR spectrum and corresponding positions of IR-active modes of crystal. "The tungstates with scheelite-type structure have eight stretching and/or bending IR-active vibrational modes" [48, 146, 147]. In our case, no more than six modes [$2A_u$, $1(A_u + E_u)$ and $3E_u$] were identified in the spectra (Figure 40).

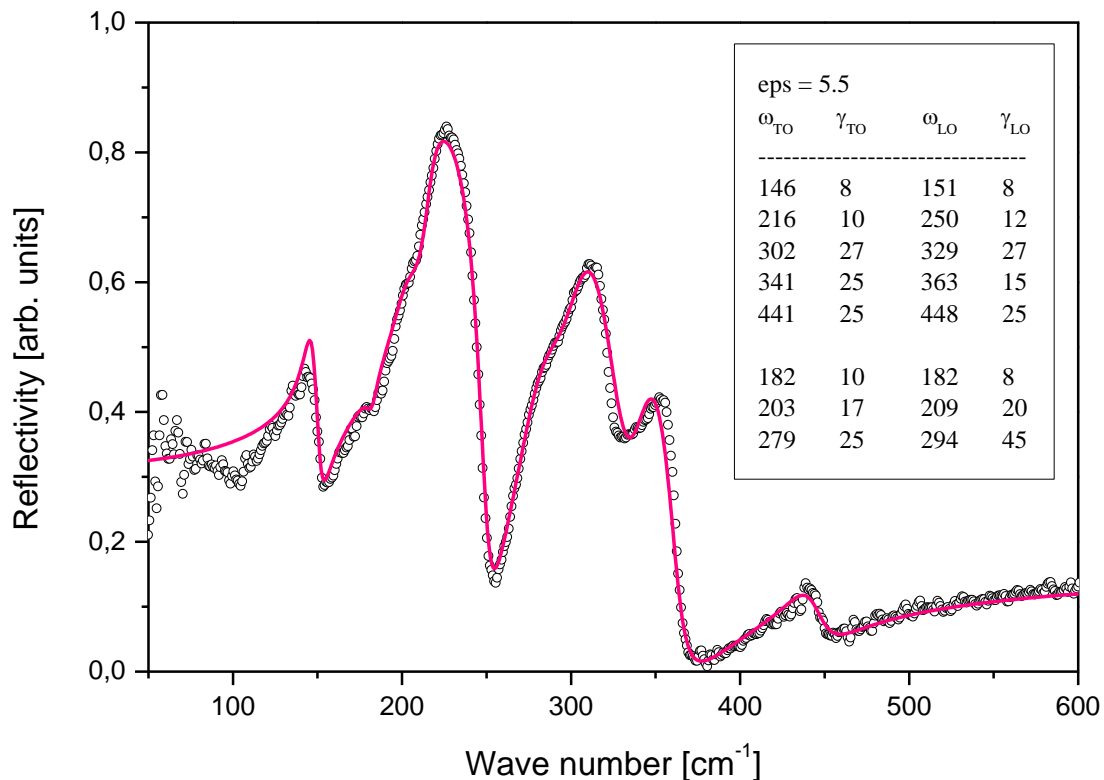


Figure 40. IR spectrum of $\text{CaWO}_4:\text{Nd}^{3+}$ single crystal, recorded at room temperature [23].

Figure 41 shows FTIR spectrum of the obtained $\text{CaWO}_4:\text{Nd}^{3+}$ at the wavenumber range of $4000\text{-}400\text{ cm}^{-1}$. The band at around 2916 cm^{-1} corresponds to the stretching vibration of the hydroxyl ion [148]. The band at 2323 cm^{-1} shows the existence of CO_2 . The bands below 1000 cm^{-1} are characteristic of the W-O bond. The absorption band at around 742 cm^{-1} and strong band at 862 cm^{-1} are attributed to the O-W-O stretches of the $[\text{WO}_4]^{2-}$ tetrahedron, because the AWO_4 -type scheelite oxides S_4 site symmetry for the WO_4 groups [148, 149]. The weak vibration band detected at 436 cm^{-1} could be ascribed to the W-O bending vibration [150]. The band at 1560 cm^{-1} corresponds to the O-H stretching and the H-O-H bending vibrations, due to small quantity of surface-absorbed water [150, 151]. From the FTIR spectrum (Figure 41), "a strong peak at 862 cm^{-1} has been obtained due to the stretching vibration of $[\text{WO}_4]^{2-}$ in scheelite structure, and a weak but sharp band at 433 cm^{-1} has also been noticed due to the metal, oxygen (Ca-O) band." [23]

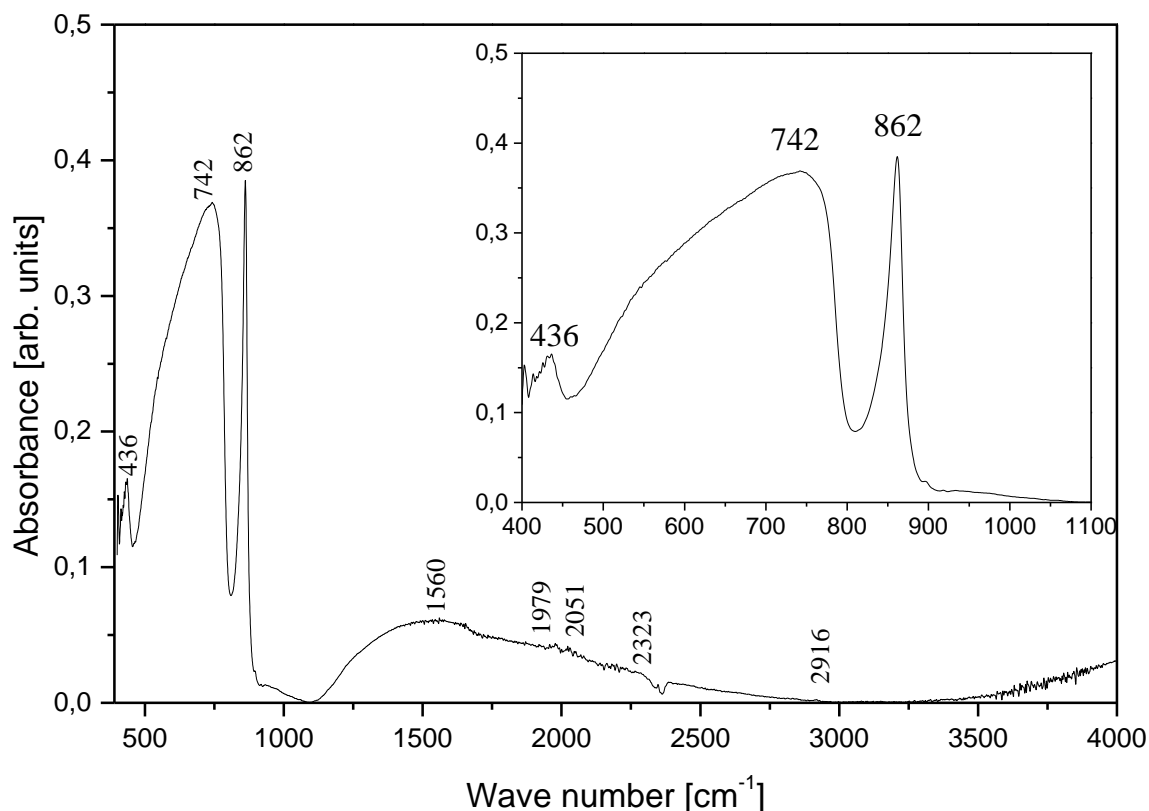


Figure 41. FTIR spectrum of $\text{CaWO}_4:\text{Nd}^{3+}$ single crystal [23].

"Near infrared luminescence of Nd^{3+} doped phosphors have received the renewed interest recently [152-154]. The time resolved optical characteristics of samples were analyzed using streak camera and Nd:YAG laser as excitation source. The setup is described in more detail in our earlier publication [124]. Here, we use pulsed laser excitation at 532 nm for time resolved analysis of $\text{CaWO}_4:\text{Nd}^{3+}$ near infrared luminescence. We have analyzed the part of the spectrum corresponding to ${}^4\text{F}_{5/2} - {}^4\text{I}_{9/2}$ and ${}^4\text{F}_{3/2} - {}^4\text{I}_{9/2}$ transitions. These transitions are of interest for remote temperature sensing, as described in [152-154]. Fluorescence intensity ratio of these two transitions is used to determine temperature sensing calibration curves. The analyzed samples of $\text{SrF}_2:\text{Nd}^{3+}$ [152], and $\text{La}_2\text{O}_2\text{S}:\text{Nd}^{3+}$ [153] phosphors were excited by CW laser at 532 nm. The extensive study of using Nd^{3+} -based luminescent nanothermometers is provided in [154]. Streak images of near infrared luminescence of Nd^{3+} doped crystal is shown in Figure 41. "[23].

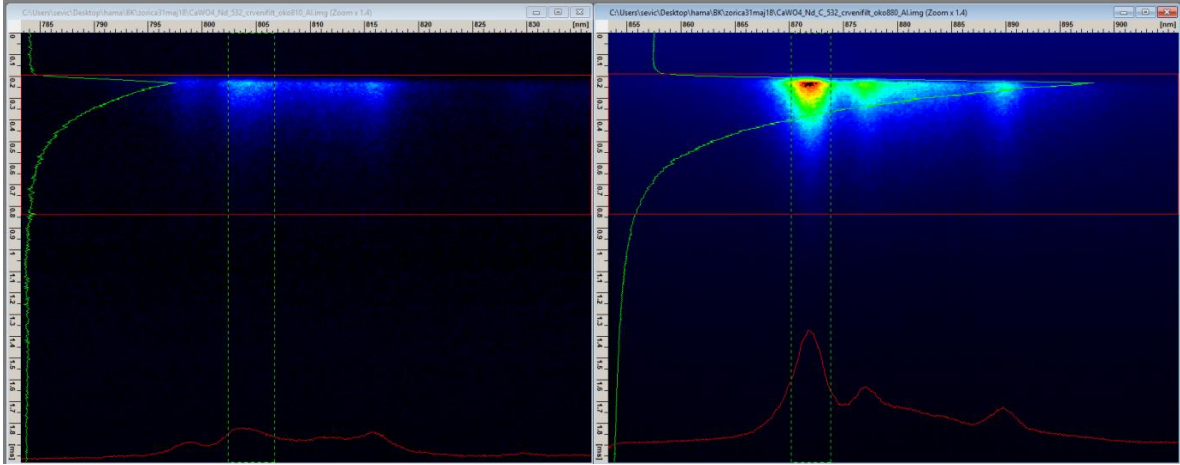


Figure 42. Streak images of $\text{CaWO}_4:\text{Nd}^{3+}$ luminescence emission, excited at 532 nm. Bands around 810 nm (${}^4\text{F}_{5/2} - {}^4\text{I}_{9/2}$ transition) and around 880 nm (${}^4\text{F}_{3/2} - {}^4\text{I}_{9/2}$ transition) were recorded separately, using diffraction grating of 300 g mm^{-1} for better wavelength resolution [23].

"We have used HPD-TA software, provided by Hamamatsu, to calculate the lifetime of $\text{CaWO}_4:\text{Nd}^{3+}$ luminescence. Estimated luminescence lifetime of ${}^4\text{F}_{5/2} - {}^4\text{I}_{9/2}$ transition is about $120 \mu\text{s}$; estimated luminescence lifetime of ${}^4\text{F}_{3/2} - {}^4\text{I}_{9/2}$ transition is about $140 \mu\text{s}$. This result (regarding the ${}^4\text{F}_{3/2} - {}^4\text{I}_{9/2}$ transition) is almost the same as provided in [154], ($\text{Gd}_2\text{O}_3:\text{Nd}^{3+}$), where corresponding lifetime at room temperature is about $142 \mu\text{s}$. Our results are not far from the value of $220 \mu\text{s}$ provided in table 4 of [155], where Nd^{3+} doped BGO crystal was analyzed. Comparing our results with a few results provided in other references, we see that the lifetimes could be strongly dependent on host [156]. Measured lifetimes for the same transitions in [152], ($\text{SrF}_2:\text{Nd}^{3+}$) are about $5 \mu\text{s}$ for ${}^4\text{F}_{5/2} - {}^4\text{I}_{9/2}$ transition and about $1230 \mu\text{s}$ for ${}^4\text{F}_{3/2} - {}^4\text{I}_{9/2}$ transition. Figure 43 shows near infrared spectrum of $\text{CaWO}_4:\text{Nd}^{3+}$ luminescence excited at 532 nm, obtained by background and sensitivity correction of streak images presented in Figure 42." [23]

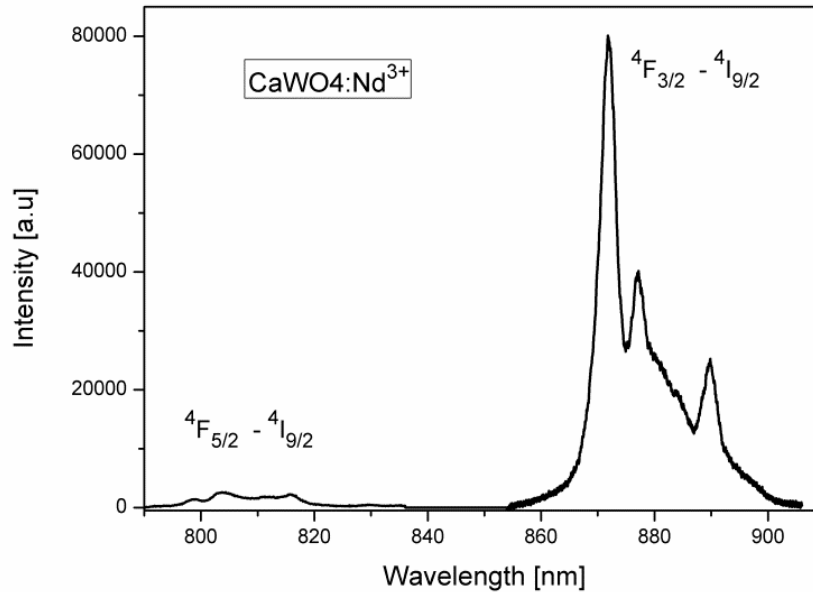


Figure 43. Near infrared spectrum of CaWO₄:Nd³⁺ luminescence excited at 532 nm [23].

The properties of the crystal, such as density of dislocations, crystallinity, and impurities concentrations, determine the optical quality.

11.2. Layered composite PMMA- CaWO₄:Nd³⁺

FTIR spectra of all studied samples are presented in Figure 44. The characteristic bands of CaWO₄:Nd³⁺ may be noticed at wavenumbers below 1000 cm⁻¹ corresponding to the W-O bond. Also, the stretching vibrations found at 781 and 852 cm⁻¹ were due to O-W-O bond stretch of [WO₄]²⁻ tetrahedron since CaWO₄:Nd³⁺ form AWO₄-type scheelite oxides [147, 148]. Vibration attributed to W-O bending was hardly noticed at ~420 cm⁻¹ wavenumber [149]. The bands corresponding to hydroxyl group vibration at ~1550 cm⁻¹ and ~3500 cm⁻¹ suggest that pre-analysis drying removed the surface-absorbed water [151].

MPTMS as a silica network was adsorbed on CaWO₄:Nd³⁺ surface by (CaWO₄:Nd³⁺)-O-Si bonds that caused the appearance of intensive peak at 552 cm⁻¹ [157]. Sharp intensity peak at 859 revealed the presence of Si-O-H stretching and OH vibrations on the surface of CaWO₄:Nd³⁺. The bands in the region 2200-1800 cm⁻¹ show the existence

of CO₂ [23]. In the infrared spectra, the band due to the S–H stretching vibration is sometimes so weak that it can be missed in dilute solutions [158]. S–H vibration occurs in the region 2600–2540 cm⁻¹ and only contours of some possible vibrations can be identified. Stretching vibration of –CH bands was noticed due to the introduction of propyl chain by MPTMS (2850–3000 cm⁻¹). Introduction of PMMA on the surface of CaWO₄:Nd³⁺ crystal, contributed to the appearance of vibration at 804 cm⁻¹ corresponding to methyl ester groups of PMMA [159]. Therefore, analyzed results from FTIR spectra showed that the experimental procedure used in this study was successful in modification of CaWO₄:Nd³⁺ crystal.

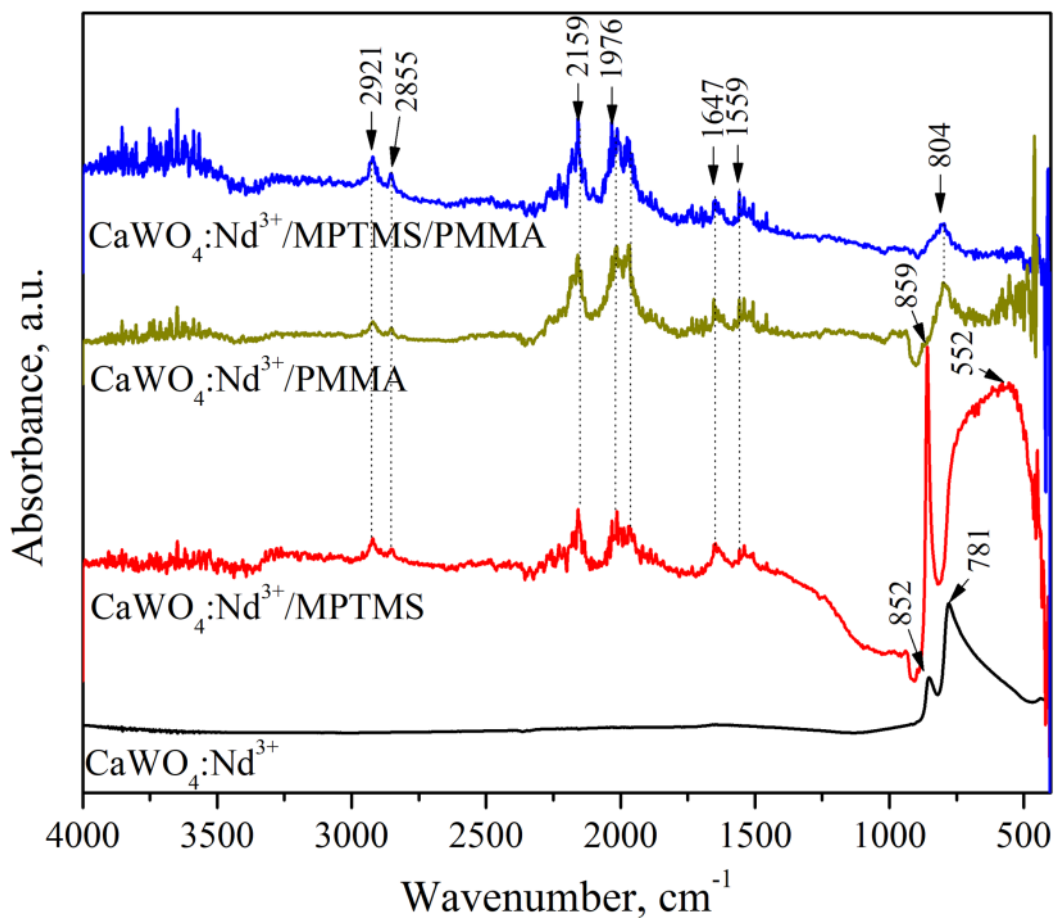


Figure 44. FTIR spectra of CaWO₄:Nd³⁺ before and after surface modification with MPTMS silane, PMMA and PMMA with MPTMPS as an adhesion primer.

In spectrum of CaWO₄:Nd³⁺/MPTMS-PMMA composite it is obvious that silane coupling agent was established some dipole-dipole secondary bond with matrix, resulting

in good transparency of obtained composite. It is supposed that bonding are established as it is presented on Figure 45.

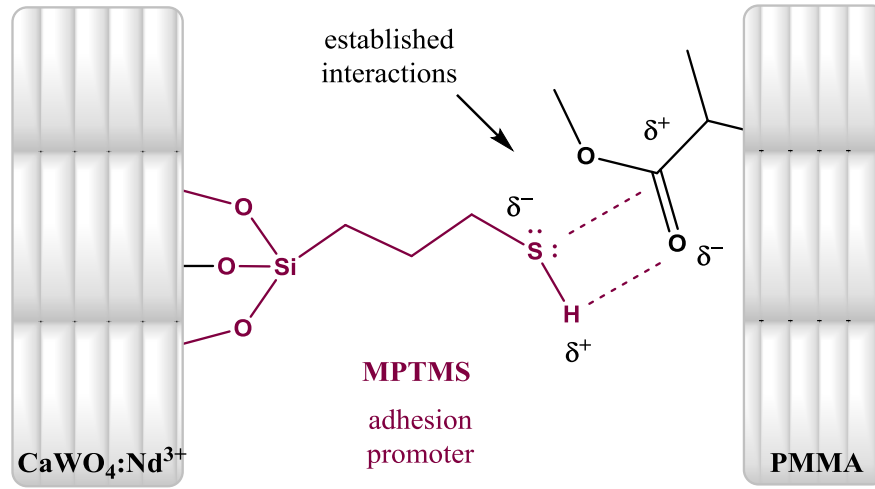


Figure 45. Schematic illustration of established interactions between inorganic and organic material ($\text{CaWO}_4:\text{Nd}^{3+}$ and PMMA) by MPTMS.

Micro Vickers hardness (HV) test was performed to determine hardness of $\text{CaWO}_4:\text{Nd}^{3+}$ and composite before and after surface modification. The advantage of HV test is determination of the hardness variations under low loads, analysis of possible surface defects, and an identification of each surface modifier contribution and characterization of microstructure gradients. HV values are determined and summarized in Table 3. The hardness of $\text{CaWO}_4:\text{Nd}^{3+}$ crystal is reduced in comparison with pure CaWO_4 because the crystal structure was change [160]. Hardness determination of polymer film on the crystal could be obtained in relation about composite hardness, because of substrate influence [161, 162].

It is interesting to note that the sample $\text{CaWO}_4:\text{Nd}^{3+}/\text{MPTMS}/\text{PMMA}$ showed higher hardness value than without MPTMS adhesion primer which was due to improved compatibility enabling effective load transfer of indentation. Comparative experimental results of HV hardness indents obtained for $\text{CaWO}_4:\text{Nd}^{3+}$ before and after surface modification are presented in Figure 46. The surface of $\text{CaWO}_4:\text{Nd}^{3+}$ sample was pretty rough before the coating and the indents were hard to notice, Figure 46a). MPTMS revealed the rigidity of $\text{CaWO}_4:\text{Nd}^{3+}$ surface which can be seen by the spread of cracks on

the edge of the imprint, Figure 46b). Very irregular imprint of $\text{CaWO}_4:\text{Nd}^{3+}/\text{PMMA}$ sample showed the inhomogeneity of surface and incompatibility of $\text{CaWO}_4:\text{Nd}^{3+}$ and PMMA, Figure 46c). Regularity of imprint can be seen on Figure 46d) of $\text{CaWO}_4:\text{Nd}^{3+}/\text{MPTMS}/\text{PMMA}$ sample with larger diagonals due to lower hardness and more uniform PMMA layer. Standard deviation is higher for samples with MPTMS or PMMA due to the non-homogeneous surface microstructure.

Improved hardness with the use of MPTMPS as an adhesion primer before PMMA indicate the manner of $\text{CaWO}_4:\text{Nd}^{3+}$ surface modification that enabled the improvement in resistance to wear, cutting and scratching. Also, this represents that the improved compatibility of $\text{CaWO}_4:\text{Nd}^{3+}$ and PMMA with MPTMS at the interface.

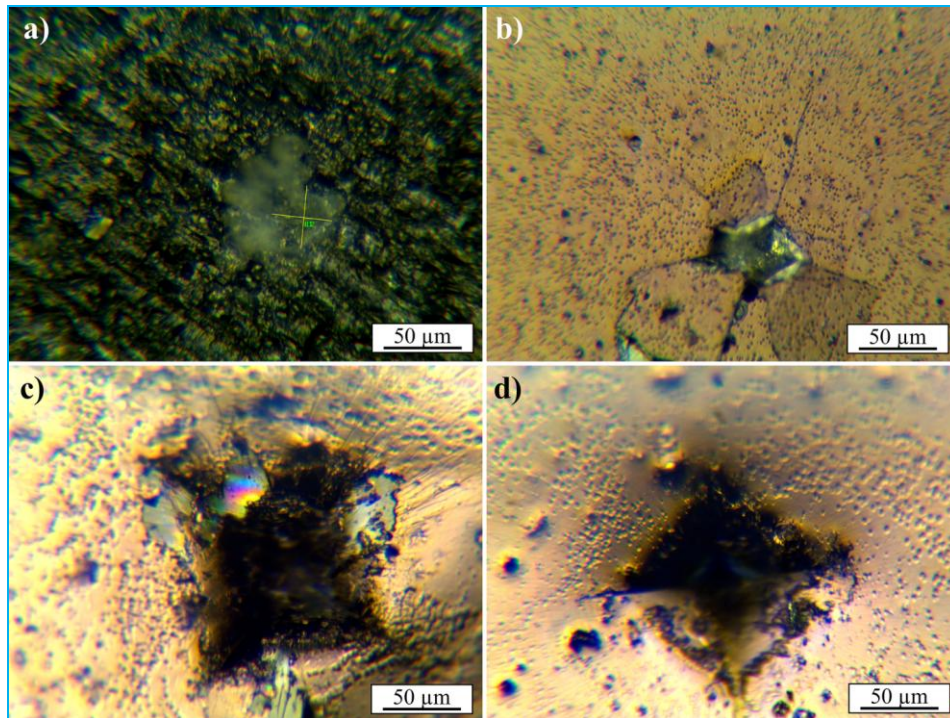


Figure 46. Micro hardness indentation imprints on the surface of: a) neat $\text{CaWO}_4:\text{Nd}^{3+}$, b) $\text{CaWO}_4:\text{Nd}^{3+}/\text{MPTMS}$, c) $\text{CaWO}_4:\text{Nd}^{3+}/\text{PMMA}$ and d) $\text{CaWO}_4:\text{Nd}^{3+}/\text{MPTMS}/\text{PMMA}$.

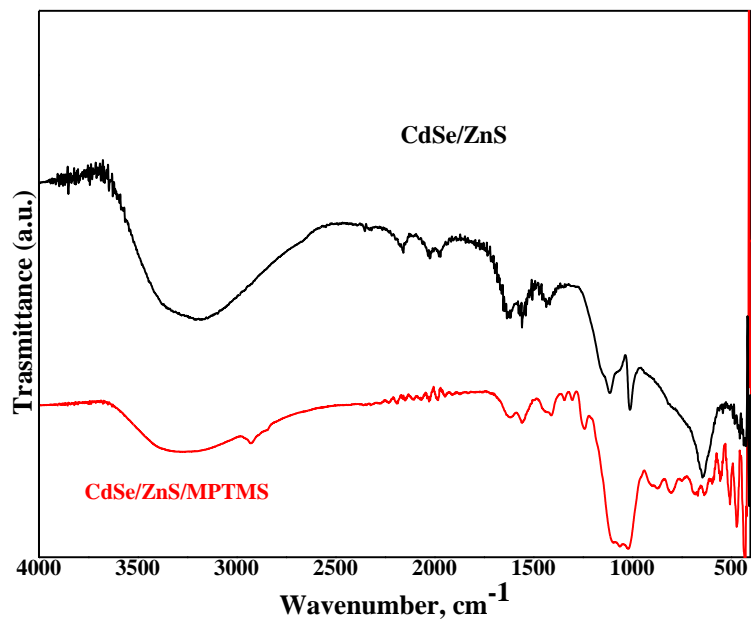
Table 3. Micro Vickers hardness of $\text{CaWO}_4:\text{Nd}^{3+}$ before and after surface modification.

Sample	HV (GPa)	Standard deviation (GPa)
$\text{CaWO}_4:\text{Nd}^{3+}$	1.156	0.011
$\text{CaWO}_4:\text{Nd}^{3+}/\text{MPTMS}$	0.973	0.063
$\text{CaWO}_4:\text{Nd}^{3+}/\text{PMMA}$	0.079	0.013
$\text{CaWO}_4:\text{Nd}^{3+}/\text{MPTMS}/\text{PMMA}$	0.098	0.002

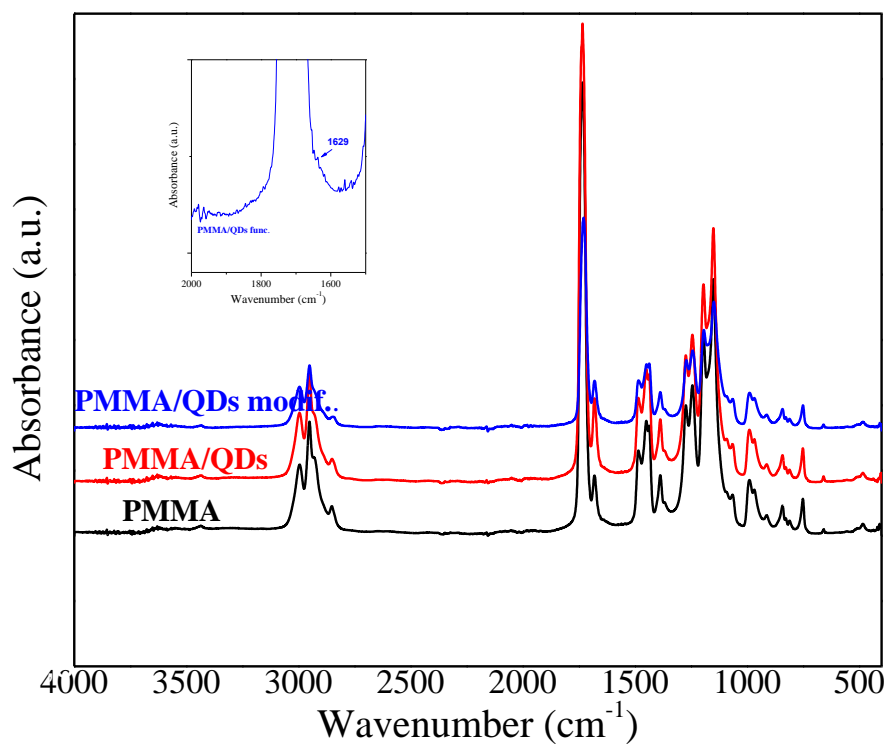
11.3. Composite films PMMA- CdSe/ZnS quantum dots

"FTIR spectrums of modified and unmodified QD`s and corresponding composites are presented in Figure 47. In the spectrum of net QD`s (Figure 47a)) the characteristic major peaks of ZnS can be observed at about 1112, 998 and 642 cm^{-1} , which are in good agreement with the reported results [105, 136, 163]. There is a band at 624.34 cm^{-1} is due to the stretching frequency of Cd–Se bond. In spectrum of modified QD`s two sharp peaks were observed at around 1620 and 1400 cm^{-1} due to the stretching vibrations of thiol capping [164]. The absence of S–H vibration at 2556-2654 cm^{-1} shows that mercapto groups molecules were bound to the ZnS surface. The absorption bands for the propyl group are appearing at 2934 and 2832 cm^{-1} due to the C–H stretching vibrations, further justifying the MPTMS anchored onto QD`s.

In the spectrum of pure PMMA and composites (Figure 47b)) exhibits typical vibration bands, *i.e.*, vibrational bands at 987 and 1453 cm^{-1} that belong to O–CH₃ bending and stretching deformation of PMMA, respectively, bands at 1730 and 1250 cm^{-1} that are assigned to stretching of C=O groups, a band at 1065 cm^{-1} that could be ascribed to the C–O stretching vibration and a band at 1197 cm^{-1} that belongs to the skeletal chain vibration. The other bands appearing in the 3000-2800 cm^{-1} , 1490-1275 cm^{-1} and 900-750 cm^{-1} spectral regions correspond to different CH₃– and CH₂– vibrational modes [165, 166]. The stretching vibration band of C=O group on MPTMS located at 1629 cm^{-1} also appears in Figure 47b) (insert), although its intensity is very weak." [118].



a)



b)

Figure 47. FTIR spectra of a) unmodified and modified CdSe/ZnS QD`s; b) pure PMMA and composites with unmodified and modified CdSe/ZnS QD`s [118].

"The morphology of PMMA films doped with unmodified QD`s and modified QD`s are presented on FESEM photos in Figure 48. It could be seen that better deagglomeration was achieved with modification of QD`s with silane. Optical properties of polymer nanocomposites are dependent on concentration, path length, temperature, and the wavelength of light used, as well as the matrix properties. With the better deagglomeration one can achieved uniformity of size and distance between nanoparticles in polymer matrix. This could be obtained by surface modification of nanoparticles embedded in polymer. As can be seen from FESEM photos, with PMMA/QD`s interface modification uniform dispersion was obtained and the better optical properties associated with that could be expect [167-169]." [118].

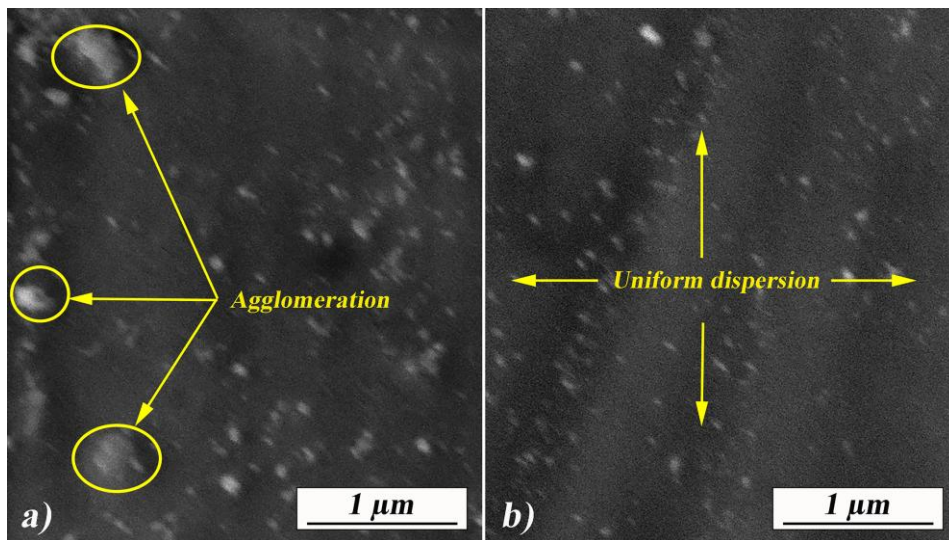


Figure 48. FESEM pictures of films a) PMMA-unmodified QD`s CdSe/ZnS, b) PMMA-modified QD`s CdSe/ZnS [118].

"The Raman spectra of the starting materials CdSe, ZnS and PMMA, quantum dots CdSe/ZnS and modified CdSe/ZnS in PMMA, in spectral range from 120 cm^{-1} to 475 cm^{-1} experimental Raman scattering spectra are analysed by the deconvolution to Lorentzian curves [118, 170, 171]. Black thick line presents resulting spectral curve. Positions of Lorentzians are given above the curves in Figure 49 [118]. The peak at 206.9 cm^{-1} in the CdSe spectrum is attributed to the first order CdSe longitudinal optical phonon. The peaks denoted as LO. Its overtone is 2LO at 410.24 cm^{-1} . The optical modes in Raman spectra of ZnS, which may be easily observed by first-order Raman scattering, are doubly degenerate

TO and single LO phonon with a higher frequency. The identity of these modes is well established by their polarization characteristics as described by published infrared and Raman studies [172-174]. Our measured TO and LO modes are located at 218.16 cm^{-1} and 348.30 cm^{-1} , which are consistent with the previous Raman studies for zinc blende ZnS [173, 174].

Raman spectra of CdSe/ZnS QD`s (previously dissolved in toluene, placed on Si-wafer and dried to eliminate solvent), PMMA film and PMMA-QD`s film in spectral range 125-470 cm^{-1} are presented in Figure 49. " [118].

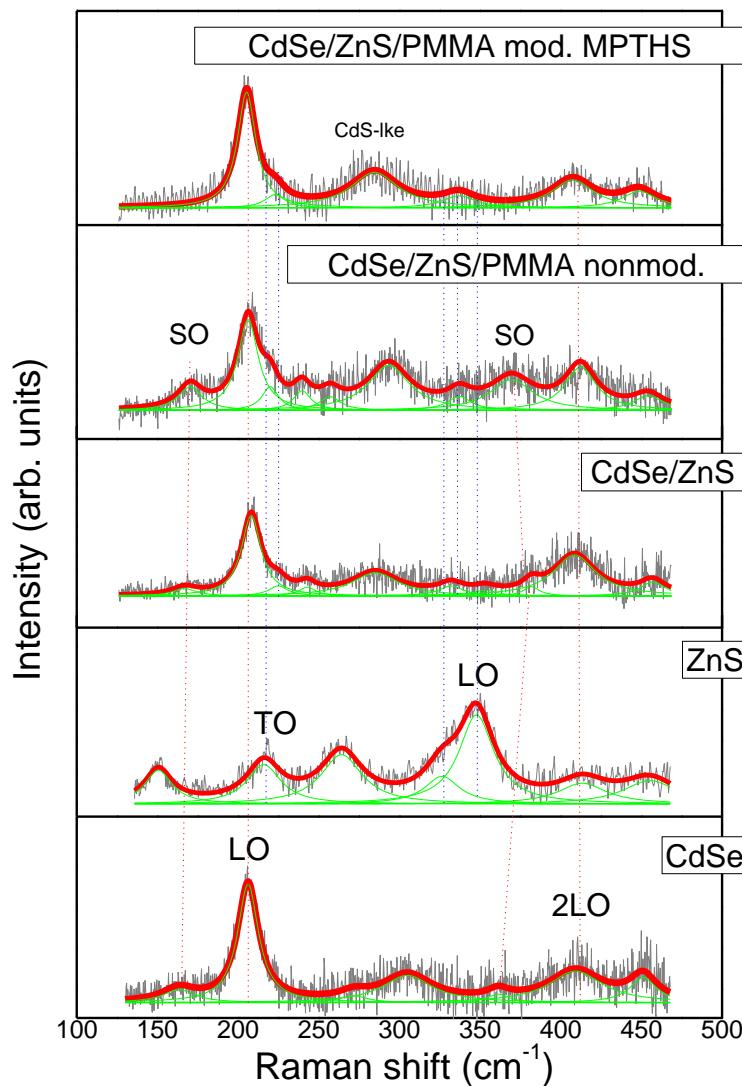


Figure 49. Raman spectra of: QD`s ZnS, QD`s CdSe, core-shell CdSe/ZnS in toluene solution, composite CdSeZnS/PMMA, composite CdSeZnS/PMMA with MPTMS modification [118].

"Observed modes are fitted by Lorentzians. In the spectrum of QD`s the most prominent Raman modes are of CdSe core. At 208.1 cm^{-1} , with FWHM 14 cm^{-1} , is LO mode and at 408.5 is its second harmonic 2LO with FWHM 32 cm^{-1} . Weak mode at 166 cm^{-1} is combination of two contributions - phonon confinement and the surface optical (SO) vibration [175]. Modes of ZnS shell are almost invisible. At 224 cm^{-1} is TO mode, at 350 cm^{-1} LO mode [174]. Little stronger modes at 243 and 332 cm^{-1} can be ascribed to the solid solution $\text{Cd}_x\text{Zn}_{1-x}\text{Se}_{1-y}\text{S}_y$. Mode at 285 cm^{-1} is CdS-like LO mode [175, 176]. Weak mode at 382 cm^{-1} is probably a surface optical (SO) mode and at about 456 cm^{-1} is a multimode feature. Raman spectrum confirms a presence of alloyed layer at the core-shell interface.

In the Raman spectrum of PMMA are clearly visible vibrations at 235 , 297.7 , 363.7 and 401.9 cm^{-1} . It is a range of vibration of $-\text{C}-\text{O}-\text{C}$ skeleton. According to Willis *at al.* [177] about 400 cm^{-1} is a bending mode $\delta(\text{C}-\text{O}-\text{C})$, about 376 cm^{-1} (363.7 in our spectrum) can be vibration of methyl methacrylate monomer. Theoretical calculations in Ref. [178] in this energy range predict C-O-C deformational modes and at 235 cm^{-1} C-O torsion mode.

In the Raman spectra of PMMA-QD`s film some peaks of PMMA are superposed to QD`s modes, but main modes of CdSe-core are clearly visible. Positions of CdSe LO and 2LO modes and corresponding FWHM are the same as in spectra of QD`s.

Raman characterization of QD`s CdSe/ZnS in PMMA is presented. The spectra of QDs CdSe/ZnS in PMMA and QD`s CdSe/ZnS are "almost identical, which could be attributed to the metal selenides and sulfides crystallites being in the pores of PMMA networks without disturbing the continuous three-dimensional network in the polymer matrices, and both are independent in their chemical behavior [179]. All of the stretching vibrations observed in the PPMA appeared in the nanocomposites with higher intensity. The van der Waals interactions between PMMA and the metal sulfide nanoparticles are very weak [180, 181], and the amount of nanoparticles used does not affect the transparency of the nanocomposites" [182, 183]. It can be concluded that presence of PMMA does not affect Raman modes of QD`s-core. 3-mercaptopropyltrimethoxy silane was chosen because promote the dipole-dipole bonding, which will not disturb optical properties. The hydrogen bonds and Van der Waals forces could be classified as two different types of intermolecular forces. In one classification, van der Waals forces must involve at least one non-permanent dipole, while hydrogen bonding involves two

permanent dipoles. Since the S-H bond is polar and PMMA is no polar molecule, it is reasonable that the Van der Waals bond is established. Also, because no intensity changes in FTIR hydroxyl region $3800-3200\text{ cm}^{-1}$ (Figure 47b)) indicates the interaction mainly due to the polarization then hydrogen bonding.

The streak image of time resolved photoluminescence spectrum of modified QD`s in PMMA material using the 360 nm excitation is presented in Figure 50 [118]. As usual, the streak image is presented in pseudo color mode." [118].

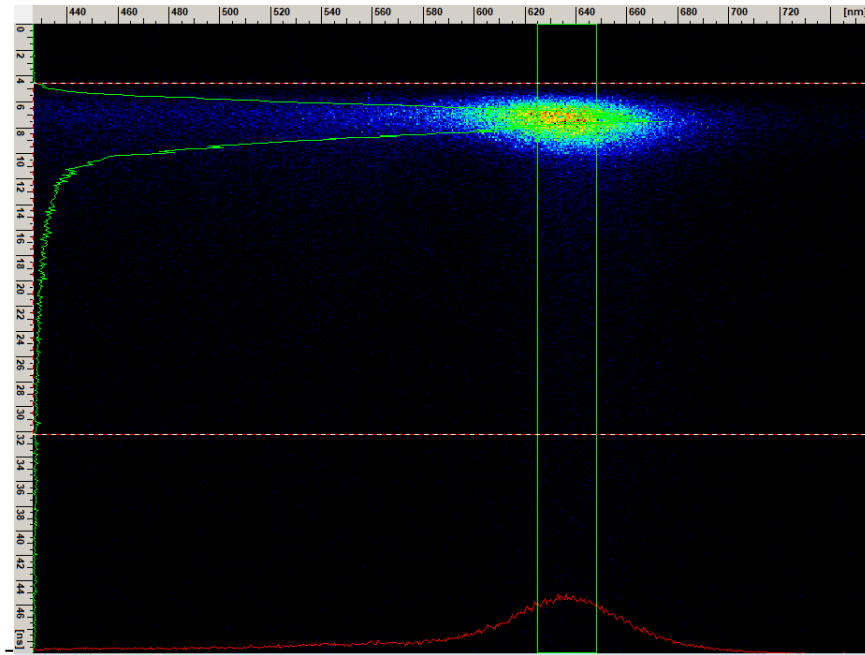


Figure 50. Streak image of time resolved photoluminescence spectrum of modified QD`s CdSe/ZnS in PMMA matrix [118].

"Fluorescence spectra of CdSe/ZnS QD`s liquid solution, QD`s in PMMA and modified QD`s in PMMA excited at 360 nm are shown in Figure 51. The spectra are integrated-in-time from the corresponding streak images using the horizontal (dotted red) frame as shown in Figure 50. It can be seen that the peak of CdSe/ZnS/PMMA nonmodified is slightly blue shifted in regard to other two spectra." [118].

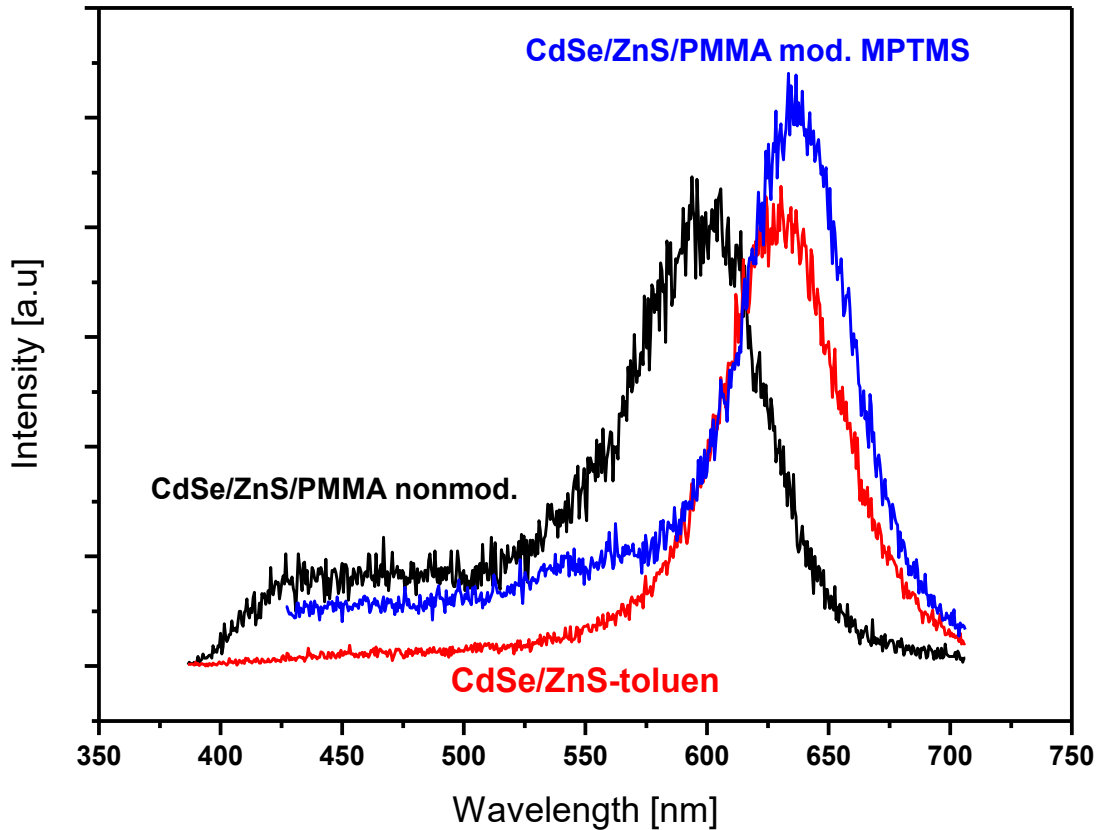


Figure 51. Fluorescence spectra of QD`s CdSe/ZnS in toluene and in PMMA composites with modified and unmodified QD`s [118].

"The line profiles used for lifetime calculations are determined from the corresponding streak images using the vertical (green) frame as shown in Figure 50. We have obtained that the lifetimes of QD`s in toluene and in PMMA composites with modified and unmodified QD`s are 1.93 ns, 1.46 ns and 1.36 ns, respectively.

The chromaticity coordinate values, CIE 1931, were calculated for our samples of CdSe/ZnS QD`s liquid solution, QD`s in PMMA and modified QD`s in PMMA and presented in Figure 52. Because of very weak PMMA luminescence in blue and green bands of visible spectrum, the points corresponding to samples with PMMA are slightly shifted to the left in CIE chromaticity diagram, away from original purple color of our QD`s.

After Raman and fluorescence spectra analysis it could be seen that the embedding of QD`s in PMMA lead to changes in spectrums relative to pure QD`s (CdS-like LO mode at Raman spectra and fluorescence peak were slightly blue shifted). But, with introducing

modification with silane were returned close to originate values for QD`s. We can say that modification with MPTMS preserved the optical functionality of QD`s." [118].

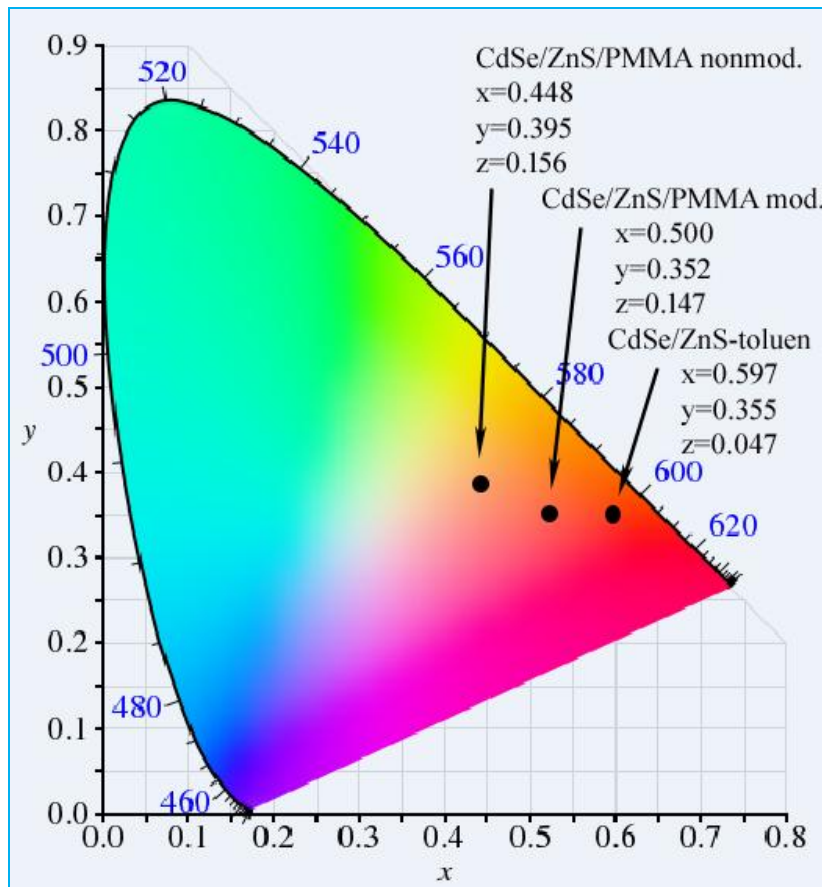


Figure 52. The CIE chromaticity diagram of emission spectra of QD`s CdSe/ZnS in toluene and in PMMA composites with modified and unmodified QD`s [118].

11.4. Composite PMMA-CdSe/ZnS nanofibers

FESEM photograph of PMMA-CdSe/ZnS film and nanofibers is presented in Figure 53. It can be seen that nanofibers were beads-free and with a smooth surface. Image analysis showed that over 70% of the fibers had diameters below 1 μm . This indicates that the chosen optimal flow resulted in favorable morphology and dimensions for the use in optical devices.

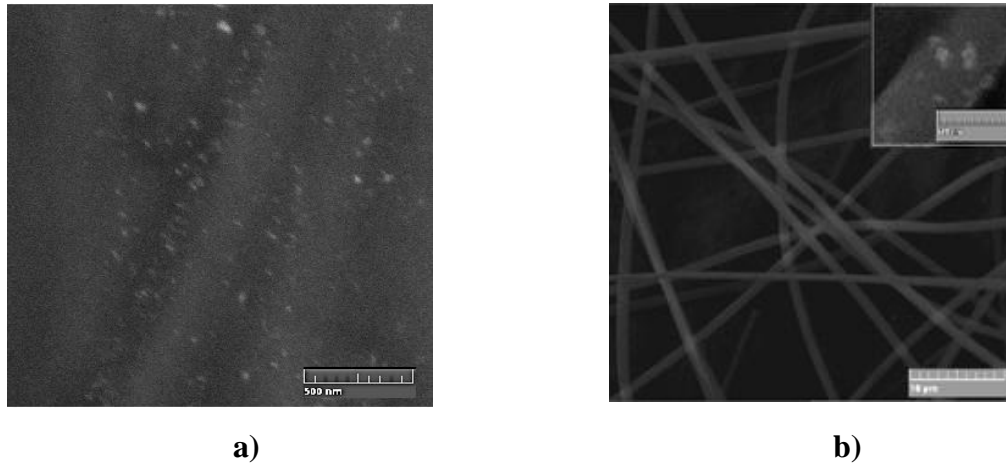


Figure 53. FESEM micrograph of CdSe/ZnS-PMMA a) film and b) fibers.

Figure 54 presents FTIR spectrums of PMMA fibers, PMMA-CdSe/ZnS fibers and film. The bands appearing in the regions $3000\text{-}2850\text{ cm}^{-1}$, $1490\text{-}1275\text{ cm}^{-1}$ and $910\text{-}750\text{ cm}^{-1}$ of all the spectrums, originate from different CH_3 and CH_2 vibrational modes [183]. Bands at 1737 cm^{-1} in spectrums are assigned to the stretching of $\text{C}=\text{O}$ groups from PMMA. While spectrum of fibers PMMA-CdSe/ZnS shows absence of $\text{C}=\text{O}$ peak coming from amide, spectrums of PMMA and PMMA-CdSe/ZnS films show peak at 1647 cm^{-1} , indicating that they were not completely dry. Vibrational bands at 1450 and 991 cm^{-1} , that belong to $\text{O}-\text{CH}_3$ stretching and bending deformation of PMMA, respectively, also appear in all the spectrums, along with the band at 1065 cm^{-1} , ascribed to the $\text{C}-\text{O}$ stretching vibration.

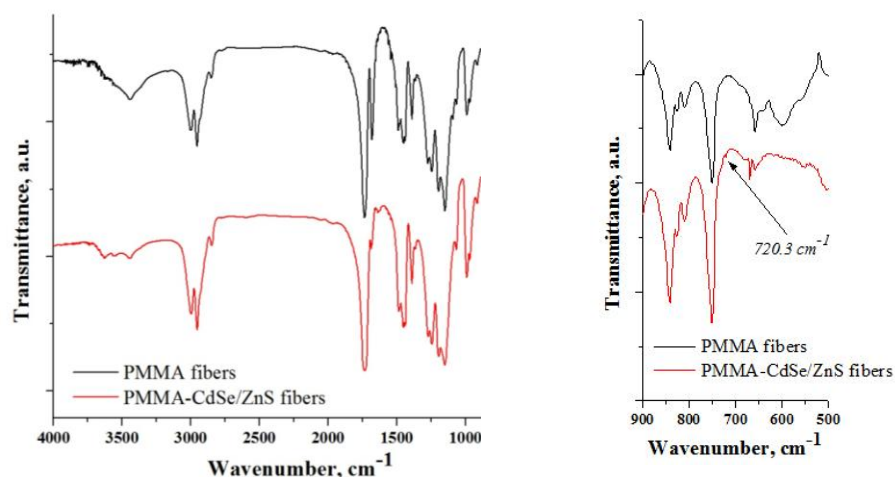


Figure 54. FTIR spectrum of PMMA and composite fibers and film.

These findings lead to the assumption that there was no formation of a new bond between quantum dots and a host material PMMA. The most prominent peak for this research appeared at 720 cm^{-1} in the spectrums of PMMA-CdSe/ZnS fibers and film, indicating the presence of CdSe active core. ZnS bond has been identified with the presence of the peak at 617 cm^{-1} [184]. These results lead to the conclusion that luminescent properties of the QDs could be preserved during the processing of the film by solution casting or fibers by electrospinning.

The results of DSC analysis are given in the Figure 55. The analyses were performed on the powder of pure PMMA, PMMA films and nanofibers and PMMA-QD films and nanofibers. The powder of PMMA shows T_g at around $113\text{ }^\circ\text{C}$. It is obvious that there was influence of solvents in both PMMA and PMMA-QD films, decreasing T_g by 22% for PMMA and nearly 26% for PMMA-QD film. There is also a typical glass transition shoulder about $55\text{ }^\circ\text{C}$ in DSC curve for PMMA-QD film, which reflects a weaker interaction between residual toluene molecules and PMMA [185, 186]. It can be noticed that the PMMA-DMF interaction is stronger in dried films because the reactions observed in that process have changed the structural characteristics of the PMMA. Opposing to the casting of films, electrospinning method gave fibers with approximately the same T_g as pure powder. This is correlated to the viscosity/polarity-dependent behavior of polymer molecules in solvent [185-187]. As Figure 55 shows, there is even a slight increase, which only further suggests that this is an appropriate technique for processing of PMMA-QD nanocomposites.

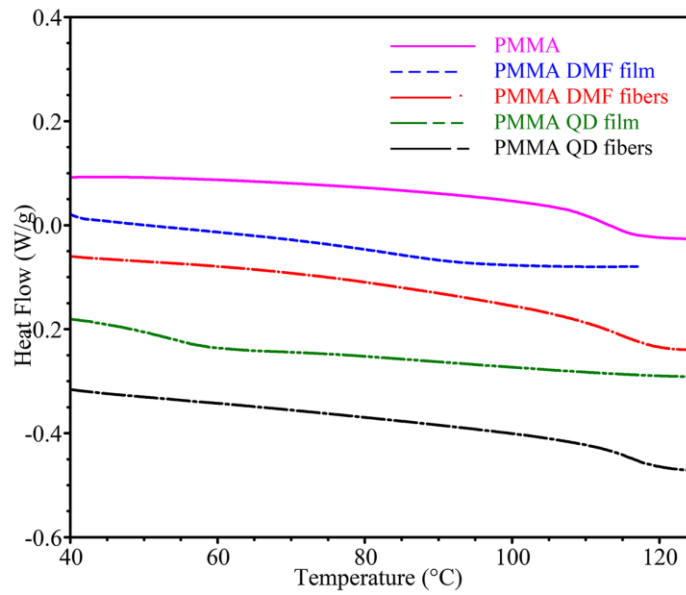


Figure 55. DSC curves.

Beside of more efficient removal of residual solvent, electrospinning ensures better dispersion of nanoparticles, hence the preservation of thermal stability of nanocomposite.

Figure 56 and Table 4 present the results obtained from nanoindentation test. Figure 56a) shows typical force–depth curves obtained in the nanoindentation tests for neat PMMA film and composites with CdSe/ZnS. The curves appear to be with continuity and without pop-in or pop-out in both loading and unloading phases. Figure 56b) displays in-situ imaging mode used for scanning the surface trace that reveals the absence of cracks and fractures around the indent.

Table 4. Results of nanoindentation test.

	E, GPa	St.dev. GPa	H, GPa	St.dev. GPa
PMMA	5.53	0.32	0.33	0.022
PMMA-CdSe/ZnS film	5.85	0.21	0.41	0.028
PMMA-CdSe/ZnS fibers	6.81	0.25	0.46	0.041

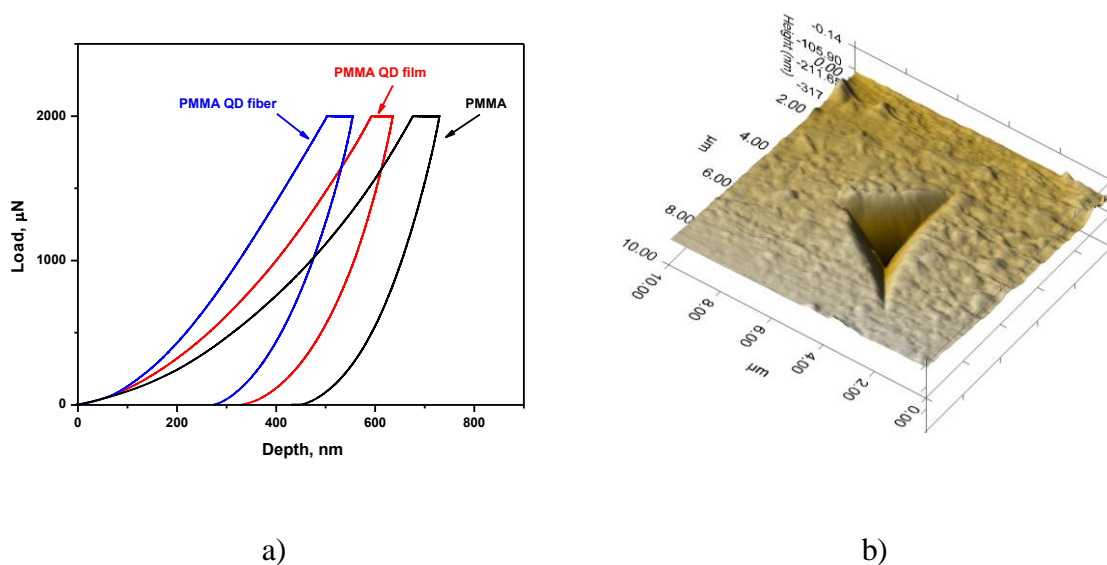


Figure 56. Nanoindentation results.

As it can be seen, with the addition of 0.06 wt% of QDs, reduced modulus increased by 6% for PMMA-CdSe/ZnS films and by 23% for PMMA-CdSe/ZnS fibers, compared to pure PMMA films.

Streak image of fluorescence spectrum of CdSe/ZnS QDs liquid solution excited at 360 nm is shown in Figure 57. The solution was prepared using one part of CdSe/ZnS toluene solution (as received) and six parts of DMF. Our aim was to check the influence of adding the DMF solvent to QDs, because PMMA host for QDs was prepared using DMF as solvent. Slight red shift from 610 nm (corresponding to the CdSe/ZnS QDs solution as received) to 630 nm could be observed. The analysis of CdSe/ZnS QDs hosted in PMMA dissolved in three different solvents (chloroform, toluene and tetrahydrofuran) was reported, however the wavelength shifts are smaller compared to our results [188].

The fluorescence lifetime based on the time resolved spectrum of the CdSe/ZnS QDs liquid solution is also presented in Figure 57. The value of about 2.4 ns was obtained, which is much shorter than the values obtained in the previous researches [102].

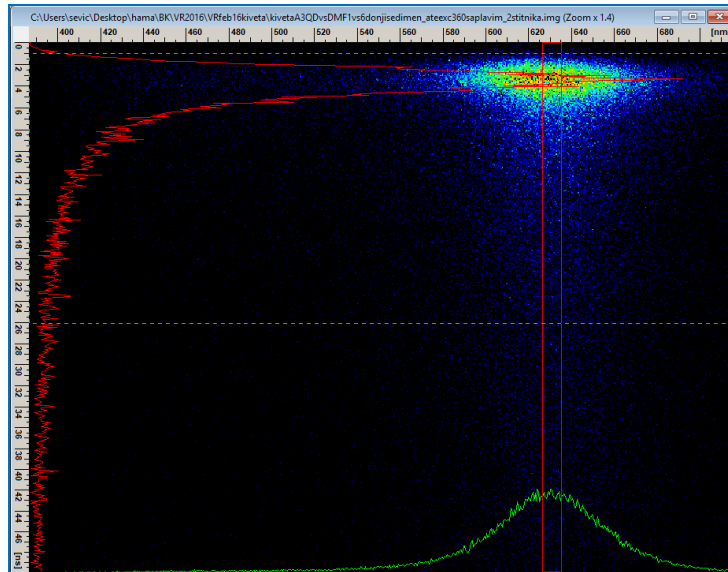


Fig. 57. Streak image of fluorescence spectrum of CdSe/ZnS QDs liquid solution excited at 360 nm.

Figure 58 shows streak images of fluorescence spectra of CdSe/ZnS QD/PMMA composite film excited at 330, 350 and 370 nm. For all excitation wavelengths the fluorescence emission is grouped into two wide bands, around 440 nm and 620 nm. It is easy to see that the band around 440 nm has longer fluorescence lifetime. Calculated fluorescence lifetime for band around 440 nm is 6.9 ns, much longer than the lifetime of QDs liquid solution. Fluorescence lifetime of band around 620 nm is about 1.6 ns, shorter than the lifetime of QDs liquid solution. Intensity ratio of these two bands depends on excitation wavelength. When excitation wavelength increases the band around 620 nm becomes more pronounced, while the band around 440 nm diminishes. Comparing with the values provided in the literature [96-99], estimated core sizes of QDs embedded in PMMA after nanocomposite fabrication process are about 2.4 nm and 5.1 nm, corresponding to the detected bands around 440 nm and 620 nm, respectively.

\

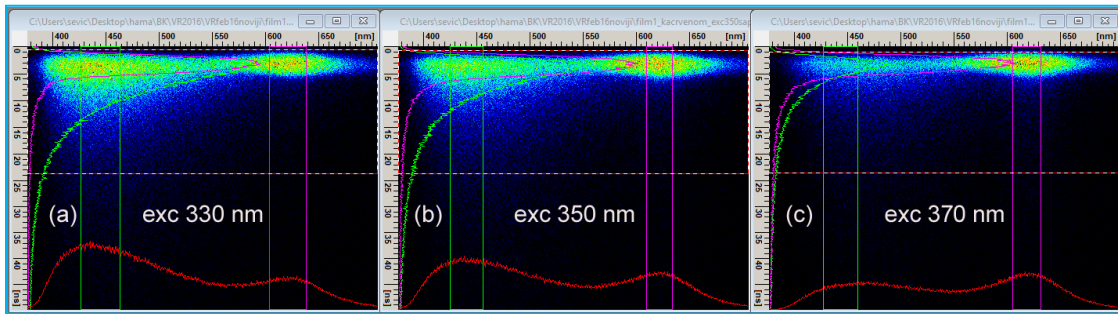


Figure 58. Streak images of fluorescence spectra of PMMA-CdSe/ZnS composite film excited at (a) 330 nm, (b) 350 nm and (c) 370 nm.

Emission intensity as a function of illumination time of PMMA-CdSe/ZnS composite film is shown in Figure 59. The pulsed OPO has frequency of 10 Hz, energy of a pulse is about 5 mJ, and estimated diameter of illuminated spot is about 100 μm . Because QDs are embedded in PMMA, there are no oxidation effects and there are no spectral shifts caused by illumination [101, 102]. Decrease of emission intensity is easy to notice, however, it seems that the bleaching effects of QDs embedded in PMMA evolve slower compared to measurements performed in nitrogen ambient.

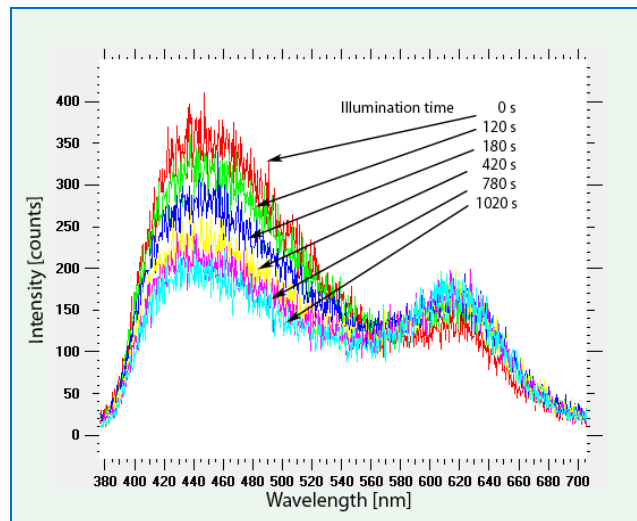


Fig. 59. Emission intensity as a function of illumination time of composite film, excited at 360 nm

Streak image of fluorescence spectrum of nanofibers excited at 360 nm is shown in Figure 60.

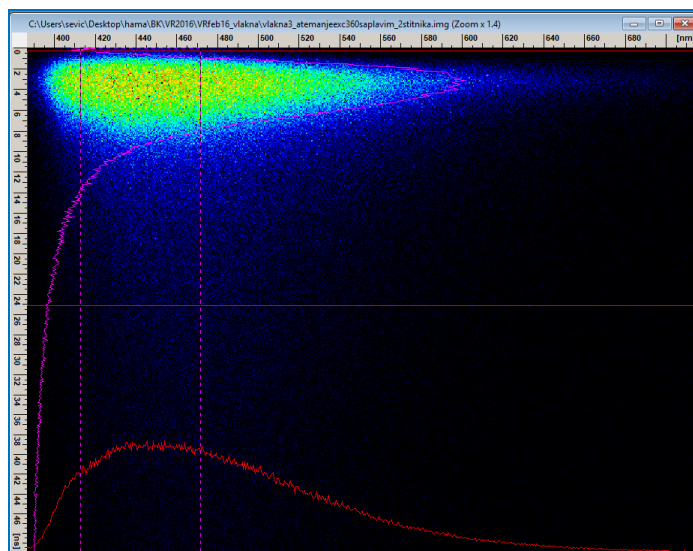


Figure 60. Streak image of fluorescence spectrum of PMMA-CdSe/ZnS nanofibers excited at 360 nm.

For all excitation wavelengths the fluorescence emissions look similar, with only one very wide band. Fluorescence lifetime of PMMA-CdSe/ZnS nanofibers optical emission is about 2.2 ns, similar to the lifetime of QDs liquid solution. Again, comparing with the values provided in the literature [96-99], estimated core size of QDs embedded in PMMA nanofibers, after the fabrication process which includes the electrospinning technique, are about 2.4 nm.

CONCLUSION

Conclusion

Functional composites with a polymer matrix represent high performance materials in which specific properties can be designed depending on the application and the requirements for exploitation. For the good physic mechanical properties of the composite it is extremely important to achieve a bonding between the matrix and the filler. In this dissertation, the possibility of modifying the surface of the single crystals during the synthesis of optoelectronic polymer composites with controlled optical properties was examined. In this way, the connection between the structure and the bond of the matrix-single crystal is improved, which will affect the physical-mechanical properties of the composite

Research was performed in two directions: synthesis of single-crystal $\text{CaWO}_4\text{-Nd}^{3+}$ as a functional carrier and embedding in the polymer matrix forming layered composite structure; and synthesis and characterization of polymer composites doped with CdSe/ZnS core shell quantum dots. All materials, started and obtained composites, were characterized with aim to investigate influence of processing parameters and components on the properties of obtained composite materials. In addition to other physical-mechanical properties, the optical properties of single crystals (unmodified and modified) have been specially examined, then the optical properties of composite itself.

Firstly, the aim of the current work was to assess obtain single crystal of calcium tungstate doped with neodymium - ($\text{CaWO}_4\text{:Nd}^{3+}$), and after that the crystal was characterized with various spectroscopic methods. The single crystal was grown from the melt using the Czochralski method in air. By optimizing growth conditions, $\langle 001 \rangle$ -oriented $\text{CaWO}_4\text{:Nd}^{3+}$ crystals up to 10 mm in diameter were grown. Number of dislocations in obtained crystal was 10^2 per cm^2 . Anisotropy in $\langle 001 \rangle$ direction was not observed. Mechanical properties of single crystal was performed by hardness micro Vickers testing. The obtained results are in good agreement with literature data. The crystal

structure was confirmed by X-ray diffraction. The obtained crystal was studied by Raman and infrared spectroscopy. Seven Raman and six IR optical active modes predicted by group theory are observed. FTIR confirmed the occurrence of all the functional groups and bonds in this material. From the FTIR spectrum, a strong peak of 862 cm^{-1} has been obtained due to the stretching vibration of WO_4^{2-} in scheelite structure, and a weak but sharp band at 433 cm^{-1} has been noticed due to the metal-oxygen (Ca-O) band. Estimated luminescence lifetime of ${}^4\text{F}_{5/2} - {}^4\text{I}_{9/2}$ transition is about $120\ \mu\text{s}$; estimated luminescence lifetime of ${}^4\text{F}_{3/2} - {}^4\text{I}_{9/2}$ transition is about $140\ \mu\text{s}$. All performed investigations show that the obtained $\text{CaWO}_4:\text{Nd}^{3+}$ single crystal has good optical quality, which was the goal of this work.

Grown bulk $\text{CaWO}_4:\text{Nd}^{3+}$ single crystal was cut into plain parallel wafers with the diamond saw. The wafers were polished with a diamond paste and surface modified with silane. Composite layered structure $\text{PMMA-CaWO}_4\text{-Nd}^{3+}$ was obtained with preserved optical properties of single crystals, whereas the thermal and mechanical properties were also improved.

FTIR analysis revealed the anchored silane onto surface of single crystal, while in spectrum of composite the dipole-dipole bonding with PMMA matrix also established. This bonding does not affect the interaction single crystal –electromagnetic rays. So, in this manner of interface modification two advantages are achieved: better mechanical properties and preserved optical activity in composite. These results lead in the direction of processing layered optic active composites with better yield and exploitation of single crystals and lower price.

In the second part of experiments core-shell quantum dots CdSe/ZnS were embedded in PMMA via electrospinning and solution casting methods. PMMA has proved to be an excellent host for quantum dots, securing the preservation of their optical properties during processing. Low content of QDs was used, only $0.06\text{ wt}\%$, in order to show that with such concentration sufficient signal strength could be achieved. FESEM provided an insight in the morphology of fibers, and it has indicated the absence of the agglomerates. FTIR analysis revealed that the structure of QDs has remained intact, with no identifying bonds coming from CdSe/ZnS in composite fibers and films. DSC analysis confirmed that the particles do not disrupt thermal properties of PMMA. The time-resolved laser induced fluorescence revealed that the optical activity of QD is preserved in composite films and

nanofibers. Fluorescence like nanoindentation also indicates that better dispersion of QD was obtained with electrospinning method.

These results confirmed PMMA as good matrix for optical composites, but improvements should be in the direction of mechanical properties also. As it is well known, the modification of interface matrix-particles improves the interactions between them. So, it was interesting to investigate how this modification influences optical interactions of single crystal in composites. With this aim, composite films with modified and unmodified core-shell QDs CdSe/ZnS was processed via solution casting. "Optical properties and fluorescence of nanocomposite were investigated as consequence of interface modification. FTIR analysis revealed the modification of QD's surface by 3-mercaptopropyltrimethoxysilane. Also, in polymer nanocomposite was established dipole-dipole bonding between S-H group of silane coupling agent and carbonyl groups of the polymer matrix. Optical properties were investigated applying Raman spectroscopy. Raman spectroscopy confirmed that PMMA matrix did not affect phonon modes of CdSe core of QD's. The obtained spectra of QDs CdSe/ZnS in PMMA and QD's CdSe/ZnS are almost identical. It could be attributed to the metal selenides and sulfides crystallites being in the pores of PMMA networks without disturbing the continuous three-dimensional network in the polymer matrices. Fluorescence revealed lifetimes of modified and unmodified QD's in PMMA are 1.46 and 1.36 ns." [118]. Those conclusions were reported in publication [118].

After wide range of characterization and different level of organization of composite structures it could be infer that during processing of composites there are many factors that could influenced the physic mechanical properties of obtained composites, particularly optical. So, it would be very important how to choice materials and methods of processing of composites relative to functionality and exploitations requirements. In this dissertation the two kind of optically active and transparent materials were used: single crystals of optoelectronic materials (on the macro, micro and nano level) and PMMA as widely used optical transparent polymer. Phenomenology on the interface polymer-crystal was followed by different methods. In the case of macro level of organization of composite (layered structures) modification of interface with silanes don't affect optical response of composite. In nano level, when different ratio surface/volume is present, and nanoparticles

tend to agglomerate, interface modification with silane leads to better dispersion and improvements both in mechanical and optical properties of obtained composites.

Results presented in this dissertation contribute to better insight on the interface phenomenology in polymer optical nanocomposites, the role of this interface both in mechanical and optical response of composites. This could be useful in design of material and process selection to obtain polymer composite with desirable properties.

REFERENCES

List of references

- [1] W. D. Callister, *Materials Science and Engineering, An Introduction*, 5-th edition, John Willey&Sons, New York, (2000).
- [2] P. K. Mallick, *Fiber-Reinforced Composites, Materials, Manufacturing, and Design*, 3rd edition, Taylor&Francis Group, Boca Raton, (2007).
- [3] Yu. I. Dimitrienko, *Composites Reinforced by Dispersed Particles, in Thermomechanics of Composite Structures under High Temperatures*, © 2018 Springer Nature Switzerland AG.
- [4] K. K. Chawla, *Composite Materials Science and Engineering*, 2nd edition, Springer-Verlag, New York, 1998.
- [5] T. W. Chou, R. L. McCullough, R. B. Pipes, *Composites, Scientific American*, 255(4), (1986) 192.
- [6] D. Hull, T. W. Clyne, *An Introduction to Composite Materials*, 2nd edition, Cambridge University Press, New York, (1996).
- [7] J. M. G. Cowie, V. Arigi, *Polymers: Chemistry and Physics of Modern Materials*, 3rd Edition, CRC Edition, Taylor &Francis GRoup, (2007).
- [8] S. F. Fennessey, R. J. Farris, *Polymer*, 45, (2004) 4217.
- [9] K. H. Lee, H. Y. Kim, Y. M. La, D. R. Lee, N. H. Sung, *J. Polymer Science: Part B: Polymer Physics*, 40(19), (2002) 2259.
- [10] L. G. Bacha, M. R. Islama, J. T. Kima, S.Y. Seob, K. T. Lima, *Applied Surface Science*, 258, (2012) 2959.
- [11] M. Shamsipur, N. Bahrami-Adeh, M. S. Hajitarverdi, F. Zarei, M. Yazdimamaghani I. Zargarlellahi *Middle-East Journal of Scientific Research*, 20 (1), (2014) 124.
- [12] G. Mohammadnezhad, M. Dinari, R. Soltani, Z. Bozorgmehr, *Applied Surface Science* 346, (2015) 182.
- [13] F. J. Tommasinia, L. da Cunha Ferreira, L. Galhardo Pimenta Tienne, V. de Oliveira Aguiar, M. H. Prado da Silva, L. F. da Mota Rocha, M. de Fátima Vieira Marques, *Materials Research*, 21(6), (2018) e20180086.
- [14] J. P. Matinlinna, L. V. J. Lassila, M. Özcan, A. Yli-Urpo, K. Vallittu, *The International Journal of Prosthodontics*, 17(2), (2004) 155 (2004).
- [15] J. Singh, *Semiconductor Devices*, John Wiley & Sons, Chichester, England, (2001).

- [16] S. Wolf, R. N. Tauber, *Silicon Processing for the VLSI Era*, Latice Press, Sunset Beach, California, (1986).
- [17] M. Madou, *Fundamentals of Microfabrication*, CRC Press LLC, Boca Raton, Florida, (1997).
- [18] E. Suhir, Y. C. Lee, C. P. Wong, *Micro-and Optoelectronic Materials and Structures: Physics, Mechanics, Design, Reliability, Packaging, Vol 1 and 2*, Springer Science+Business Media. Inc., (2007).
- [19] M. Nikl, P. Bohacek, N. Mihokova, M. Kobayashi, M. Ishii, Y. Usuki, Y. Usuki, V. Babin, A. Stolovich, S. Zazubovich, M. Bacci, *J. Lumin.*, 87-89, (2000) 1136.
- [20] A. Baranov, E. Tourney, *Semiconductor Lasers: Fundamentals and Applications*, Woodhead Publishing Series in Electronic and Optical Materials, 1st Edition, Woodhead Publishing Limited, Cambridge, UK, (2013).
- [21] V. L. Pushparaj, M. M. Shaijumon, A. Kumar, S. Murugesan, L. Ci, R. Vajtai, R. J. Linhardt, O. Nalamasu, P. M. Ajayan, *Proc. Natl. Acad. Sci. USA*, 104, (2007) 13574.
- [22] E. Sunden, J. K. Moon, C. P. Wong, W. P. King, S. Graham, *J. Vac. Sci. Technol. B*, 24, (2006) 1947.
- [23] R. M. Abozaid, Z. Ž. Lazarević, V. Radojević, M. S. Rabasović, D. Šević, M. D. Rabasović, N. Ž. Romčević, *Sci. Sinter.*, 50, (2018) 445.
- [24] G. Jia, C. Wang, S. Xu, *J. Phys. Chem. C*, 114, (2010) 17905.
- [25] X. Yan-Ling, Z. Hong, W. Rui, Z. Chun-Yu, *Chin. Phys. Lett.*, 6, (2011) 064210.
- [26] H. Lei, S. Zhang, XZ. Zhu, Y. Sun, Y. Fu, *Mater.Lett.*, 64, (2010) 344.
- [27] D. Errandonea, R. S. Kumar, X. Ma, C. Tu, *J. Solid State Chem.*, 181, (2008) 355.
- [28] V. I. Balakshy, K. Asratyan, V. Y. Molchanov, *J. Opt. A: Pure Appl. Opt.*, 3, (2001) S87.
- [29] L. Fan, Y. X./ Fan, Y. H. Duan, Q. Wang, H. T. Wang, G. H. Jia, C. Y. Tu, *Appl. Phys. B: Lasers Opt.*, 94, (2009) 553.
- [30] J. Sulc, H. Jelinkova, T. T. Basiev, M. E. Doroschenko, L. I. Ivleva, V. V. Osiko, P. G. Yverev, *Opt. Mater.*, 30, (2007) 195.
- [31] P. G. Yang, J. Liu, H. Yang, X. Yu, Y. Guo, Y. Zhou, J. Liu, *J. Mater. Chem.*, 19, (2009) 3771.
- [32] J. Bi, L. Wu, Y. Zhang, Z. Li, j. Li, X. Fu, *Appl. Catal. B*, 91, (2009) 135.
- [33] J. Yu, L. Qi, B. Cheng, X. Zhao, *j. Hazard. Mater.*, 160, (2008) 621.

- [34] J. Liu, H. Lian, C. shi, *Opt. Mater.*, 29, (2007) 1591.
- [35] J. Liao, B. Qiu, H. Wen, J. Chen, W. You, *Mater. Res. Bull.*, 44, (2009) 1863.
- [36] J. Liao, B. Qiu, H. Wen, J. Chen, W. You, L. Liu, *J. Alloys Compd.*, 487 (2009) 758.
- [37] A. V. Vereswnikova, B. K. Lubsandorzhev, I. R. Barabanov, P. Grabmayr, D. Greiner, J. Jochum, M. Knapp, C. Ostwald, R. V. Poleshuk, F. Ritter, B. A. M. Shaibonov, Y. E. Vyatchin, G. Meierhofer, *Nucl. Instrum. Methods Phys. Res. Sect. A*, 603, (2009) 529.
- [38] V. B. Mikhailika, S. Henrya, H. Krausa, I. Solskii, *Nucl. Instrum. Methods Phys. Res. Sect. A*, 583, (2007) 350.
- [39] I. Annenkov, O. A. Buzanov, F. A. Danevich, A. Sh. Georgadze, S. K. Kim, H. J. Kim, Y. D. Kim, V. V. Kobychhev, V. N. Kornoukhov, M. Korzhik, J. I. Lee, O. Missevitch, V. M. Mokina, S. S. Nagorny, A. S. Nikolaiko, D. V. Poda, R. B.Podviyanuk, D. J. Sedlak, O. G. Shkulkova, J. H. So, I. M. Solsky, V. I. Tretyak, S. S. Yurchenko, *Nucl. Instrum. Methods Phys. Res. Sect. A*, 584, (2008) 334.
- [40] G. K. Choi, J. R. Kim, S. H. Yoon, K. S. Hong, *J. Eur. Ceram. Soc.*, 27, (2007) 3063.
- [41] G. K. Choi, S. Y. Cho, J. S. An, K. S. Hong, *J. Eur. Ceram. Soc.*, 26, (2006) 2011.
- [42] H. Kraus, V. B. Mikhailik, *Nucl. Instrum. Methods Phys. Res. Sect. A*, 621, (2010) 395.
- [43] J. Ninkovic, G. Angloher, C. Bucci, C. Cozzini, T. Frank, D. Hauff, H. Kraus, B.Majorovits, V. Mikhailik, F. Petricca, F. Probat, Y. Ramachers, W. Rau, W. Seidel, S.Uchaikin, *Nucl. Instrum. Methods Phys. Res. Sect. A*, 537, (2005) 339.
- [44] I. Trabelsi, M. Dammak, R. Maalej, M. Kamoun, *Phys. B*, 406, (2011) 315.
- [45] W. Wang, P. Yang, S. Gai, N. Niu, F. He, J. Lin, *J. Nanopart. Res.*, 12, (2010) 2295.
- [46] Q. Xiao, Q. Zhou, M. Li, *J. Lumin.*, 130, (2010) 1092.
- [47] A. B. Campos, A. Z. Simões, E. Longo, J. A. Varela, V. M. Longo, A. T. De Figueiredo, F. S. de Vicente, A. C. Hernandez, *Appl. Phys. Lett.*, 91, (2007) 051923.
- [48] L. S. Cavalcante, V. M. Longo, J. C. Sczancoski, M. A. P. Almeida, A. A. Batista, J. Varela, M. O. Orlandi, E. Longo, M. Siu Li, *Cryst. Eng. Comm.*, 14, (2012) 853.
- [49] I. V. Andreiev, V. P. Bondarenko, L. G. Tarasenko, *Sci. Sinter.*, 48, (2016) 191.
- [50] C. Tablero, *Chem. Phys. Lett.*, 635, (2015) 190.
- [51] R. M. Hazen, L. W. Finger, J. W. E. Mariathan, *J. Phy. Chem. Solids*, 46 (1985) 253.
- [52] A. Golubovic, R. Gajic, Z. Dohcevic, S. Nikolic, *Sci. Sinter.*, 38, (2006) 265.

- [53] A. Golubovic, R. Gajic, Z. Dohcevic-Mitrovic, S. Nikolic, *J. Alloys Compd.*, 415, (2006)16.
- [54] W. Shockley, G. L. Pearson, *Phys. Rev.*, 74, (1948) 74.
- [55] L. T. Canham, *Appl. Phys. Lett.*, 57, (1990) 1046.
- [56] J. A. Sekhar, *J. Cryst. Growth*, 109, (1991) 113.
- [57] S. Kuppurao and J. J. Derby, *J. Cryst. Growth*, 172, (1997) 350.
- [58] R. Nacker, N. Jahrab, *Mineral Geol.*, 2, (1915) 133.
- [59] J. Czochralski, *Physik Z. Chem.*, 92, (1918) 219.
- [60] G. Tamman, *Metallography*, Trans. Dean and Svenson, Chemical catalog Co. New York, (1925).
- [61] Obreimov and L. W. Shubnikov, *Physik. Z.*, 25, (1924) 31.
- [62] P. W. Bridgeman, *Proc. Am. Acad. Arts. and Sci.*, 60, (1925) 305.
- [63] A. Verneuil, *Compt. Rend.*, 135, (1902) 791.
- [64] A. Verneuil, *Ann. Chim. Phys.* 3, (1904) 20.
- [65] C. H. L. Goodman (ed.), *Crystal Growth*, Springer Science+Business Media New York, (1978).
- [66] W. G. Pfann, *Zone Melting*, Wiley, New York, 2nd edn., (1964).
- [67] W. G. Pfann, *Principles of zone-melting*, Trans. AIME 194 747, (1952).
- [68] X. Zhang, S. Friedrich, B. Friedrich, *J. Crysta. Proc. Tech.*, 8, (2018), 33.
- [70] J. C. Brice, *The growth of Crystals from the melt*, North Holland, (1965).
- [71] J. Czochralski, *Physik Z. Chem.*, 92, (1918) 219.
- [72] L. de Broglie, *Ann. Phys.*, 3, (1925) 22.
- [73] D. A. Tomlin, J. M. J Frechet, *J. Polym. Sci. Part A. Polym. Chem.*, 40, (2002) 2719.
- [74] I. Gerdova, A. Haché, *Opt. Commun.*, 246, (2005) 205.
- [75] U. Woggon, *J. Appl. Phys.*, 101, (2007) 081727.
- [76] B. Bhattacharjee, C.H. Hsu, C.H. Lu, W.H. Chang, *Physica E*, 33, (2006) 388.
- [77] V. I. Klimov, S. A. Ivanov, J. Nanda, M. Achermann, I. Bezel, J. A. McGuire, A. Piryatinski, *Nature*, 447(24), (2007) 441.
- [78] D. Vasudevan, Rohit Ranganathan Gaddam, Adrian Trinchi, Ivan Cole, *J. Alloy Compd.*, 363, (2015) 395.
- [79] E. Sharon, R. Freeman, I. Willner, *Anal. Chem.*, 82, (2010) 7073.
- [80] I. L. Medintz, H. T. Uyeda, E. R. Goldman, H. Mattoussi, *Nat. Mater.*, 4, (2005) 435.

- [81] R. Bakalova, Z. Zhelev, I. Aoki, H. Ohba, Y. Imai, I. Kanno, *Anal. Chem.*, 78, (2006) 5925.
- [82] H. Kobayashi, Y. Hama, Y. Koyama, *Nano Lett.*, 7, (2007) 1711.
- [83] Y. Chan, J. Steckel, P. Snee, J. Caruge, J. Hodgkiss, D. Nocera, M. G. Bawendi. *Appl. Phys. Lett.*, 86, (2005) 0731021.
- [84] Z. Tan, F. Zhang, T. Zhu, J. Xu, A. Y. Wang, J. D. Dixon, L. Li, Q. Zhang, S. E. Mohney, J. Ruzyllo, *Nano Lett.*, 7, (2007) 3803.
- [85] I. Gur, N. A. Fromer, M. L. Geier, A. P. Alivisatos, *Science*, 310, (2005) 462.
- [86] B. S. Sun, J. Henry, A. S. Dhoot, S. G. Westenhoff, C. Neil, *J. Appl. Phys.*, 97, (2005) 014914.
- [87] K. E. Plass, M. A. Filler, J. M. Spurgeon, B. M. Kayes, S. Maldonado, B. S. Brunschwig, H. A. Atwater, N. S. Lewis, *Adv. Mater.*, 21, (2009) 325.
- [88] V. L. Pushparaj, M. M. Shaijumon, A. Kumar, S. Murugesan, L. Ci, R. Vajtai, R. J. Linhardt, O. Nalamasu, P. M. Ajayan, *Proc. Natl. Acad. Sci. USA*, 104, (2007) 13574.
- [89] E. Sunden, J. K. Moon, C. P. Wong, W. P. King, S. Graham, *J. Vac. Sci. Technol. B*, 24, (2006) 1947.
- [90] Y. J. Jung, S. Kar, S. Talapatra, C. Soldano, G. Viswanathan, X. S. Li, Z. L. Yao, F. S. Ou, A. Avadhanula, R. Vajtai, S. Curran, O. Nalamasu, P. M. Ajayan, *Nano Lett.*, 6, (2006) 413.
- [91] N. R. Raravikar, A. S. Vijayaraghavan, P. Koblinski, L. S. Schadler, P. M. Ajayan, *Small*, 1, (2005) 317.
- [92] E. B. Sansom, D. Rinderknecht, M. Gharib, *Nanotechnology*, 19, (2008) 035302.
- [93] M. P. Zach, K. Inazu, K. H. Ng, J. C. Hemminger, R. M. Penner, *Chem. Mater.*, 14, (2002) 3206.
- [94] S. A. Morin, F. F. Amos, S. Jin, *J. Am. Chem. Soc.*, 129, (2007) 3776.
- [95] D. Meissner, R. Memming, B. Kastening, *Chem. Phys. Lett.*, 96, (1983) 34.
- [96] V. Pilla, L. P. Alves, M. T. T. Pacheco, E. Munin, *Opt. Commun.*, 281, (2008) 5925.
- [97] L. P. Alves, V. Pilla, D. O. A. Murgu, E. Munin, *J. Dent.*, 38, (2010) 149.
- [98] B. O. Dabbousi, J. Rodriguez-Viejo, F. V. Mikulec, J. R. Heine, H. Mattoussi, R. Ober, K. F. Jensen, M. G. Bawendi, *J. Phys. Chem. B*, 101, (1997) 9463.
- [99] V. Pilla, L. P. Alves, A. N. Iwazaki, A. A. Andrade, A. Antunes, E. Munin. *Appl. Spectrosc.*, 67, (2013) 997.

- [100] R. Z. Stodilka, J. J. L. Carson, K. Yu, Md. B. Zaman, C. Li, D. Wilkinson, *J. Phys. Chem. C*, 113, (2009) 2580.
- [101] W. G. J. H. M. van Sark, P. L. T. M. Frederix, D. J. Van den Heuvel, H. C. Gerritsen, A. Bol, J. N. J. van Lingen, C. de Mello Donegá, A. Meijerink, *J. Phys. Chem. B*, 105, (2001) 8281.
- [102] W. G. J. H. M. van Sark, P. L. T. M. Frederix, A. A. Bol, H. C. Gerritsen, A. Meijerink, *Blueing, Chemphyschem.*, 3, (2002) 871.
- [103] L. Liu, Q. Peng, Y. Li, *Inorg. Chem.*, 47, (2008) 5022.
- [104] I. Suarez, H. Gordillo, R. Abargues, S. Albert, J. Mart, I. Pastor, *Nanotechnology*, 22, (2011) 435202.
- [105] R. M. Dukali, I. Radovic, D. B. Stojanovic, P. S. Uskokovic, N. Romcevic, V. Radojevic, R. Aleksic, *J. Alloy Compd.*, 583, (2014) 376.
- [106] E. B. Gibelli, J. Kai, E. E. S. Teotonio, O. L. Malta, M. C. F. C. Felinto, *J. Photochem. Photobiology A: Chemistry*, 251, (2013) 154.
- [107] M. Rosemal, H. M. Harisa, S. Kathiresan, S. Mohan, *Der Pharma Chemica*, 2, (2010) 316.
- [108] A. Chapiro, *Radiation Chemistry of Polymeric Systems*, John Wiley&Sons, New York, (1962).
- [109] R. G. Jagger, *J. Prosthet. Dent.*, 76, (1996) 573.
- [110] L. Woo, M. T. K. Ling, S.Y. Ding, S. P. Westphal, L. Woo, M. T. K. Ling, S. Y. Ding, S. P. Westphal, *Thermochim. Acta*, 324, (1998) 179.
- [111] H. Song, S. Lee, *Nanotechnology*, 18, (2007) 055402.
- [112] A. M. Alam, Y. Liu, M. Park, S. J. Park, H. Y. Kim, *Polymer*, 59, (2015) 35.
- [113] Z. M. Huang, Y. Z. Zhang, M. Kotaki, S. Ramakrishna, *Compos. Sci. Technol.*, 63, (2003) 2223.
- [114] A. Frenot, I. S. Chronakis, *Curr. Opin. Colloid In.*, 8, (2003) 64.
- [115] L. Daelemans, S. van der Heijden, I. De Baere, H. Rahier, W. Van Paepegem, K. De Clerck, *Compos. Sci. Technol.*, 117, (2015) 244.
- [116] Y. Zhang, S. Zhuang, X. Xu, J. Hu, *Opt. Mater.*, 36, (2013) 169.
- [117] G. Mohammadnezhad, M. Dinari, R. Soltani, Z. Bozorgmehr, *Appl. Surf. Sci.*, 346, (2015) 182.
- [118] R. M. Abozaid, Z. Ž. Lazarević, I. Radović, M. Gilić, D. Šević, M. S. Rabasović, V. Radojević, *Optical Materials*, 92, (2019) 405.

- [119] D. Dragoman, M. Dragoman, *Optical Characterization of Solids*, Springer-Verlag, Berlin, (2002).
- [120] W. H. Bragg, W. L. Bragg, *The Reflexion of X-rays by Crystals*, *Proc. R. Soc. Lond. A*, 88(605), (1913) 428.
- [121] P. R. Griffiths, J. A. De Haseth, *Fourier Transform Infrared Spectrometry*, John Wiley & Sons, (2007).
- [122] B. Schrader, *Infrared and Raman Spectroscopy*; VCH Publishers Inc., New York, (1995) Chapter 4.
- [123] O. C. Wells, *Scanning Electron Microscopy*, McGraw-Hill, New York, (1974).
- [124] C. Moulin, I. Laszak, V. Moulin, C. Tondre, *Applied Spectroscopy*, 52, (1998) 528.
- [125] M. S. Rabasovic, D. Sevic, M. Terzic, B. P. Marinkovic, *Nucl. Instrum. Methods Phys. Res. B*, 279, (2012) 16.
- [126] A. Alavudeen, N. Venkateshwaran, J. T. Winowlin Jappes, *A Textbook of Engineering Materials and Metallurgy*, Firewall Media, 2006
- [127] E. Pungor, *A Practical Guide to Instrumental Analysis*, Florida, Boca Raton, (1995) 181.
- [128] H. I. Elswie, Z. Ž. Lazarević, V. Radojević, M. Gilić, M. Rabasović, D. Šević, N. Ž. Romčević, *Sci. Sinter.*, 48, (2016) 333.
- [129] A. A. Algellai, M. M. Vuksanovic, N. Tomić, A. Marinković, M. Dojčinović, T. Volkov-Husović, R. Jančić Heinemann, *Improvement of cavitation resistance of composite films using functionalized alumina particles*, *Hemijska Industrija* 2018, <http://dx.doi.org/10.2298/HEMIND180308011A>
- [130] ASTM E384 - 16 - *Stand. Test Method Microindentation Hardness Mater.*, 201528.
- [131] R. W. Cheary, A. Coelho, *J. Appl. Crystallography*, 25, (1992) 109.
- [132] Z. V. Popovic, *Center of Excellence in Optical Spectroscopy Applications in Physics, Material Science and Environmental Protection*, 2009.
- [133] M. A. Almessiere, *Sci. Sinter.*, 50 (2018) 63.
- [134] M. Petrović, M. Gilić, J. Ćirković, M. Romčević, N. Romčević, J. Trajić, I. Yahia, *Sci. Sinter.*, 49 (2017) 167.
- [135] *Safety Data Sheet according to EC 1907/2006 (REACH) and 1272/2008 (CLP)*.
- [136] H. El-Swie, I. Radovic, D. B. Stojanovic, D. M. Sevic, M. S. Rabasovic, P. Uskokovic, V. Radojevic, *J. Optoelectr. Adv. Mat.*, 2017, 19, 228.
- [137] W. C. Oliver, G. M. Pharr, *J. Mater. Res.*, 7, (1992) 1564.

- [138] M. Crane, R. L. Frost, P. A. Williams, J. T. Kloprogge, *J. Raman Spectrosc.*, 33, (2002) 62.
- [139] R. L. Rousseau, R. P. Bauman, S. P. Porto, *J. Raman Spectrosc.*, 10, (1981) 253.
- [140] D. Christofilos, G. A. Kourouklis, S. Ves, *J. Phys. Chem. Solids*, 56, (1995) 1125.
- [141] S. P. S. Porto, J. F. Scott, *Phys. Rev.*, 157, (1967) 716.
- [142] M. Nicol, J. F. Durana, *J. Chem. Phys.*, 54, (1971) 1436.
- [143] T. T. Basiev, A. A. Sobol, Y. K. Voronko, P. G. Zverev, *Opt. Mater.*, 15, (2000) 205.
- [144] A. Phuruangrat, T. Thongtem, S. Thongtem, *J. Exp. Nanosci.*, 5, (2010) 263.
- [145] T. T. Basiev, A. A. Sobol, P. G. Zverev, I. I. Ivleva, V. V. Osiko, R. C. Powell, *Opt. Mater.*, 11, (1999) 307.
- [146] A. S. Barker Jr., *Phys. Rev.*, 135, (1964) A742.
- [147] Z. C. Ling, H. R. Xia, D. G. Ran, F. Q. Liu, S. Q. Sun, J. D. Fan, H. J. Zhang, J. Y. Wang, L. L. Yu, *Chem. Phys. Lett.*, 426, (2006) 85.
- [148] P. Suneetha, Ch. Rajesh, M. V. Ramana, *Mater. Res. Express*, 4, (2017) 085020.
- [149] Q. Li, Y. Shen, T. Li, *J. Chem.*, 2013, (2013) 952954.
- [150] N. A. Sabu, X. Francis, J. Anjaly, S. Sankararaman, T. Varghese, *Eur. Phys. J. Plus*, 32, (2017) 290.
- [151] X. Lai, Y. Wei, D. Qin, Y. Zhao, Y. Wu, D. Gao, J. Bi, D. Lin, G. Xu, *Integr. Ferroelec.*, 142, (2013) 7.
- [152] N. Rakov, G. S. Maciel, *J. Appl. Phys.*, 121, (2017) 113103.
- [153] G. Jiang, X. Wei, S. Zhou, Y. Chen, C. Duan, M. Yin, *J. Lumin.*, 152, (2014) 156.
- [154] S. Balabhadra, M. L. Debasu, C. D. S. Brites, L. A. O. Nunes, O. L. Malta, J. Rocha, M. Bettinellie, L. D. Carlos, *Nanoscale*, DOI: 10.1039/c5nr05631d.
- [155] F. Chen, M. Ju, G. L. Gutsev, X. Kuang, C. Lu, Y. Yeung, *J. Mater. Chem. C*, 5, (2017) 3079.
- [156] X. Fu, Z. Jia, Y. Li, D. Yuan, C. Dong, X. Tao, *Opti. Mat. Express*, 2, (2012) 1242.
- [157] S. M. Salili, A. Ataie, M.R. Barati, Z. Sadighi, *Mater. Charact.*, 106, (2015) 78-85.
- [158] G. Socrates, *Infrared and Raman Characteristic Group Frequencies Tables and Charts*, Third Edition, John Wiley & Sons Ltd, Baffins Lane, Chichester, West Sussex PO19 IUD, England, (2001).

- [159] N. Z. Tomić, A. D. Marinković, Ž. Radovanović, K. Trifković, M. Marinović-Cincović, R. Jančić-Heinemann, *J. Polymer Research*, 25(4), (2018) 96, DOI: 10.1007/s10965-018-1493-7.
- [160] C. Palache, H. Berman, and C. Frondel (1951) *Dana's system of mineralogy*, (7th edition), v. II, 1075–1077
- [161] [161] J. Lamovec, V. Jović, D. Randjelović, R. Aleksić, V. Radojević, Analysis of the composite and film hardness of electrodeposited nickel coatings on different substrates, *Thin Solid Films* 516 (2008) 8646-8654.
- [162] [162] A. A. Algellai, M. M. Vuksanović, N. Z. Tomić, A. D. Marinković, K. D. Obradović-Đuričić, V. J. Radojević, R. M. Jančić Heinemann, The implementation of image analysis for the visualization of adhesion assessment of a composite film, *Mater. Lett.* 227 (2018) 25-28.
- [163] Kuppayee, G. K. Vanathi Nachiyar, V. Ramasamy, *Appl. Surf. Sci.*, 257, (2011) 779.
- [164] S. Reghuran, A. Arivarasan, R. Kalpana, R. Jayave, *J. Experimental Nanoscience*, 10, (2015) 787-802.
- [165] I. S. Elashmawi, N. A. Hakeem, *Polym. Eng. Sci.* 48 (2008) 895-901.
- [166] F. Goldibi, G. Asghari, *Res. J. Biol. Sci.* 4 (2009) 244-249.
- [167] T. T. M. Phan, N. C. Chu, V. B. Luu, H. N. Xuan, D. T. Pham, I. Martin, P. Carriere, *J. Science: Advanced Materials*, 1, (2016) 90.
- [168] H. C. Kim, H. G. Hong, C. Yoon, H. Choi, I. S. Ahn, D. C. Lee, Y. J. Kim, K. Lee, *J. Colloid. Interf. Sci.*, 393, (2013) 74.
- [169] O. O. Akinwunmi, G. O. Egharevba, E. O. B. Ajayi, *J. Mod. Phys.*, 5, (2014) 257.
- [170] B. H. Henry, J. R. Daring (Eds.), *Raman Spectroscopy: Sixty Years On*, vol. 10, Elsevier, Amsterdam, (1990).
- [171] J. Trajić, R. Kostić, N. Romčević, M. Romčević, M. Mitrić, V. Lazović, P. Balaž, D. Stojanović, *J. Alloys Compd.*, 637, (2015) 401.
- [172] O. Brafman, S. S. Mitra, *Phys. Rev.*, 171, (1968) 931-934.
- [173] W. G. Nilsen, *Phys. Rev.*, 182, (1969) 838.
- [174] Y. C. Cheng, C. Q. Jin, F. Gao, X. L. Wu, W. Zhong, S. H. Li, P. K. Chu, *J. App. Phys.*, 106, (2009) 123505-1-123505-5.
- [175] V. M. Dzhagan, M. Ya. Valakh, A. E. Raevskaya, A. L. Stroyuk, S. Ya. Kuchmiy, D. R. T. Zahn, *Nanotechnology*, 18, (2007) 285701.

- [176] M. Isarov, N. Grumbach, G. I. Maikov, J. Tilchin, Y. Jang, A. Sashchiuk, E. Lifshitz, *Lithuanian J. Phys.*, 55, (2015) 297.
- [177] H. A. Willis, V. J. I. Zichy, P. J. Hendra, *Polymer*, 10, (1969) 737.
- [178] J. Dubal, S. Krimm, *Macromolecules*, 23, (1990) 1301.
- [179] S. Agarwal, D. Patidar, N. S. Saxena, *J. Appl. Polym. Sci.*, 123, (2012) 2431.
- [180] Z. Li, J. Zhang, J. Du, T. Mu, Z. Liu, J. Chen, B. Han, *J. Appl. Polym. Sci.*, 94, (2004), 1643.
- [181] C. Guan, C. Lu, Y. Cheng, S. Song, B. Yang, *J. Mater. Chem.*, 19, (2009) 617.
- [182] J. Z. Mbese, P. A. Ajibade, *Polymers* 6, (2014) 2332-2344
- [183] R. M. Dukali, I. M. Radović, D. B. Stojanović, D. M. Šević, V. J. Radojević, D. M. Jocić, R. R. Aleksić, *J. Serb. Chem. Soc.*, 79, (2014) 867.
- [184] S. Ummartyotin, N. Bunnak, J. Juntaro, M. Sain, H. Manuspiya, *Solid State Sci.* 14, (2012) 299.
- [185] N. Patra, A. C. Barone, M. Salerno, *Adv Pol Tech*, 30(1), (2011) 12.
- [186] M. Eriksson, H. Goossens, T. Peijs, *Nanocomposites*, 1, (2015) 36.
- [187] S. S. Musbah, V. Radojević, I. Radović, P. S. Uskoković, D. B. Stojanović, M. Dramićanin, R. Aleksić, *J. Min. Metall. Sect. B-Metall.*, 48, (2012) 309.
- [188] V. Pilla, L. P. Alves, E. Munin, M. T. T. Pacheco, *Opt. Commun.*, 280, (2007) 225.

Prilog 1.

Izjava o autorstvu

Прилог 1.

Изјава о ауторству

Потписани-а Rouaida Mohamed Abozaid
број индекса 4015/2014

Изјављујем

да је докторска дисертација под насловом

**Физичко механичка својства полимерних композита са
наномодификованим монокристалима**

**Physic mechanical properties of polymer composites with nanomodified single
crystals**

- резултат сопственог истраживачког рада,
- да предложена дисертација у целини ни у деловима није била предложена за добијање било које дипломе према студијским програмима других високошколских установа,
- да су резултати коректно наведени и
- да нисам кршио/ла ауторска права и користио интелектуалну својину других лица.

Потпис докторанда

У Београду, _____



Prilog 2.

Izjava o istovetnosti štampane i elektronske verzije doktorskog rada

Прилог 2.

Изјава о истоветности штампане и електронске верзије докторског рада

Име и презиме аутора _____ Rouaida Mohamed Abozaid _____

Број индекса _____ 4015/2014 _____

Студијски програм _____ Инжењерство Материјала _____

Наслов рада Физичко механичка својства полимерних композита са
наномодификованим монокристалима

Physic mechanical properties of polymer composites with
nanomodified single crystals

Ментори _____ Радојевић Весна _____

_____ Зорица Лазаревић _____

Потписани/а _____

Изјављујем да је штампана верзија мог докторског рада истоветна електронској верзији коју сам предао/ла за објављивање на порталу **Дигиталног репозиторијума Универзитета у Београду**.

Дозвољавам да се објаве моји лични подаци везани за добијање академског звања доктора наука, као што су име и презиме, година и место рођења и датум одбране рада.

Ови лични подаци могу се објавити на мрежним страницама дигиталне библиотеке, у електронском каталогу и у публикацијама Универзитета у Београду.

У Београду, _____

Потпис докторанда



Prilog 3.

Izjava o korišćenju

Прилог 3.

Изјава о коришћењу

Овлашћујем Универзитетску библиотеку „Светозар Марковић“ да у Дигитални репозиторијум Универзитета у Београду унесе моју докторску дисертацију под насловом:

Физичко механичка својства полимерних композита са наномодификованим монокристалима

Physic mechanical properties of polymer composites with nanomodified single crystals

која је моје ауторско дело.

Дисертацију са свим прилозима предао/ла сам у електронском формату погодном за трајно архивирање.

Моју докторску дисертацију похрањену у Дигитални репозиторијум Универзитета у Београду могу да користе сви који поштују одредбе садржане у одабраном типу лиценце Креативне заједнице (Creative Commons) за коју сам се одлучио/ла.

1. Ауторство
2. Ауторство - некомерцијално
3. Ауторство – некомерцијално – без прераде
4. Ауторство – некомерцијално – делити под истим условима
5. Ауторство – без прераде
6. Ауторство – делити под истим условима

(Молимо да заокружите само једну од шест понуђених лиценци, кратак опис лиценци дат је на полеђини листа).

У Београду, _____

Потпис докторанда



1. Ауторство - Дозвољавате умножавање, дистрибуцију и јавно саопштавање дела, и прераде, ако се наведе име аутора на начин одређен од стране аутора или даваоца лиценце, чак и у комерцијалне сврхе. Ово је најслободнија од свих лиценци.
2. Ауторство – некомерцијално. Дозвољавате умножавање, дистрибуцију и јавно саопштавање дела, и прераде, ако се наведе име аутора на начин одређен од стране аутора или даваоца лиценце. Ова лиценца не дозвољава комерцијалну употребу дела.
3. Ауторство - некомерцијално – без прераде. Дозвољавате умножавање, дистрибуцију и јавно саопштавање дела, без промена, преобликовања или употребе дела у свом делу, ако се наведе име аутора на начин одређен од стране аутора или даваоца лиценце. Ова лиценца не дозвољава комерцијалну употребу дела. У односу на све остале лиценце, овом лиценцом се ограничава највећи обим права коришћења дела.
4. Ауторство - некомерцијално – делити под истим условима. Дозвољавате умножавање, дистрибуцију и јавно саопштавање дела, и прераде, ако се наведе име аутора на начин одређен од стране аутора или даваоца лиценце и ако се прерада дистрибуира под истом или сличном лиценцом. Ова лиценца не дозвољава комерцијалну употребу дела и прерада.
5. Ауторство – без прераде. Дозвољавате умножавање, дистрибуцију и јавно саопштавање дела, без промена, преобликовања или употребе дела у свом делу, ако се наведе име аутора на начин одређен од стране аутора или даваоца лиценце. Ова лиценца дозвољава комерцијалну употребу дела.
6. Ауторство - делити под истим условима. Дозвољавате умножавање, дистрибуцију и јавно саопштавање дела, и прераде, ако се наведе име аутора на начин одређен од стране аутора или даваоца лиценце и ако се прерада дистрибуира под истом или сличном лиценцом. Ова лиценца дозвољава комерцијалну употребу дела и прерада. Слична је софтверским лиценцама, односно лиценцама отвореног кода.

Biography

Rouaida Mohamed Abozaid was born on January, 07. 1976. in Tripoli Libya, she graduated in 2000 and got her BSc. in Physic from Tripoli University, Faculty of Science. She got her MSc. degree from Szent Istvan University Hungary, in the Faculty of Mechanical Engineering (2004-2006). Then she went back to Libya and worked for Zawia University at the department of computer science as an assistant lecturer also as a head of the department between 2007-2009. She taught some subjects such as basics of computer, numerical analysis and she also supervised some final BSc. projects. In 2009 she got a scholarship to pursue her higher education. Using her experience with Engineering and Physics sciences she started doing her PhD program in 2014 at the Faculty of Technology and Metalurgy, Department of Material Science and Engineering, Belgrade University and passed all exams by platform of these studies.

Biografija

Rouaida Mohamed Abozaid rođena je 07.01.1976. godine u Tripoliju, Libija. Fakultet je završila je na Tripoli Univerzitetu, Libija, Departman Fizika. Master studije na Szent Istvan University, Madjarska na Departmanu Mašinstvo odbranila je 2006. godine. Radila je na Zawia University, Libija Departman za Kompjuterske nauke od 2007-2009. godine. Doktorske studije upisala je 2014. godine na Univerzitetu u Beogradu, Tehnološko-metalurški fakultet, profil Inženjerstvo materijala.

